AN INVESTIGATION OF THE POSSIBILITY OF CHARGED PARTICLE DETECTION USING TUNNELING BETWEEN SUPERCONDUCTORS

by

GORDON HARVEY WOOD

B.A.Sc., University of British Columbia, 1963

A THESIS SUBMITTED IN PARTIAL FULFILMENT OF

THE REQUIREMENTS FOR THE DEGREE OF

MASTER OF APPLIED SCIENCE

in the Department

of

PHYSICS

We accept this thesis as conforming to the

required standard

THE UNIVERSITY OF BRITISH COLUMBIA

September, 1965

In presenting this thesis in partial fulfilment of the requirements for an advanced degree at the University of British Columbia, I agree that the Library shall make it freely available for reference and study. I further agree that permission for extensive copying of this thesis for scholarly purposes may be granted by the Head of my Department or by his representatives. It is understood that copying or publication of this thesis for financial gain shall not be allowed without my written permission.

Department of Physics

The University of British Columbia
Vancouver 8, Canada

Date October 1, 1965

ABSTRACT

A study has been made which demonstrates the feasibility of developing a nuclear particle detector utilizing tunneling between superconductors.

For optimum detector performance, temperatures lower than $1.2^{o}K$ are mandatory. Accordingly, a He^{4} cryostat capable of being modified to a He^{3} cryostat has been constructed and tested.

The detectors, which have been fabricated and tested at $1.4^{o}K$, consist of thin aluminum and lead films separated by an insulating layer of aluminum oxide. The d-c tunneling currents have been observed and are found to compare favourably with the results of previous workers.

The d-c response of the device to gamma radiation was, as expected, unobservable.

TABLE OF CONTENTS

	Page
Chapter I - INTRODUCTION	1
Chapter II - PRESENT METHODS OF MEASURING CHARGED PARTICLE ENERGY SPECTRA	5
A. Introduction	5
B. Momentum Measurement	5
C. Energy Measurement	9
1. Gas Filled Counter	9
2. Scintillation Counter	12
3. Solid State Counters	16
D. Velocity Measurement	19
1. The Cerenkov Detector	19
2. Time-of-Flight Method	23
E. Comparison of Three Methods of Spectrometry	24
1. Energy Resolution (R)	25
2. Detector Efficiency.	25
3. Solid Angle.	25
4. Arbitrary Figure of Merit	26
5. Energy Loss/Ion Pair.	26
6. Time Resolution	26
7. Available Sizes	27
8. Environment Required	27
Chapter III - THEORY OF THE PROPOSED SUPERCONDUCTING NUCLEAR PARTICLE DETECTOR	30
A. Introduction.	30
B. Physical Characteristics of Detector	30

Page

C. Tunneling 32

1. Introduction 32

2. "Cooper Pairs" and the Energy Gap 34

3. Density of States 35

4. Tunneling Current between Normal Metal and a Superconductor. 37

5. Tunneling between two Similar Superconductors 41

6. Tunneling between two Dissimilar Superconductors 42

7. Résumé. 44

D. Excitation Energy and Energy Resolution 44

1. Excitation Energy 44

2. Energy Resolution 49

E. Tunneling Probability and Recombination Time 50

F. Diffusion Velocity 56

G. Signal and Noise 57

1. Signal Size 57

2. Shot Noise in the Leakage Current 62

3. Thermal Noise 62

4. Generation-Recombination (GR) Noise in Leakage Current . 64

5. Input Noise of Amplifier 65

6. GR Noise in Signal 66

7. Net Contribution of Noise to Resolution 67

8. Signal to Noise Ratio 67

H. Josephson Tunneling 69

I. Comparison Between Solid State and Superconducting Detectors. 71

Chapter IV - FABRICATION OF TUNNELING JUNCTIONS 73

A. Preparation of Substrate 73

B. Evaporation Procedure 73

C. Geometric Effects 74

Page

Chapter V - CRYOGENIC APPARATUS 77

A. Introduction 77

B. Dewars 77

C. Pumps 80

D. Pressure-Temperature Measurement 80

E. Cryostat 80

F. Cryostat Cap and Sample Mount 81

Chapter VI - ELECTRICAL MEASUREMENT TECHNIQUES 85

A. Power Supply 85

B. High-Pass Filter 85

C. Electrical Connections 87

D. Measuring Circuitry 87

Chapter VII - RESULTS 91

A. Normal Metal Junction Resistance 91

B. Time Dependence of Junction Resistance 92

C. Superconductive Tunneling 96

D. Effect of Radioactive Source 99

Chapter VIII - CONCLUSION 102

Appendix A - EFFECT OF THERMAL CONTRACTION ON JUNCTION THICKNESS AND TUNNELING PROBABILITY 105

Appendix B - CALCULATION OF DIFFUSION VELOCITY AND RECOMBINATION TIME . 110

Appendix C - ESTIMATE OF THE THICKNESS OF LEAD AND ALUMINUM FILMS . . . 113

Appendix D - ESTIMATE OF HEAT LEAKAGE AND RESULTING LIQUID HELIUM LOSS 117

Appendix E - PROCEDURE FOR LIQUID HELIUM RUN. 119

Bibliography 121

LIST OF TABLES

Table		Page
I	Comparison of Nuclear Particle Detectors (Part 1)	28
II	Comparison of Nuclear Particle Detectors (Part 2)	29
III	Comparison of Solid State and Superconducting Detectors	72
IV	Relation Between Oxidation Time and Junction Resistance for $Al-Al_2O_3-Pb$ Sandwiches	92

LIST OF FIGURES

Figure		Page
1.	Sector Field Spectrometer (60^{o})	8
2.	Schematic of Ionization Chamber	10
3.	Schematic of Scintillation Counter	10
4.	Schematic of Silicon Junction Detector	17
5.	Depletion Region and Charge Density	17
6.	Construction to Show Formation of Cerenkov Radiation	21
7.	Time-of-Flight Schematic.	21
8.	Junction Thickness v/s Junction Resistance	33
9.	Density of States near the Fermi Surface	36
10.	Single Particle Energy Spectrum for M-B-S	36
11.	I-V Characteristic for M-B-S Structure	40
12.	Single Particle Energy Spectrum for S-B-S'	40
13.	Typical I-V Characteristic for S-B-S' Structure	43
14.	I-V Characteristic for S_1-B-S_2 Structure	43
15.	Single Particle Energy Spectrum for S_1-B-S_2	45
16.	Modes of Excitation	47
17.	Recombination Times of Electrons in Superconducting Lead	52
18.	Variation of Theoretical Diffusion Velocity with Temperature	58
19.	Junction Equivalent Circuit and Amplifier	59
20.	Model for Voltage Pulse Estimate	59
21.	Theoretical Signal Pulse Shape	59
22.	Evaporation Procedure	75
23.	Cryogenic Apparatus (Schematic)	78
24.	Cryostat (Simplified)	82

Figure		Page
25.	Cryostat Cap and Specimen Mount	83
26.	Electrical Circuit (Schematic)	86
27.	Twin D.C. Amplifiers (Schematic)	89
28.	I-V Characteristic for Normal Metal Junction	93
29.	Time Dependence of Junction Resistance in Various Environments .	94
30.	I-V Characteristic for Al-Al_2O_3-Pb Sandwich	97
31.	I-V Characteristic for Al-Al_2O_3-Pb Sandwich	98
32.	Geometry of Evaporator	114
33.	Geometry for Molecular Effusion	114

ACKNOWLEDGEMENTS

My sincere thanks go to Dr. B. L. White for his generous assistance and enthusiastic supervision throughout the duration of this work.

The many valuable discussions with Drs. J. Brown, P. Critchlow, M. Crooks and P. Matthews concerning cryostat design and operation are acknowledged with gratitude.

Special thanks are due my wife Linda for her continuing encouragement and her limitless patience in typing this thesis.

The financial assistance received from the National Research Council in the form of two scholarships is also gratefully acknowledged.

CHAPTER I

INTRODUCTION

The products of nuclear reactions provide, in effect, a window into the interior of the atomic nucleus and it is through the analysis of the energy distribution of these products that a great deal of the present knowledge of nuclear physics has been obtained. Because of the immediate rewards in more reliable data, much effort has gone into the development of radiation detectors so that the science of nuclear particle spectroscopy has grown into a complex and sophisticated one (cf., Yuan, 1961; Ajzenberg-Selove, 1960). Consequently, adequate detectors are now available for most experimental requirements; room always exists, however, for improvement. It is the intent of this thesis, therefore, to outline the theory of a new type of particle detector based on the principle of tunneling between superconductors and to report on some related preliminary developmental work.

A theoretical study of the feasibility of developing a superconducting nuclear particle detector has been carried out and its findings indicate that there is no fundamental reason why the proposed counter should not work. In addition, a He^4 cryostat has been designed, constructed and tested. Presently it is capable of reaching temperatures near $1.2^{\circ}K$ but is designed in such a way that, if still lower temperatures are required for optimum detector operation, conversion of the cryostat to He^3 refrigerating gas could be readily performed. Tunneling junctions consisting of evaporated aluminum and lead films separated by a thin layer of aluminum oxide have also been prepared and tested.

During the course of developing junction fabrication techniques, an aging effect was noted in the tunneling junctions. As a result considerable time and effort was spent in attempting to understand and thence control this undesirable property.

The motivation for conducting such an experiment is transparent. At the very least, much important information should be gained concerning fundamental processes in the tunneling of electrons between superconductors (Chapter III). In addition, there exists the exciting possibility of developing a new particle detector, superior in energy resolution to the best solid state device, and constituting therefore a significant advance in the science of nuclear spectroscopy.

The pioneering work of Giaever and Megerle (1961) first drew attention to the tunneling of excited or "normal" electrons between superconductors separated by a thin insulating barrier. Soon afterward, Burstein, et al (1961) proposed the use of these tunneling "sandwiches" or junctions to detect microwave and submillimetre-wave radiation and showed that, except for some purely technological problems, the device was quite feasible. The gist of their proposal was that the energy lost in the superconducting junction by the impinging photons would give rise to a sharp increase in the current due to tunneling electrons. The magnitude of this photon-assisted tunneling current is proportional to the number of photons striking the junction so that by monitoring the tunneling current, one could "detect" electromagnetic radiation. Similarly, recent experiments have been reported by Lax (1965) and Abeles (1965) in which microwave phonon-assisted tunneling was observed in superconducting junctions. By analogy, the proposed superconducting nuclear

particle detector can loosely be said to depend on ionizing particle-assisted tunneling.

Some of the physical parameters affecting the operation of the superconducting counter are not presently well understood (Chapter III). For example, Ginsberg (1962), Schrieffer (1962) and Rothwarf (1963) have made experimental and theoretical estimates of the lifetime of an excited electron which are, at best, very approximate. Also, little is known of the mechanism by which excited electrons are generated in a superconductor by a nuclear particle nor is much known about the velocity at which those electrons would diffuse through the superconductor. It is almost certain that experiments pertaining to the superconducting detector will furnish information concerning these questions and, for that reason alone, are well worth carrying out.

The investigations concerning the superconducting counter are presented in the following sequence. Chapter II gives a survey of the present methods of measuring charged particle energy spectra. Several types of detectors are considered in each of three broad classifications: momentum measurement, energy loss determination and velocity measurement. Specifically, a magnetic spectrometer, scintillation counter and solid state detector are compared (Tables I and II) with respect to energy resolution, detection efficiency, solid angle, time resolution, size and operating environment. In this way, a firm basis is established for judging the merit of the proposed detector.

The theory behind the superconducting particle detector is discussed in Chapter III where, first of all, the physical characteristics of the detector are described. Then, in considerable detail, the concepts from superconductivity essential to an understanding of the device are set forth and incorporated

into a derivation of the thermal tunneling current. In order to predict the effect of charged particles in a superconductor an estimate is made of the energy that must be lost by the particle to produce one excited electron. The three different ways an excited electron can decay back to the ground state are then discussed and it is shown that an appreciable fraction of the excited electrons will tunnel only if low experimental temperatures and very thin junctions are employed. Following this, a rough estimate is made of the excited electron diffusion velocity; it is found to be sufficiently high as to not be a limiting factor in detector performance. Leakage current noise, signal noise, the signal to noise ratio and the resultant energy resolution are then examined in some detail. Josephson tunneling is briefly considered but is found to not be a serious threat to successful detector operation. At the end of the chapter, the superconducting and solid state detectors are compared (Table III) with respect to several figures of merit.

Chapters IV, V and VI describe the experimental work that has been done. In particular, Chapter IV deals with the method of preparing the tunneling junctions, Chapter V describes the cryogenic apparatus that was constructed and Chapter VI outlines the techniques used in making electrical measurements.

Preliminary results on the developmental work are set forth in Chapter VII. Finally, in Chapter VIII, the conclusions which may be drawn from theory and experiment are briefly summarized.

CHAPTER II

PRESENT METHODS OF MEASURING CHARGED PARTICLE ENERGY SPECTRA

A. Introduction

Many methods are available for measuring the numbers and energies of charged particles resulting from a nuclear reaction. Broadly speaking, the methods are based either on the deflection of charged particles in magnetic or electric fields or on the energy loss of charged particles when passing through matter. For purposes of this discussion, it is convenient to divide the methods into three major categories: momentum measurement, energy determination and velocity measurement.

B. Momentum Measurement

Of all the ways of measuring the momentum of a charged particle, the most common and precise are those founded on the well-known interaction of electric and magnetic fields with charged particles (Yuan, 1961). Analyzers or spectrometers based on this concept use the principle that rays of particles diverging from a point source at small angles will, after having been bent into circular trajectories by the field, converge again at some point. At this point is situated an appropriate nuclear particle detector. Shutters and baffles are employed to define a small focal point so that the detector sees only particles having very nearly the same initial momentum. It is this high resolution or ability to distinguish between particles having very small differences in momentum that makes the spectrometer so valuable a device for nuclear spectroscopy.

For reasons set out clearly by Yuan (1961), spectrometers employing magnetic fields are much more widely used than either those using electric fields or those using a combination of both electric and magnetic fields. Therefore, the rest of this discussion will relate specifically to magnetic field spectrometers.

To gain an appreciation of the physical size of a magnetic spectrometer, consider a particle of charge q moving with a velocity v in a plane perpendicular to a uniform magnetic field B. Then, if ρ is the radius of curvature, $qvB = mv^2/\rho$ or, in a more useful form, $B\rho = p/q$. Now, in nuclear reactions, the energies encountered are usually such that the required magnetic field is sufficiently high that, for reasons of economy, magnetic circuits using iron are required. It is essential that the field distribution be independent of the magnitude of the actual field if the trajectories of the particles transmitted through the instrument are to remain constant. With iron, saturation effects appear at higher fields which limits the maximum field to about 12,000 gauss (Ajzenberg, 1960). The $B\rho$ product for a 5 Mev alpha particle is about 300 kilogauss-cm. which corresponds to a radius of curvature of about 10 inches. Clearly, an instrument capable of handling such particle trajectories requires fairly large amounts of iron and occupies a considerable volume.

Before considering some of the types of magnetic spectrometers commonly used, it is expedient to choose some figures of merit as a basis for comparison; resolution and efficiency are two natural choices. Resolution R is related to the capability to distinguish between particles of different momenta and is defined as

$$R = \frac{\Delta(B\rho)}{B\rho}$$

where $B\rho$ is the particle momentum, the particles being assumed monoenergetic, and $\Delta B\rho$ the line width at half maximum. Efficiency is stipulated by the spectrometer transmission T which is the effective solid angle in steradians expressed as a percentage of 4π. In other words, T is the probability that a particle emitted from an isotropic point source will be transmitted from the source to the detector. Spectrometers have intrinsically high resolution and low efficiency and one can only be increased at the expense of the other.

Several types of spectrometer in general use are described in some detail by Ajzenberg (1960), Bueckner (1956), and Yuan (1961). The semicircular focusing spectrometer, the double focusing spectrometer and the sector field spectrometer are three of the most common. As the name implies, the semicircular focusing spectrometer brings charged particles of the same momenta to a focus at a point 180° and a distance 2ρ from the source. Only radial focusing is obtained. Since both the source and detector are in the magnetic field, this spectrometer has less flexibility than others but is good for high precision work as the particles do not pass through any fringing fields. In the double focusing spectrometer, the magnetic field is shaped so that both radial and axial focusing obtain. In general, the two focii do not coincide but by careful design and choice of field they can be made to coincide after a deflection of about 256°. Adjusted for the same resolution as the semicircular instrument, the double focusing spectrometer has about three times the efficiency of the former. Sector field spectrometers, see figure 1 , are often designed to give 60° or 90° deflections. The magnetic field is wedge shaped thereby reducing the amount of iron required and permitting both the source and detector to be located outside the field. By causing the charged particles to enter the pole faces at oblique angles, the fringing fields can

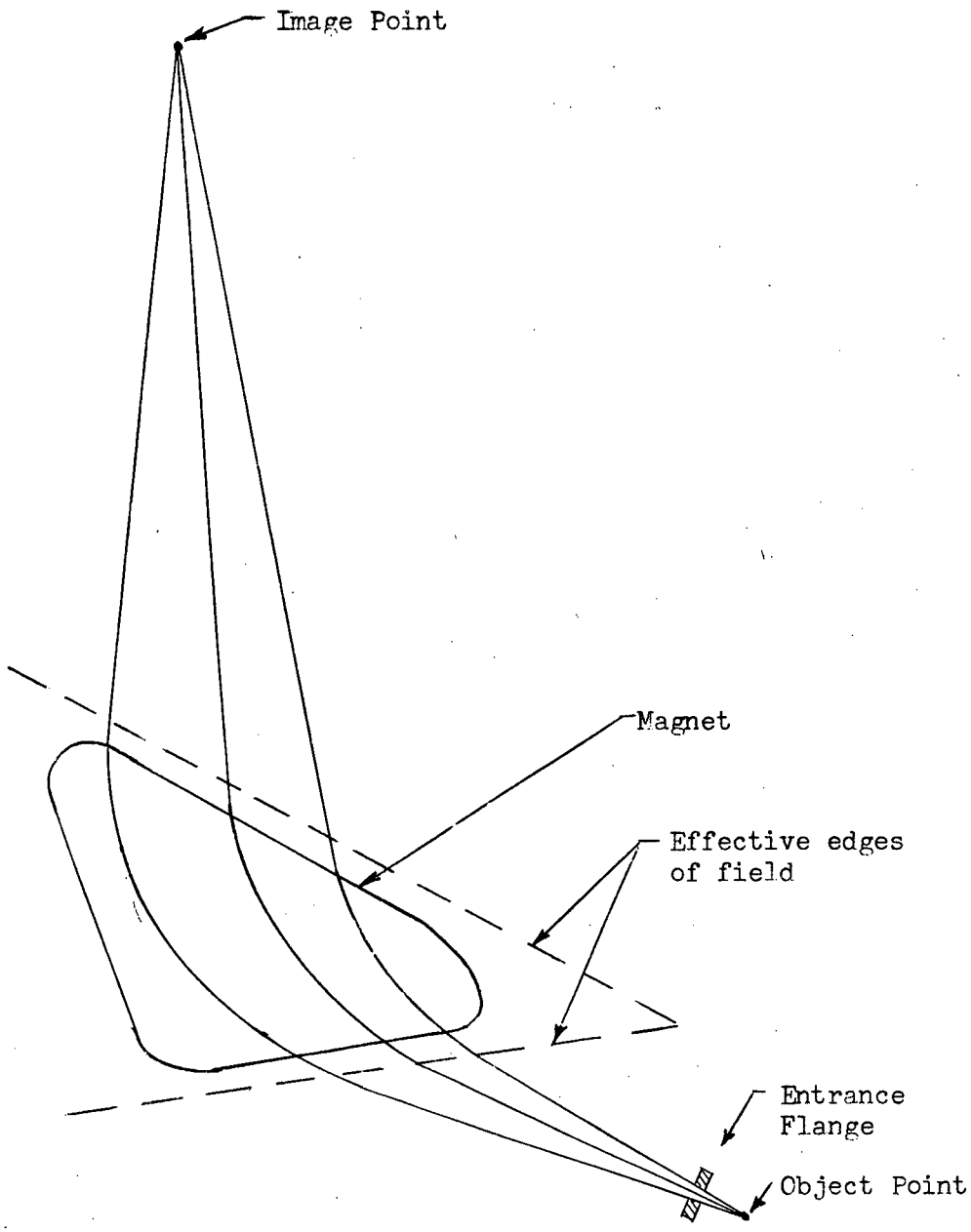

Figure 1: Sector Field Spectrometer (60^{o})

be used to provide double focusing (Cross, 1951). Because of the large distance between source and detector, the instrument is capable of high resolution, but, when adjusted for the same resolution as the above-mentioned spectrometers, the sector focusing spectrometer has a considerably lower transmission.

C. Energy Measurement

When a charged particle passes through matter, it loses energy through the excitation and ionization of atoms situated close to the path of the particle. This property has been exploited in the development of several types of particle detectors. Three of special interest are the gas-filled counter, the scintillation counter and the solid-state counter.

1. Gas-Filled Counter

Basically, a gas-filled counter is a metal chamber that is fitted with an anode and cathode and filled with an accurately defined volume of gas. The ionization chamber, the proportional counter and the Geiger-Muller counter belong to this classification, but since the last two are merely modifications of the ionization chamber a discussion of its properties will suffice to outline the basic principles on which gas-filled particle detectors operate.

A typical ionization chamber is shown schematically in figure 2 . The passage of an energetic charged particle through a suitable "window" into the gas volume, causes electrons to be removed from some of the gas molecules, thereby producing electron-positive ion pairs. Under the influence of the electric field, the electrons are attracted to the anode and the positive ions are attracted to the cathode. This movement of charge

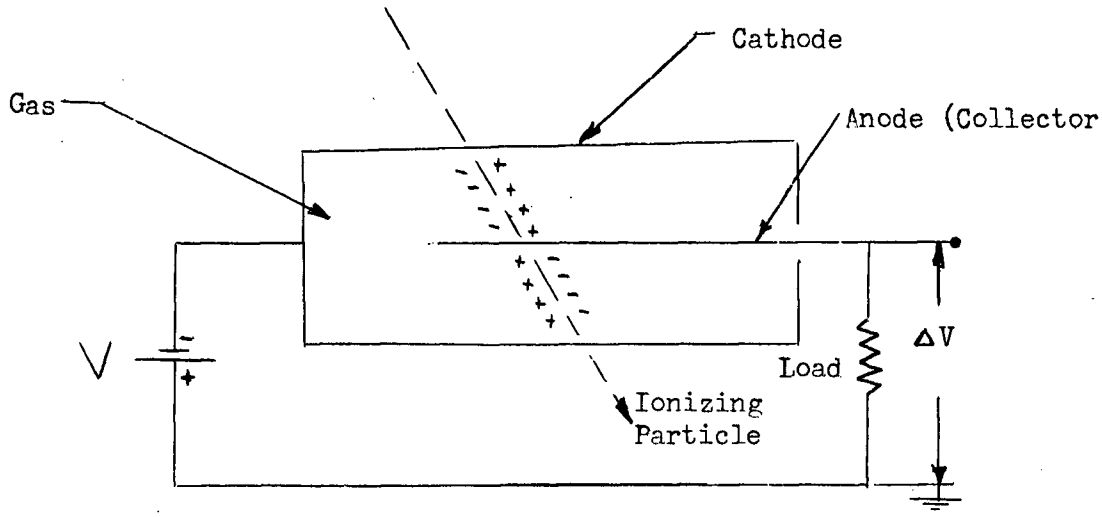

Figure 2: Schematic of Ionization Chamber

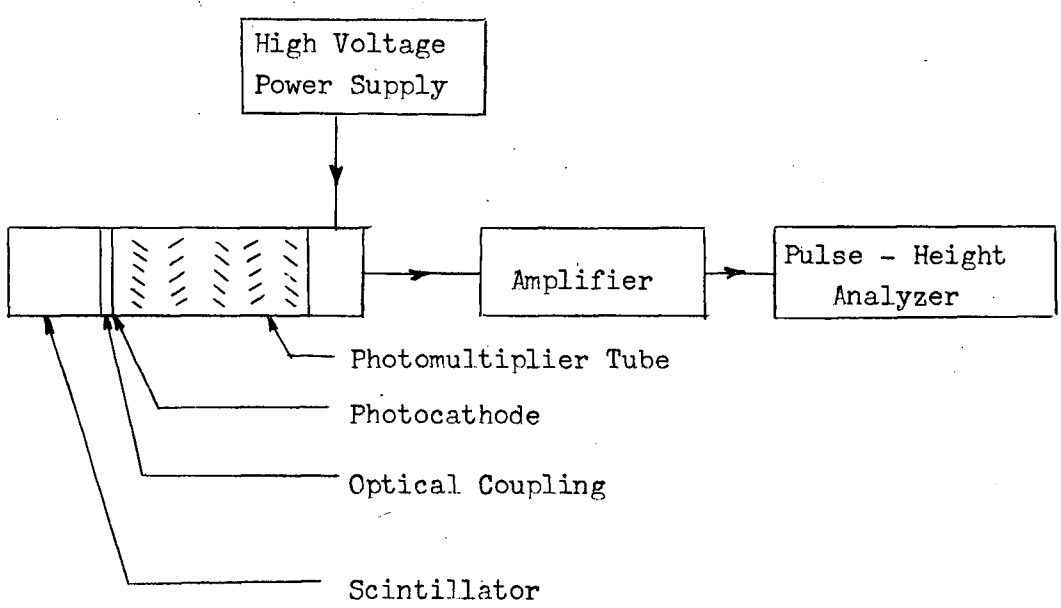

Figure 3: Schematic of Scintillation Counter

induces image charges on the electrodes and it is clear that if the electrodes have a capacitance C and the ionizing particles induce a charge Q then the change in voltage appearing across the load resistor is $\Delta V = Q/C$ as long as RC is long compared with the charge collection time. Now the average number of electron-positive ion pairs created per unit energy--about 1 pair per 30 ev--lost in the chamber is virtually independent of the energy and type of the charged particle (Yuan, 1961). Therefore, since C is fixed for a given counter configuration, the amplitude of the voltage pulse ΔV is a measure of the energy lost by the particle in the chamber and, if the particle is completely stopped in the chamber, the amplitude of the pulse is proportional to the energy of the ionizing particle.

A practical counter, of course, requires modifications to overcome the problems inherent in the fact that the electron mobility is approximately 1000 times that of the positive ions. An outline of these innovations, including for example suitable gas mixtures and the introduction of a grid, is contained in books by Rossi and Staub (1949), Wilkinson (1950) and Yuan (1961).

The energy resolution is directly related to variations in the pulse height. Contributions to the fluctuations in the amplified pulse height come from particle energy straggling caused by the windows defining the gas volume, statistical variations in the number of ionization events, and electrical noise in the external amplifying circuitry. In practice, these factors combine to make the best line width observed (Dearnaley and Northrop, 1963) for a 5 Mev alpha particle to be about 30 kev, a resolution of 0.6%. More typically, resolution is about 1% (Bromley, 1961).

The time resolution strongly depends on the drift velocities of the electrons and positive ions. Voltage pulses resulting from the passage of a charged particle have a fast-rising part due to electron collection and a much slower-rising part due to positive-ion collection. The introduction of a grid to raise the counting rate by clipping the slow-rising part and of appropriate pulse-shaping circuitry to remove track orientation dependence by integrating the fast-rising part, results in a time resolution of about 10^{-4} sec.

Though rapidly being superseded by more recent types of detectors, the gas-filled counter is still used in certain special applications. A common and very practical application is to fill the ionization chamber with the gas being studied and use it as both target and detector. With this technique, for example, studies have recently been carried out at U.B.C. on the photodisintegration of He-3 (MacDonald), photodisintegration events in Argon (Reimann) and neutron thresholds (Healey). The tremendous variations in size from 1 to 10^5 cm^3 (Segrè, 1964) permit the ionization chamber to be used in dosimetry, where it might be the size of a fountain pen, or to be used in cosmic-ray studies where its size might approach a cubic metre. Because of its transmission properties, a "thin" gas-filled counter is frequently used in tandem with a scintillation counter to form a specific ionization and particle detector (Ajzenberg, 1960). Finally, the capability of varying the gas pressure makes the ionization chamber useful for identifying particles by range measurements.

2. Scintillation Counter

The scintillation counter features high efficiency, relatively good energy resolution and fast response. Detailed accounts of design and operation are found in works by Curran (1953) and Birks (1953) with more

general discussions found in Yuan (1961) and Chase (1961).

A typical scintillation counter arrangement is shown in figure 3 . The scintillating phosphor--crystal, liquid, plastic solid or gas--is optically coupled to a photomultiplier tube whose output signal is proportional to the energy of the charged particles striking the phosphor. If necessary, the output signal is amplified and fed into appropriate analyzing instruments.

The operating principle of the scintillation counter is relatively straightforward. When an ionizing particle strikes the phosphor, the energy dissipated causes loosely bound electrons in the material to be excited into the conduction band. Then, at imperfection sites in the crystal, they proceed to fall back to their ground state by one of two main mechanisms. Either they emit a photon and fall back directly to the ground state or they fall into a metastable state where they may either absorb sufficient thermal energy to raise them again to their initial excited state from which they subsequently fall to the ground state after emission of a photon or fall from the metastable state to the ground state via a radiationless transition. The direct process is called fluorescence; the indirect process is called phosphorescence. Because the latter process lags the former by about 10^{-8} sec., it is a nuisance and considerable steps are taken to make it minimal. The photons emitted during fluorescence strike the photocathode of the photomultiplier tube thereby ejecting photoelectrons.

Both organic and inorganic phosphors are commonly used. In the organic phosphor, fluorescence is a property of the molecules rather than of the lattice whereas in the inorganic phosphor, fluorescence is greatly

dependent on crystal form and perfection and consequently may be beneficially altered by variation of impurities. Anthracene and trans-Stilbene are used commonly as organic scintillators; thallium activated sodium iodide and cesium iodide are perhaps the most common inorganic scintillators. These have been found to satisfactorily meet the three main requirements of a scintillator, which are: short duration of phosphorescence, transparency to its own luminescent radiation and frequency of radiation matching the response of a photomultiplier tube.

Unlike that of the gas-filled counter, the energy response of the scintillation detector does vary with particle energy and type. In inorganic scintillators, the variation of light output with particle energy is slightly non-linear, especially at energies below about 0.5 Mev for protons and below about 15 Mev for alpha particles. In organic scintillators the variation is considerably more non-linear, this non-uniformity being attributed to "damage" suffered by the molecule during large energy transfers (Yuan, 1961). A strong variation of light output per unit particle energy with the type of particle detected is reported by Dearnaley and Northrop (1963). As an example, it is quoted that the pulse amplitude in NaI(Tℓ) due to a 5 Mev alpha particle is roughly one-half the amplitude due to an electron of the same energy. This lower conversion efficiency for excitation by heavily ionizing particles is thought to result from an increase in the proportion of non-radiative transitions. These transitions ensue from states which are more readily excited by the low-energy electrons produced by a heavy ionizing particle.

Potentially, the scintillation counter has 100% efficiency for detection of charged particles, since every charged particle striking the phosphor expends all or part of its kinetic energy. But the conversion

efficiency from kinetic to light energy to photoelectrons is at best roughly 10%. This means that, even under optimum conditions, more energy must be expended in a scintillator to produce a photoelectron than in a gas or a semiconductor to produce an ion pair (see Table II). Consequently, although every charged particle entering the phosphor may be ultimately detected, the conversion inefficiencies will, as pointed out in the succeeding paragraph, inhibit energy resolution. Understandably, the situation is even more unfavourable for detection of gamma radiation with detection efficiency dropping to about 60% (Siegbahn, 1955).

Energy resolution depends mainly on fluctuations in $\sqrt{N}$ where N is the number of photoelectrons produced by the photons from the scintillator. Now, as was just discussed, the number of photoelectrons produced by a scintillator will be significantly lower than the number of ion pairs produced by a particle of the same energy in an ionization chamber or a semiconductor; hence as anticipated theoretically and found experimentally, the energy resolution of the scintillation counter is relatively poorer than some competing devices. Dearnaley and Northrop (1963) report, for an alkali phosphor, an optimum line width of about 150 kev for monoenergetic 5 Mev alpha particles which is 3% resolution.

The excellent time resolution of the scintillation counter is one of its main attractions. Usually, the light intensity is a maximum immediately after the passage of a charged particle and the light amplitude decays exponentially thereafter with a time constant τ characteristic of the phosphor. Again, considerable differences exist between organic and inorganic scintillators. Yuan (1961) lists decay times for several scintillators with typical values being 10^{-8} sec. to a few $x10^{-9}$ sec. for $\tau_{organic}$ and 10^{-6} sec.

for $\tau_{inorganic}$. An improvement in time resolution by a factor of 100-1000 over that of a gaseous counter is immediately evident.

3. Solid State Counters

The principal features of the solid state counters are their fast response time, linearity with particle energy, high efficiency and superior energy resolution. Books by Taylor (1963) and Dearnaley and Northrop (1963) deal thoroughly with these detectors giving details on theory and application.

Semiconductors silicon and germanium are most often used as the stopping medium. Two chief types, the "diffused junction" and the "surface barrier", are prevalent but because the only significant difference between them is the manner in which they are prepared, it is convenient to discuss their properties and characteristics together. A typical P-N silicon junction detector is shown schematically in figure 4 .

The principle of operation of these counters is fundamentally analogous to that of the gas-filled counters. In order to be specific, the diffused junction detector will be considered. A P-N junction is formed close to one face of a slab of high resistivity P type silicon which is necessarily of high perfection to minimize trapping. Typically, the junction is within $\frac{1}{2}\mu$ of the one face and is very abrupt. When the junction is reverse biased, a depletion region is created which forms the sensitive volume of the counter (see figure 5). Depending on the doping and the magnitude of reverse bias applied, the depth of the sensitive volume, $x = x_n + x_p$, may range from 10μ to 0.8 mm. The conductivity of the surface layer and even of the bulk P-type crystal are vastly greater than that of the depletion region, hence this section

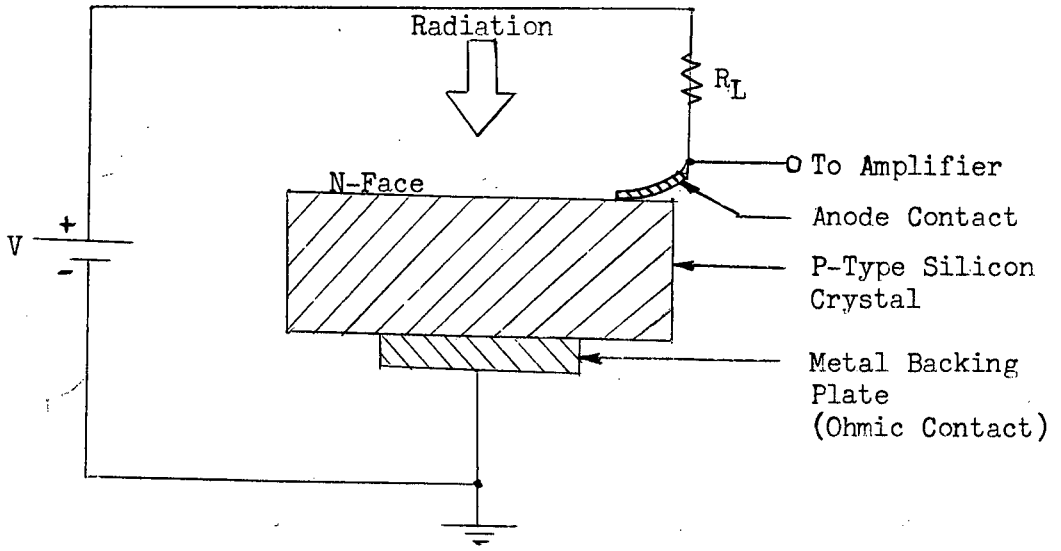

Figure 4: Schematic of Silicon Junction Detector (After Taylor, 1965)

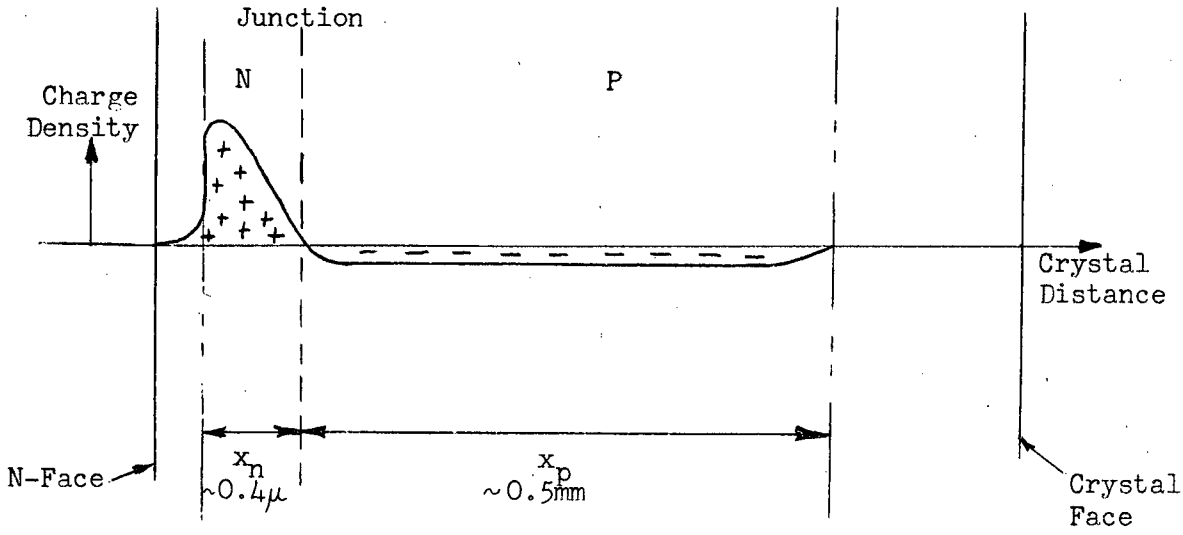

Figure 5: Depletion Region and Charge Density

resembles a distributed dipole or the parallel-plate capacitor of the gas-filled chamber. When an ionizing particle passes through the depletion region, electron-hole pairs are generated by inelastic collisions with the silicon atoms. These carriers are then swept apart by the strong electric field in the depletion region and a pulse results.

A remarkable feature of the energy response of the semiconducting counter is the linearity of pulse amplitude with particle energy regardless of the particle type. Yuan (1961) quotes results showing strict proportionality up to 10 Mev for protons, 40 Mev for alpha particles and 100 Mev for heavy ions and fission fragments. Such strict proportionality, however, is not achieved trivially. The depletion zone depth must be sufficient to stop all the particles concerned; the insensitive surface layer, or "window", must be negligibly thick; the decay time constant must be sufficiently large to ensure almost complete carrier collection.

As previously mentioned, the most fundamental contribution to the limit of energy resolution is the fluctuation in the number of ion pairs produced by a particle. Therefore, since the mean energy per ion pair generated in a semiconductor is about 3.5 ev compared to mean energies per ion pair of 30 and 300 ev in gas-filled and scintillation counters respectively, one expects and obtains superior energy resolution in the solid state device. Taylor (1963) makes an interesting comparison, on purely a statistical basis, between the resolution of a gas-filled counter and a silicon counter and finds that for a 5.3 Mev alpha particle the resolution is 0.4 and 0.2% respectively.

The time required for collection of all the carriers generated by an ionizing particle depends on the bulk and contact resistance of the

crystal, bias voltage and depletion layer depth. Tove and Falk (1961) estimate a collection time of about 6 nsec. for a 10K P type Silicon detector operating at a 500V bias with a depletion layer of 700μ. Thus, the effective time resolution of the solid state detector approaches that of the best scintillator, that is, approximately 10^{-9} sec.

Surface leakage current is the major contribution to electrical noise in the solid state counter. The reverse current, though merely a few microamps, makes an additional noise contribution and, being a strong function of the applied voltage, sets an upper limit to the reverse bias of about 300-400 volts for silicon and 50-100 volts for germanium. Operating solid state detectors, especially those made from germanium, at liquid nitrogen temperatures, significantly reduces reverse current and thermal noise. Semiconducting counters are susceptible to electrical interference and so must be screened. They have not been discovered, however, to be susceptible to magnetic fields as high as 50 kilogauss and therefore find profitable use with magnetic spectrometers.

D. Velocity Measurement

Two of the foremost methods for determining charged particle velocities are Cerenkov radiation detection and time-of-flight measurements. Both methods are described in considerable detail in Yuan (1961); Chase (1961) and Ajzenberg (1960) deal with Cerenkov radiation in particular; Neiler and Good (1960) describe comprehensively various time-of-flight techniques.

1. The Cerenkov Detector

When a charged particle traverses a medium with a velocity

that is greater than the velocity of light in that medium, light is emitted but essentially only in directions making acute angles with the direction of motion of the particle. This light, called Cerenkov radiation, emanates from any relatively transparent optical material and differs from ordinary fluorescence not only in its production mechanism but also in that it is partially polarized and its intensity is independent of temperature changes of the substance.

The analogy between Cerenkov radiation and the pressure shock wave caused by a supersonic projectile is very close. By using a simple wave-front construction (see figure 6), one easily obtains the relation between the angle of propagation of Cerenkov radiation and the particle velocity. Clearly, if β is the ratio of the charged particle velocity v_p to the velocity of light in vacuum c, and $n(\nu)$ is the index of refraction of the medium at the frequency ν of the emitted photon, and $\Delta\tau$ is the time interval for the particle to pass from P_1 to P_6, then

$$\cos\theta = 1/\beta n(\nu) \tag{2-1}$$

The intensity I, or the number of photons emitted per unit path length, is given in each of the above references as

$$I = \frac{2\pi Z^2 (\Delta\nu) \sin^2\theta \quad \text{photons}}{137c \qquad\qquad \text{unit path length}} \tag{2-2}$$

where Z is the particle atomic number and $\Delta\nu$ the frequency interval, in cycles per second, of the emitted radiation.

Equation 2-1 and 2-2 demonstrate the relation of the particle velocity to the direction and intensity of the Cerenkov radiation thereby illustrating why Cerenkov radiators are employed mainly to define a velocity range for the particles being counted. A lower bound for the velocity is

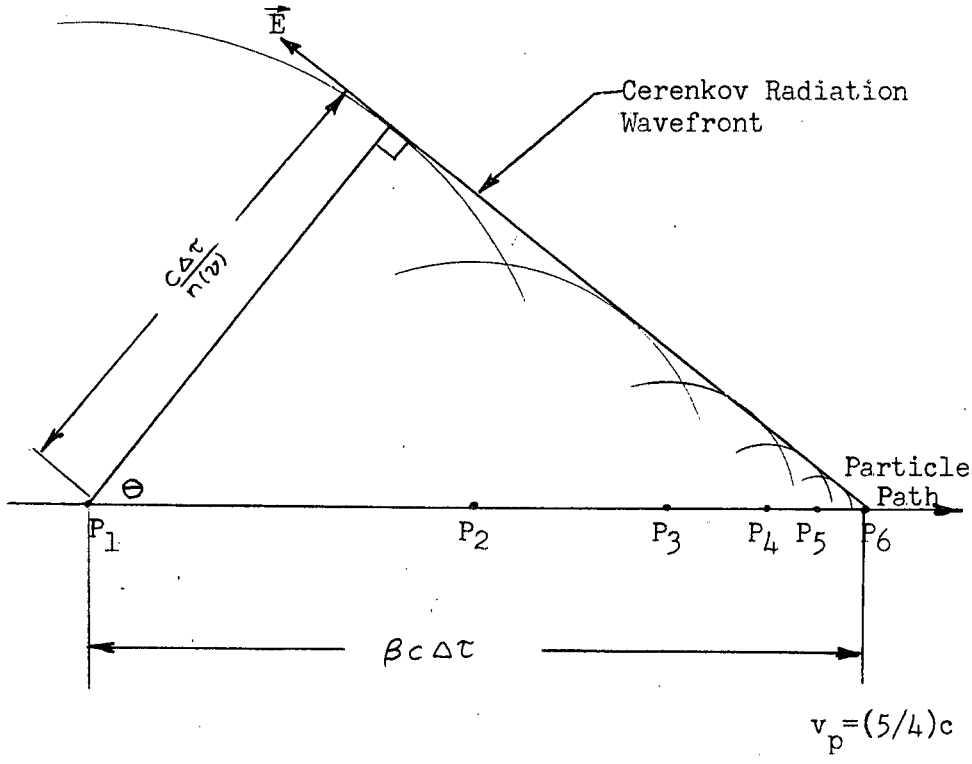

Figure 6: Construction to Show Formation of Cerenkov Radiation

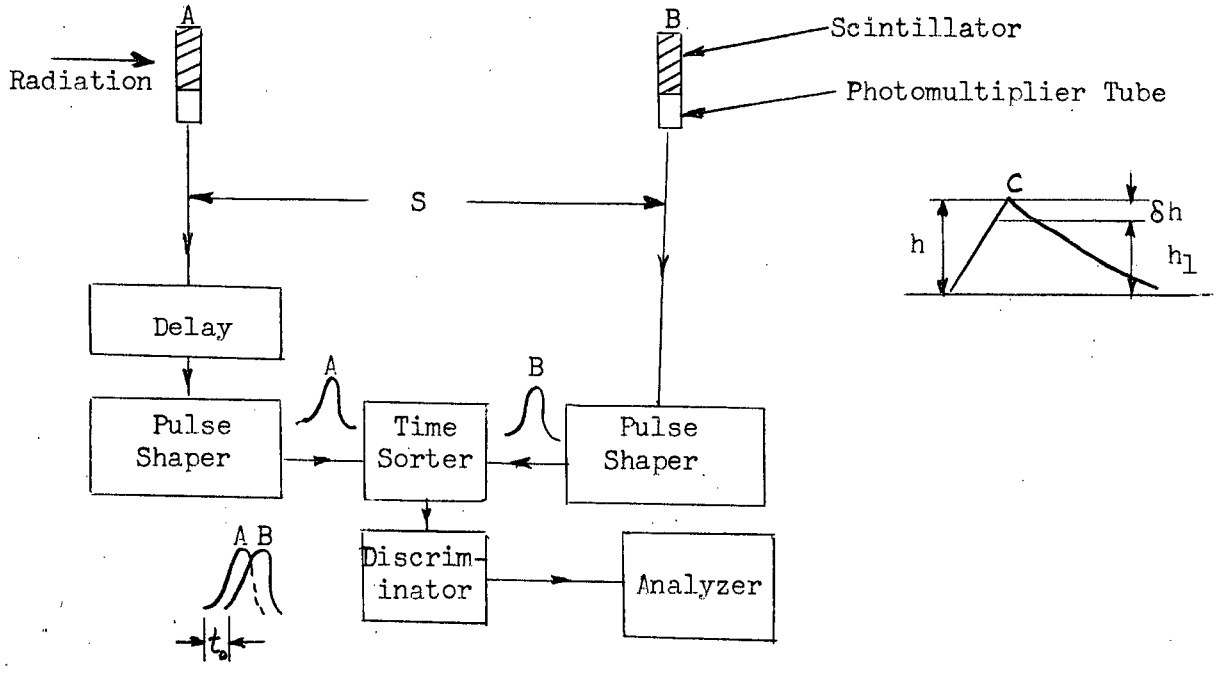

Figure 7: Time-of-Flight Schematic

automatically established since the detector responds only to particle velocities exceeding a specific threshold value $(n(\nu)/c)$; a measurement of the angular range of the Cerenkov photons restricts the particle velocity to a range $v_{p_1}<v_p<v_{p_2}$ where v_{p_1} and v_{p_2} are established by the details of the measuring system and the medium's index of refraction.

The velocity resolution of a Cerenkov detector is given by

$$R_v = \partial\theta/\partial\beta = 1/\beta^2 \, n \sin\theta$$

Since β changes slowly with energy, satisfactory resolution obtains only if R_v is large. Now, for relativistic particles, β approaches 1 and since n is close to 1,

$$R_v \sim 1/\sin\theta$$

and it is evident that θ must be kept small. It must be recalled from equation 2-2, however, that intensity is proportional to $\sin^2\theta$ --clearly a compromise in θ is required. The index of refraction must therefore be chosen such that θ can be sufficiently small to enhance the resolution and yet not so small as to reduce the intensity below an acceptable limit. Generally, gases under low pressure serve well as low index of refraction media, and with these, resolution of changes in β of less than 1/1000 have been reported (Yuan, 1961).

In practice, the photons generated in a Cerenkov detector are collected in a photomultiplier tube where they generate photoelectrons. Because the number of photoelectrons generated by a scintillation counter is about 30 to 50 times greater than the number of photoelectrons generated by a Cerenkov counter for the same charged particle over the same path length, it is evident that the Cerenkov counter is the more difficult to use and consequently is not employed unless conventional detectors are unable to render the required accuracy. Nevertheless, the Cerenkov detector has numerous advantages. It is

exceedingly fast being limited basically only by the delays of the ancillary apparatus such as photomultiplier tubes and amplifying circuits. This property makes it especially useful in large fluxes of particles where "pile-up" might occur in slower systems. In addition, gases may be used to provide a variable index of refraction thus allowing the detector to cover a range of velocities. Finally, the directional property of Cerenkov radiation makes it possible to ascertain the direction of a charged particle as well as its speed.

2. Time-of-Flight Method

Charged particle velocities can be measured fairly accurately using this method where, as implied by the name, the time taken for a particle to pass between two fixed points is measured. The experimental arrangement, see figure 7 , is typically two scintillators spaced an accurately measured distance s apart. The particle traverses the distance in a time $\Delta t = s/v$ where v is the particle velocity. It is evident that the accuracy of this method relies chiefly on the precision to which Δt is determined.

The usual methods of measuring Δt is the time-to-amplitude conversion technique depicted in figure 7 . The pulse from photomultiplier tube A is purposely delayed long enough (t_D) to cause it to arrive at the time sorter almost coincidentally with the pulse from tube B. A pulse (c), whose amplitude (h) is proportional to the overlap time (t_O) between pulses A and B, is then fed from the time sorter to a discriminator. The discriminator selects only those pulses c whose amplitude is between h_1 and $h_1 + \delta h$ and sends them to an analyzer where they are counted. In this way, $t = t_D \pm \delta t_O$, where δt_O is proportional to δh, can be measured to within one or two nanoseconds and, since s is known precisely, v is easily and accurately calculated. Another

method, though not as precise, is the direct measurement of the pulse separation on an oscilloscope display.

The major factors limiting the time resolution to about 10^{-9} sec. are the following: the delay-time of signals from the detectors, the transit time dispersion in the photomultiplier tube, the rise time of output signals from the photomultiplier tube, the resolution time of the coincidence circuit and the rise time of any amplifying circuits used. The last factor may be eliminated as the output signal of some photomultiplier tubes is sufficiently large as to not require amplification. Substituting semiconductor detectors for the scintillation detectors obviates the photomultipliers and electron-hole transit time then becomes a limiting factor.

The time of flight method is used normally for particles having energies from several kev to roughly 1 Bev. For higher energy particles, the Cerenkov detector is invoked.

E. Comparison of Three Methods of Spectrometry

In this section an attempt is made to compare three of the above-mentioned methods for measuring charged particle energy spectra; they are the magnetic spectrometer, the scintillation counter and the solid state counter. These three are selected in particular because they lend themselves more readily to a meaningful comparison and because they are the devices which would be in direct competition to the proposed superconducting detectors if it proves practicable.

The comparison, as shown in tables I and II, is made with respect to the figures of merit listed below:

1. Energy Resolution (R)

Energy resolution is a measure of the detector's ability to distinguish between particles having nearly the same energy. Primarily, it is dependent upon the width of the peak appearing in a spectrum and arises from statistical fluctuations in the pulse heights, as recorded, from a nominally monoenergetic source of charged particles. A very common definition for energy resolution, and the one used in this table, is the ratio of the full line width of the peak at half maximum (FWHM) to the nominal particle energy, expressed as a percentage. (Strictly speaking, the resolution quoted for the magnetic spectrometer is momentum resolution).

2. Detector Efficiency (η)

$$\eta = \text{detector efficiency} = \frac{\text{Number of particles detected}}{\text{Number of particles striking detector}} \times 100\%$$

The application of this definition to the scintillation and solid state counters is obvious. In the case of the magnetic spectrometer, however, the definition is more meaningfully restated as

$$\eta = \frac{\text{Transmission}}{\text{Gathering Power}} = \frac{\text{Number of Particles passing through exit baffle}}{\text{Number of Particles passing through entrance baffle}}$$

3. Solid Angle (ω)

For purposes of this comparison, solid angle is taken as the percentage of particles leaving an isotropic source and striking the detector.

This is commonly called the "gathering power" of a magnetic

spectrometer and is typically small--never larger than 1%.

By boring a small hole in the scintillator and placing a source inside, solid angles of 100% are attainable. Typical values would be 50% or less.

It is possible to place a source directly onto the "window" of a solid state counter thus subtending a maximum solid angle of 50%.

4. Arbitrary figure of merit ($F = \Im\omega/R$)

Because efficiency is usually gained at the expense of loss in resolution and vice versa, a practical means of comparing devices is the ratio of these two factors times the solid angle.

F should be as large as possible.

5. Energy Loss / Ion Pair (W)

W is the average energy that must be expended in a medium by a charged particle to create an ion pair. This is of interest since energy resolution depends on statistical variations in the square root of the number N of ion pairs produced by an ionizing particle and N is directly related to the particle energy E by the relation $N = E/W$

6. Time Resolution

Time resolution is a measure of the smallest time interval which can occur between pulses that are distinguished and recorded as separate entities.

7. Available sizes

For the scintillation and solid state counters, the sizes quoted are for the detecting medium only. No estimate is included for photomultiplier tubes and preamplifiers.

8. Environment required

This section includes operating temperature, source size limitations, portability and ancillary items such as cooling water, power supplies and amplifiers.

The references for the figures quoted in this table are as follows:

(1) Bromley (1961)

(2) Yuan (1961)

(3) Leigh (1964)

(4) Dearnaley and Northrop (1963)

(5) Chase (1961)

(6) Segrè (1964)

(7) "Simtec" catalogue (1965)

(8) Smith (1961)

METHOD	R ENERGY RESOLUTION (%)		η DETECTOR EFFICIENCY (%)		ω SOLID ANGLE % (BEST VALUE)	$F = \frac{\eta\omega}{R}$
	CHARGED PARTICLE	GAMMA RAY (ENERGY)	CHARGED PARTICLE	GAMMA RAY (ENERGY)		
MAGNETIC SPECTROMETER	.01-.5 (1)		50 (2)		1 (.1 for U.B.C.) (8)	200
SCINTILLATION COUNTER	2 - 3 (1)		100		100	4,000
		6.2 (3) (1.25 Mev)		60 (3) (1.25 Mev)		970
		3.9 (3) (6.14 Mev)		57 (3) (6.14 Mev)		1,500
SOLID STATE COUNTER	0.3-0.7 (1)		100		50 (7)	10,000
		6 (4) (120 kev)		0.58 (4) (120 kev)		5

TABLE I

METHOD	W (ev) / Energy / Ion Pair	TIME RESOLUTION (SEC.)	AVAILABLE SIZES	ENVIRONMENT REQUIRED
MAGNETIC SPECTROMETER	--	Limited by frequency response of detector used in conjunction with it	Bulky U.B.C. spectrometer eg. - has 60^{o} sector with 15" radius of curvature - occupies 30 sq. ft. of floor space - is 8 ft. high	Firm Foundation Cooling Water Vacuum System Well regulated Magnet Power Supply Source size severely limited by dispersion in ion paths (8)
SCINTILLATION COUNTER	ORGANIC 1000 (4)	10^{-9} (5)	Crystals available from $1 - 10^{4}$ cm^{3} (6)	Portable Easily mounted in arrays Room Temperature Operation Stable High Voltage Power Supply Amplifier sometimes necessary Source size not critical
	INORGANIC 300	10^{-6} (5)		
SOLID STATE COUNTER	3 - 4	10^{-8} (4)	.025 - 5 cm^{3} (7)	Portable Easily mounted in arrays (at focus of mag. spectr.) Room Temperature or Liquid Nitrogen Operation No Special Power Supply Operate in dark Requires Amplifying Electronics Source size not critical

TABLE II

CHAPTER III

THEORY OF THE PROPOSED SUPERCONDUCTING NUCLEAR PARTICLE DETECTOR

A. Introduction

It has been shown in Chapter II that the science of nuclear particle detection is sufficiently advanced that adequate detectors are now available for most experimental requirements. This chapter outlines the theory behind a new type of detector, based on the principle of tunneling between superconductors, which is being investigated at U. B. C.

B. Physical Characteristics of Detector

Basically, the detector is a "sandwich" or junction composed of one superconducting thin film separated from another superconducting thin film by an insulating barrier (S_1 -B-S_2). The two superconductors used are aluminum and lead; the barrier is aluminum oxide. Details of the junction size and the methods of fabrication are given in Chapter IV.

It is planned to permit nuclear particles to impinge on the superconducting lead. If the lead is sufficiently thick, the particles will either be stopped or slowed down, and in so doing will lose energy through ionizing collisions with lead atoms. The excited electrons eventually generated by this process (Sections C and D) then have a finite probability of tunneling through the insulating barrier to the superconducting aluminum (Section C). The act of tunneling in essence reduces the effective resistance of the junction so that if the device is powered by a constant current source,

(Chapter VI), a voltage pulse should then result. Since the number of excited electrons is proportional to the energy lost by the ionizing particle, it follows that the amplitude of the voltage pulses obtained from the detector will be a measure of incident particle energy.

It will be shown later (Section D) that the chief improvement in this detector over existing ones would be in energy resolution. Efficiency and solid angle should be comparable to those of solid state detectors. The time resolution obtained will depend heavily on two quantities, tunneling time and recombination time, which are not well known at present (Section E).

In addition to the tunneling and recombination times, there are two other key factors which are presently not well understood and it is hoped the investigation of the superconducting counter will yield valuable information about them. The first is the excitation process (Section D). Little is known of the actual mechanism by which the superconducting electrons are excited, hence no firm estimates can be made of the excitation energy. The second factor is the velocity at which excited electrons diffuse from their point of "creation" to the barrier (Section F).

Fortunately, a fair amount is known about some of the other parameters affecting the operation of the detector. The energy gap existing in the electronic energy spectrum of superconductors is of fundamental importance (Section C). Its magnitude and variation with temperature and magnetic field has been described theoretically by Bardeen, Cooper and Schrieffer (BCS, 1957) and determined experimentally by, for example, Giaever and Megerle (1961) and Douglass and Meservey (1964 a,b). The tunneling current due to thermally excited electrons is fairly well understood (Section C) as is the Josephson tunneling current (Section H).

C. Tunneling

1. Introduction

It is well known that a current can flow between two metals separated by a thin insulating film because of the quantum-mechanical tunneling of electrons. Quantum mechanics says that an electron on one side of a barrier has a non-zero probability of tunneling through it if there exists an allowed state of equal or lower energy available for it on the other side.

During the past 30 years, extensive calculations have been made relating the tunneling current density to barrier thickness. Simmons (1963 a,b) gives a short bibliography to the literature on this subject and presents quite general calculations describing tunneling currents at low, intermediate and high voltages between electrodes of both similar and dissimilar metals. A typical curve is shown in figure 8 where K is the dielectric constant, ϕ is the height of the barrier above the Fermi surface of the metals and $\triangle\phi$ is the difference between the work functions of the metals. The values chosen approximate most closely the lead-aluminum oxide-aluminum system. A notable feature of figure 8 is that an increase in barrier thickness of only 5 $\mathring{A}$ causes the resistance to increase by a factor of 10^4.

The discovery of tunneling currents between a normal metal and a superconductor was first reported by Giaever (1960) in an experiment to measure the size of the electronic energy gap. Nicol, et al (1960) and Giaever and Megerle (1961) then extended the study to the case of tunneling between two superconducting metals. A proposal to use superconducting tunneling junctions to detect microwave and submillimetre-wave radiation, put forward

Figure 8: Junction Thickness v/s Junction Resistance
(After Simmons, 1963b)

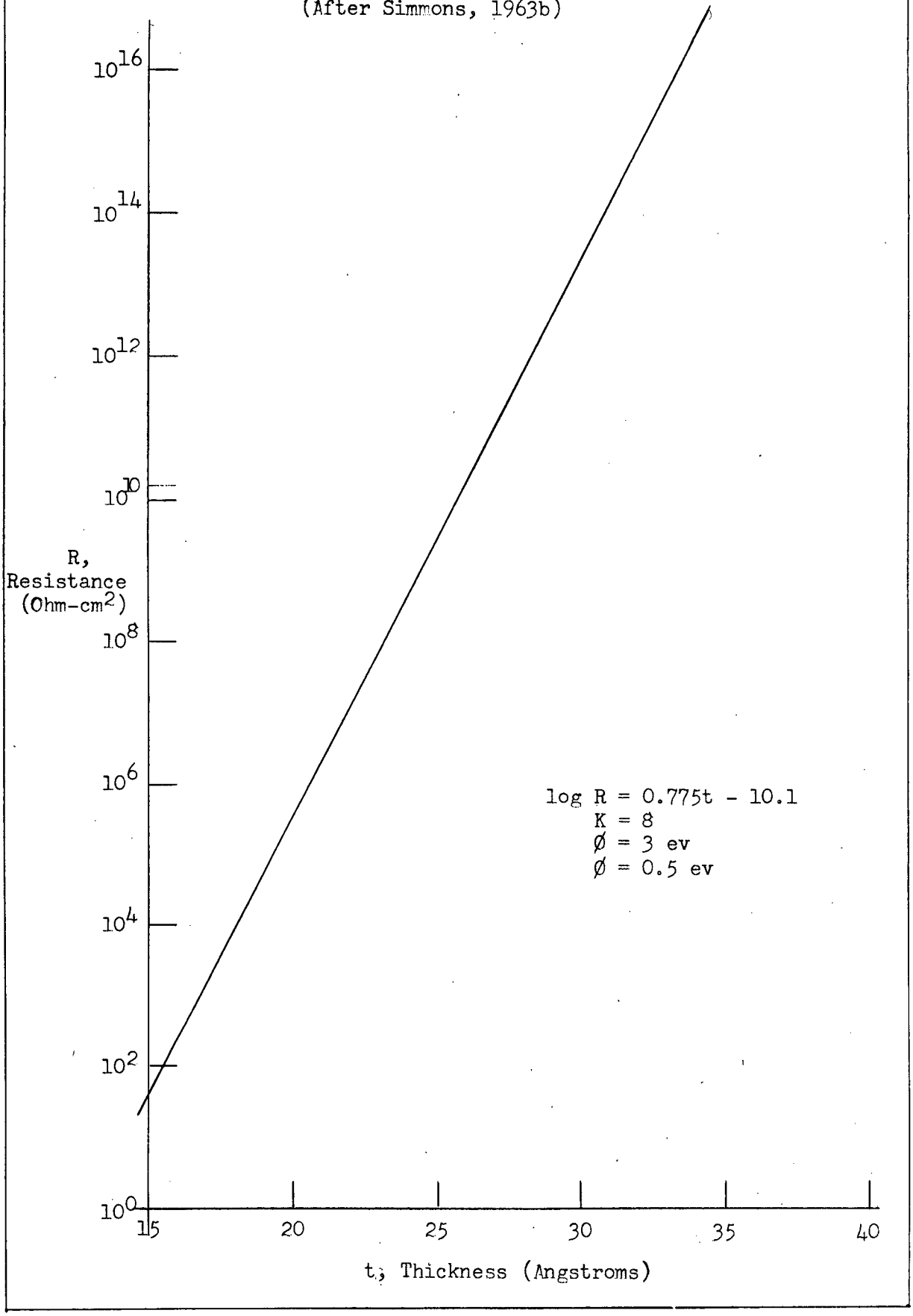

by Burstein, et al (1960), provides a basis for the present study of nuclear particle detection.

2. "Cooper Pairs" and the Energy Gap

The basic hypothesis of the BCS theory is that at $0^{\circ}K$ the superconducting ground state is a highly correlated one in which in momentum space the electron states in a thin shell near the Fermi surface are to the fullest possible extent occupied by pairs of electrons--"Cooper pairs"--of opposite spin and momentum. The energy of this ground state is lower than that of the normal metal by a finite amount. Thus, this state has the important property that a finite quantity of energy is required to excite even a single "normal" unpaired electron (Lynton, 1962). The reason for this is as follows.

When an attempt is made to excite an electron from the pair which are instantaneously in state $\vec{k}$ and $-\vec{k}$, say, so that one electron remains in state $\vec{k}$ while the other goes to a new state $\vec{k}'$, it turns out that although the state of only one of the electrons has been altered, both have effectively been excited since the possibility of two sets of pairs $\pm\vec{k}$ and $\pm\vec{k}'$ has been destroyed. The energy required to do this is therefore not just $E_k = (\varepsilon_k^2 + \varepsilon_o^2)^{\frac{1}{2}}$ (BCS, 1957) but $E_k + E_{k'}$ where ε_k is the kinetic energy of an electron in the normal state relative to the Fermi surface and ε_o is one-half the gap energy. It follows from this that even for the smallest possible excitation, $\varepsilon_k = \varepsilon_{k'} = 0$, it is impossible to break up a "Cooper pair" unless energy of at least $2\varepsilon_o$ is available. In this way, the BCS theory introduces an energy gap of magnitude $2\varepsilon_o$ between the ground and excited states of a superconductor (Rosenberg, 1963).

That such an energy gap exists had been deduced experimentally by Daunt and Mendelssohn in 1946 and Goodman in 1953 from thermal conductivity experiments. Its presence is fundamental to a successful explanation of the thermal and electromagnetic behaviour of superconductors. The size of the gap E_g is estimated in the BCS theory (1957) to be $E_g(0) = 3.50\ kT_c$ at $T = 0^\circ K$ where k is Boltzmann's constant and T_c is the critical temperature. For lead, $E_g(0)$ is 2.18×10^{-3}ev which, compared to the experimental value of 2.68×10^{-3}ev obtained by Giaever and Megerle (1961) at $1^\circ K$, illustrates that the agreement between theory and experiment is rather good, especially in light of the gross simplifications inherent in the BCS theory.

A complete summary of present knowledge about the energy gap can be found in a recent review article by Douglass and Falicov (1964,c).

3. Density of States

The density of states per unit energy interval in a superconductor is given (BCS, 1957) as

$$N_s(E) = \frac{dN(\varepsilon)}{d\varepsilon}\frac{d\varepsilon}{dE} = N_s(0)\frac{E}{(E^2 - \varepsilon_o^2)^{\frac{1}{2}}} \qquad (3\text{-}1)$$

where $N_s(0) = dN(\varepsilon)/d\varepsilon$ is the density of states at the Fermi surface of the superconductor when in the normal state and $E = (\varepsilon^2 + \varepsilon_o^2)^{\frac{1}{2}}$ where the subscript K has now been suppressed. (The Fermi level of a superconductor is taken to lie in the middle of the energy gap.) Noting that there exists a singularity at $E = \varepsilon_o$ and that for E greater than $3\varepsilon_o$, $N_s(E)$ tends to $N_s(0)$, one obtains the density of states in the vicinity of the Fermi surface as shown in figure 9 .

The electrons and holes that exist in a superconductor at

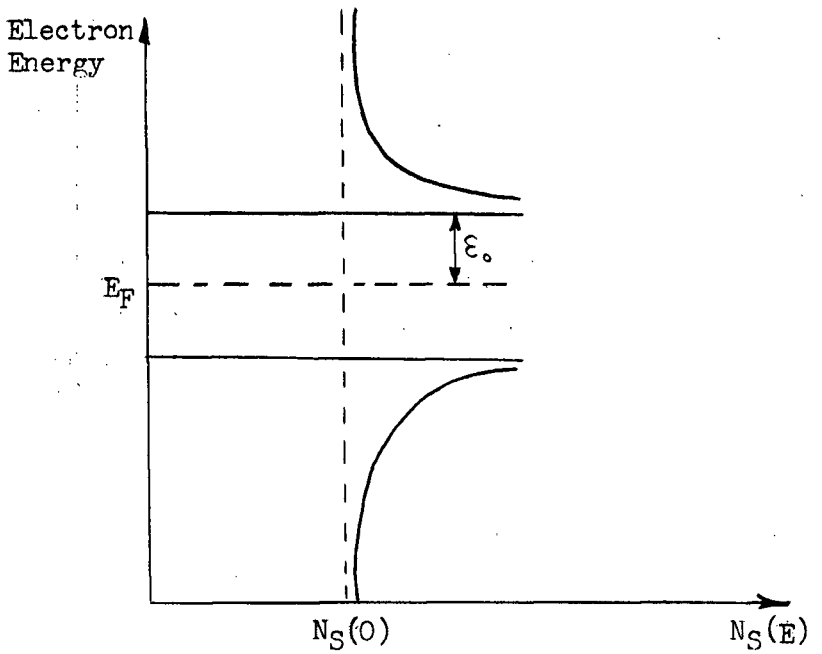

Figure 9: The Density of States Near the Fermi Surface

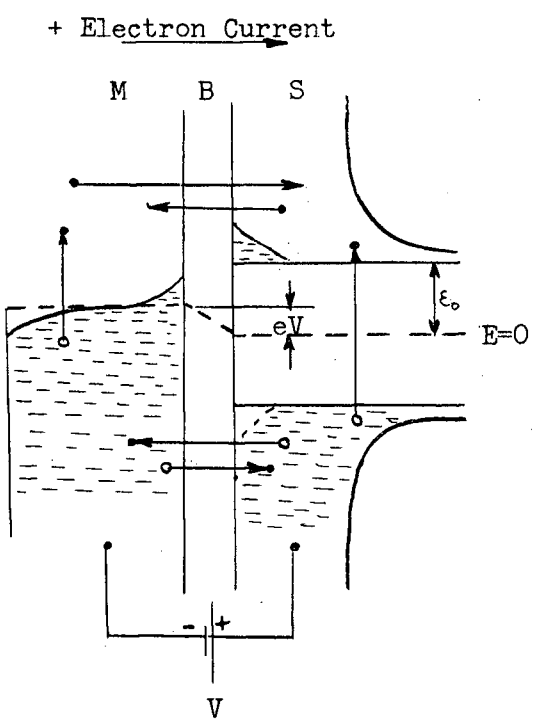

Figure 10: Single Particle Energy Spectrum For M-B-S (After Burstein)

finite temperatures obey Fermi statistics and it can be shown (Douglass and Falicov, 1964 c) that their energy distribution is given by the Fermi function

$$f(E) = (\exp(\beta E) + 1)^{-1} \qquad (3\text{-}2)$$

where $\beta = 1/kT$. In analogy with normal metals, the energy $E = (\varepsilon^2 + \varepsilon_o^2)^{\frac{1}{2}}$ can be thus interpreted as the quasi-particle or "normal" electron energy with its zero at the Fermi surface.

From the foregoing, it is evident that the BCS theory regards superconductors from a two-fluid point of view. As the temperature increases above 0^oK, more electrons are thermally excited into quasi-particle states. These excitations are similar to those in a normal metal for they are readily scattered and can gain or lose further energy in arbitrarily small amounts; hence they are usually referred to as normal electrons. These co-exist with the "Cooper pairs" which display superconducting behaviour and are difficult to scatter or excite.

4. Tunneling Current between a Normal Metal and a Superconductor

Before considering the tunneling in a superconducting "sandwich", it is expedient to consider the simpler case of tunneling in a normal metal-barrier-superconductor (M-B-S) structure (see figure 10).

The one way tunneling current for electrons going from the metal to the superconductor will be proportional to the integral over all energies of the product of the number of electrons in the metal and the number of holes (unoccupied states) in the superconductor. In the notation of Burstein (1961), this current is

$$I_e(MS) = A \int_{\varepsilon_o}^{\infty} |M|^2 [N_m(E-eV)\, f(E-eV)]\, [N_s(E)\, (1-f(E))]\, dE \qquad (3\text{-}3)$$

where A is a constant, $|M|^2$ is the matrix element for the tunneling transition and $N_m(E)$ is the density of states function for the normal metal. Bardeen (1961) showed that for small applied voltages, it is plausible to take $|M|^2$ as constant and may therefore be removed from the integral.

The reverse electron current can be written

$$I_e(SM) = -A|M|^2 \int_{\mathcal{E}_o}^{\infty} [N_m(E-ev)(1-f(E-ev))]\,[N_s(E)\,f(E)]\,dE \qquad (3\text{-}4)$$

so that the net electron current $I_e = I_e(MS) + I_e(SM)$ is

$$I_e = A|M|^2 \int_{\mathcal{E}_o}^{\infty} N_m(E-ev)\,N_s(E)(f(E-eV) - f(E))\,dE \qquad (3\text{-}5)$$

There is also, of course, a net current of holes which is given by

$$I_h = A|M|^2 \int_{\mathcal{E}_o}^{\infty} N_s(E)\,N_m\,(E+eV)(f(E) - f(E+eV))\,dE \qquad (3\text{-}6)$$

making the total current

$$I_T = I_e + I_h = A|M|^2 \int_{\mathcal{E}_o}^{\infty} N_m(E+eV)\,N_s(E)(f(E-eV) - f(E+eV))\,dE \qquad (3\text{-}7)$$

Equation 3-7 can be simplified with the assumptions that $N_m\,(E+eV) \approx N_m(0)$ = constant near the Fermi surface and that for sufficiently low voltages and temperatures ($kT \ll |\mathcal{E}_o - eV|$),

$$f\,(e) = e^{-E/kT}$$

Consequently, the net current is

$$I_T \approx A|M|^2\,N_m(0) \int_{\mathcal{E}_o}^{\infty} N_s(E)\,f(E)(e^{eV/kT} - e^{-eV/kT})\,dE$$

which since $eV \gg kT$ for conditions of interest, can be written as

$$I_T = A|M|^2\,N_m(0)\,n_o\,e^{eV/kT} \qquad (3\text{-}8)$$

where $n_o = \int_{\varepsilon_o}^{\infty} N_s(E)\, f(E)\, dE$ is the thermal equilibrium density of electrons or holes in the superconductor.

For $T = 1^{\circ}K$, $kT \approx 0.1$ mev so that one can see qualitatively when eV is close to $\varepsilon_o \approx 1.0$ mev, the tunneling current will increase rapidly with voltage (figure 11) and approach the values that would be obtained if both metals were normal.

One noteworthy result of this derivation is that, although I_T is proportional to n_o, it arises almost entirely from the tunneling of carriers from the metal to the superconductor (Burstein, 1961). From equations 3-4 and 3-6, the tunneling current due to electrons and holes tunneling from the superconductor to the metal is given by

$$
\begin{aligned}
I(SM) &= I_e(SM) + I_h(SM) \\
&= -A|M|^2 \int_{\varepsilon_o}^{\infty} N_m(E-eV)(1-f(E-eV))\, N_s(E)\, f(E)\, dE \\
&\quad + A|M|^2 \int_{\varepsilon_o}^{\infty} N_m(E+eV)(1-f(E+eV))\, N_s(E)\, f(E)\, dE \\
&\cong A|M|^2 N_m(0) \int_{\varepsilon_o}^{\infty} N_s(E)\, f(E)(f(E-eV) - f(E+eV))\, dE \\
&= -A|M|^2 N_m(0) \int_{\varepsilon_o}^{\infty} N_s(E)\, f^2(E)\, (e^{eV/kT} - e^{-eV/kT})\, dE \\
&\cong -A|M|^2 N_m(0)\, n_o\, e^{eV/kT}\, (\tfrac{1}{2}\, e^{-E_g/kT})^{\frac{1}{2}}
\end{aligned}
$$

Comparing the magnitudes of I(SM) and I_T, one readily observes that $I(SM) = (\frac{1}{2} \exp(-\beta E_g))^{\frac{1}{2}}\, I_T$. As mentioned previously, $\beta \varepsilon_o$ is typically about 10 so that I(SM) is roughly e^{-10} smaller than I_T and therefore negligible. Thus it is clear that changes in the density of electrons and holes effected in the superconductor by nuclear radiation would have little effect on the current.

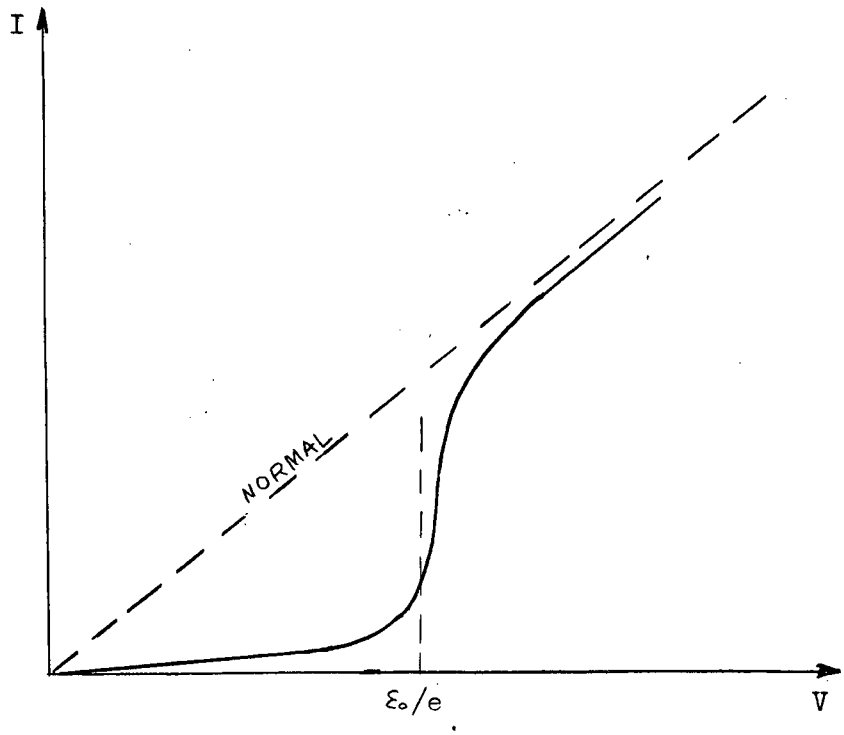

Figure 11: I-V Characteristic for M-B-S Structure

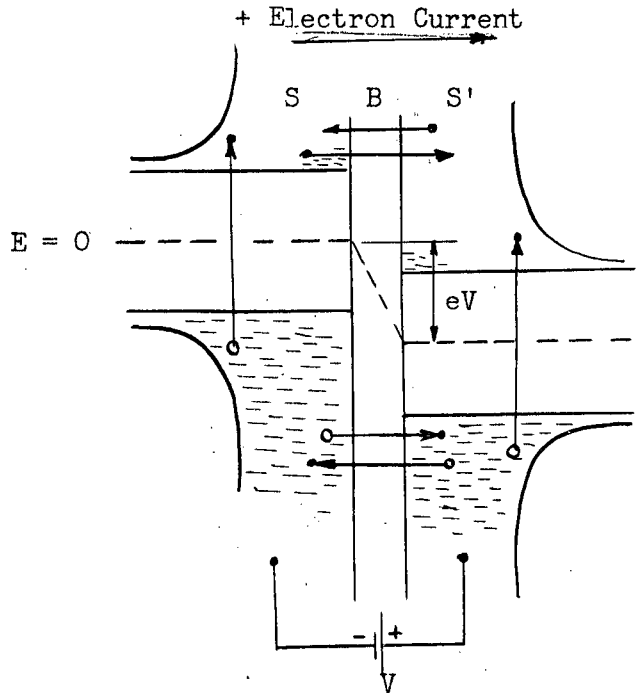

Figure 12: Single Particle Energy Spectrum for S-B-S' (After Burstein)

In other words, radiation induced currents in the M-B-S structure would depend not on the extremely favourable excitation properties of the superconductor but on the adverse excitation properties of the normal metal. The normal metal excitations quickly decay back to thermal equilibrium, whereas superconducting excitations are above the energy gap and can decay only by recombination.

5. Tunneling Between two Similar Superconductors

In this section the tunneling current in a symmetrical junction of superconductor-barrier-superconductor (S-B-S') is considered where S and S' are the same type of metal (figure 12).

Following the same reasoning as in section 4, one can write the electron current from S to S' as

$$I_e\ (SS') = A|M|^2 \int_{\mathcal{E}_o}^{\infty} \left[N_S(E)\ f(E)\right]\left[N_{S'}\ (E + eV)(\ 1-f(E + eV)\right]\ dE \quad (3\text{-}9)$$

Similarly, the expression for current due to electrons tunneling from S' to S is

$$I_e\ (S'S) = -A|M|^2 \int_{\mathcal{E}_o}^{\infty} N_{S'}\ (E + eV)\ f(E+eV)\ N_S(E)\ (\ 1-f(E))\ dE$$

Now, if the bias voltage and temperature are low such that $kT \ll eV$ and $eV < E_g$ (as sketched in figure 12) the vast majority of excited electrons in superconductor S' can "see" only forbidden states on the other side of the barrier and hence cannot tunnel. A similar situation holds for the holes in superconductor S. Consequently, most of the tunneling current will consist of electrons tunneling from S to S' and holes tunneling from S' to S. Furthermore, it is within the spirit of this estimate to assume the two contributions are equal so that the total current is

$$I_{SC} \approx 2\,A|M|^2 \int_{\mathcal{E}_o}^{\infty} N_s(E)\, f(E)\, N_s(E+eV)\, (1-f(E+eV))\, dE \qquad (3\text{-}10)$$

Making the additional approximations that, for energies of interest, $N_s(E + eV) \approx N_s(0)$ for $eV \approx 2\mathcal{E}_o$ and $1 - f(E + eV) \approx 1$, equation 3-10 becomes

$$I_{SC} \approx 2A|M|^2 N_s(0)\, n_o \qquad (3\text{-}11)$$

Though a very rough estimate, this result does illustrate the important fact I_{SC} is due entirely to excited carriers in the superconductors. This implies that a change Δn in the density of excited carriers in either superconductor will cause a change in tunneling current:

$$\Delta I_{SC} = 2\,A|M|^2 N_s(0)\Delta n = I_{SC}\,(\Delta n/n_o) \qquad (3\text{-}12)$$

It can be seen from equation 3-11 that for eV slightly less than E_g, I_{SC} is approximately independent of the bias voltage. This behaviour has been observed experimentally (see figure 13) by Giaever (1961). Note that the current rises quite quickly with increasing voltage at first, levels off until $eV \approx 2\mathcal{E}_o$, and then increases rapidly to values obtained for the metals in their normal state.

6. Tunneling Between two Dissimilar Superconductors

Calculations for the more general case of the tunneling current between superconductor (1) - barrier-superconductor (2) (S_1-B-S_2) are quite difficult but have been performed for several structures by Shapiro, et al (1962). The predicted characteristics (figure 14) agree remarkably well with the experimental results of Giaever (1961).

The shape of this I-V characteristic can be explained qualitatively from an examination of the density of states for the S_1-B-S_2

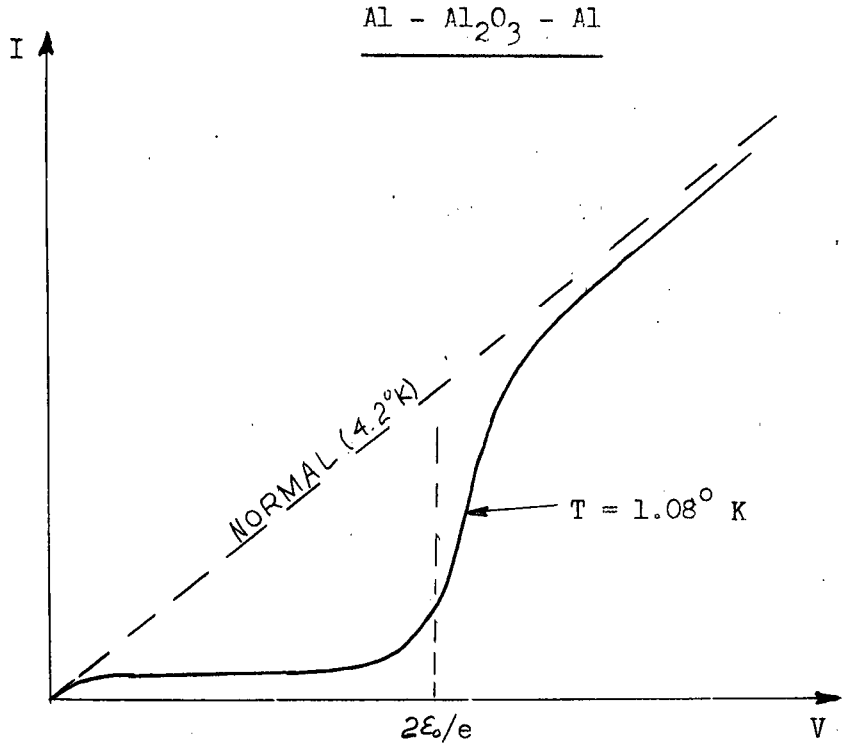

Figure 13: Typical I-V Characteristic for S-B-S' Structure (After Giaever, 1961)

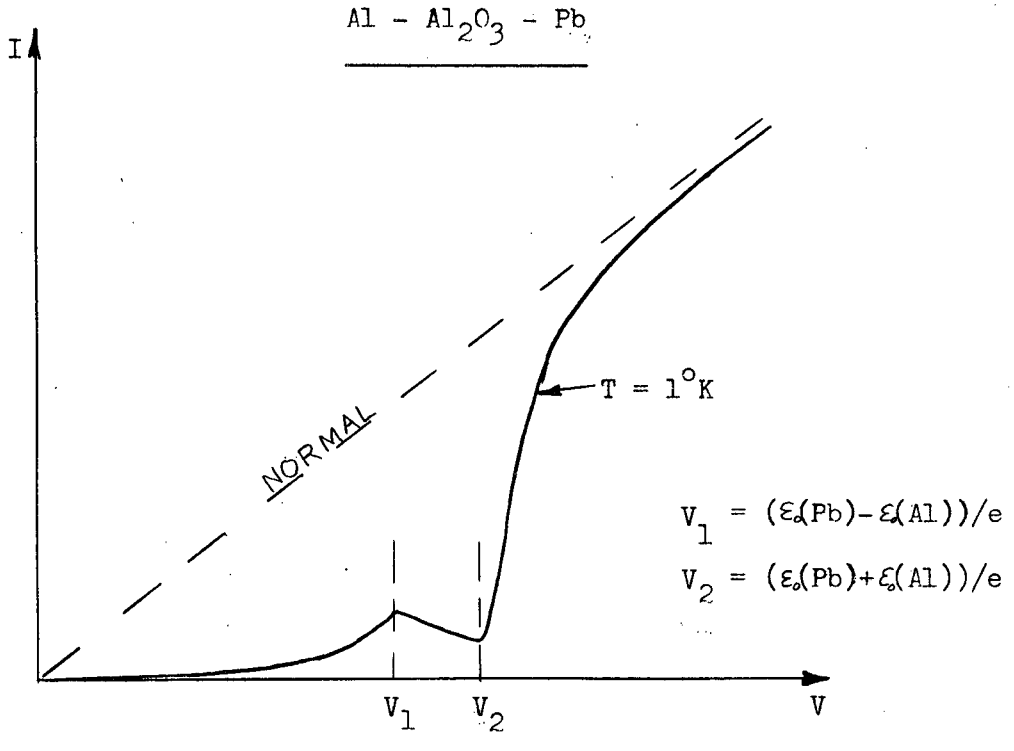

Figure 14: I-V Characteristic for S_1-B-S_2 Structure (After Shapiro, 1962)

case (figure 15). Applying a potential V between the two superconductors is equivalent to sliding one density of states curve with respect to the other. It is readily seen that when eV is near but slightly less than $\mathcal{E}_o(Pb) - \mathcal{E}_o(Al)$ the current will increase due to the sharp increase in the number of final hole states near the bottom edge of the gap. When $\mathcal{E}_o(Pb) - \mathcal{E}_o(Al) < eV < \mathcal{E}_o(Pb) + \mathcal{E}_o(Al)$, however, the density of final states available to all carriers is decreasing with increasing voltage which gives rise to the small negative resistance region in the I-V characteristic. At the point when eV is slightly greater than $\mathcal{E}_o(Pb) + \mathcal{E}_o(Al)$, which corresponds to the upper edge of the gap in the aluminum being level with the lower edge of the gap in the lead, the density of final states becomes favourable once more and a rapid increase in current with voltage is observed.

7. Résumé

A fairly complete study of tunneling currents has been made from which the following conclusions can be drawn:

(a) Either an S-B-S' or S_1-B-S_2 structure is essential

(b) To take advantage of the large changes in voltage produced by a small change in the density of excited carriers, the junction should be biased at a voltage V such that

$$eV < \mathcal{E}_o(1) - \mathcal{E}_o(2)$$

D. Excitation Energy and Energy Resolution

1. Excitation Energy

In section C, the dependence of the tunneling current on the density of excited carriers has been shown; this section will endeavour to determine the energy required by a nuclear particle to generate excited carriers.

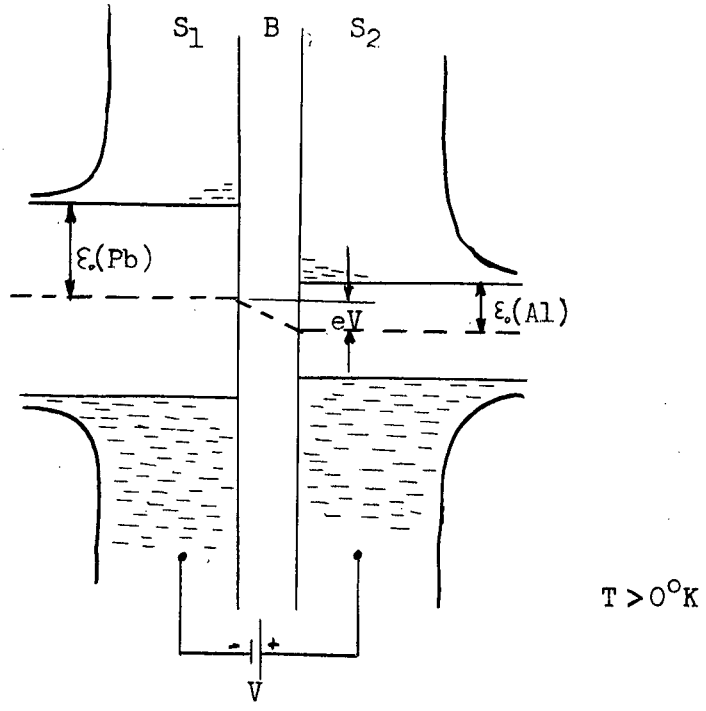

Figure 15: Single Particle Energy Spectrum for S_1-B-S_2

Shin (1964) has pointed out that excitation may take place in three different ways (figure 16):

(a) across the energy gap

(b) within the paired band

(c) within the excited or unpaired band

He showed however that for $\mathcal{E}_o/kT \gg 1$, which is valid for liquid helium temperatures, the first process very strongly dominates the others.

Because of the analogy between superconductors and semiconductors, Sherman (1962) suggested that the Shockley (1961) mean energy formula for semiconductors, which agrees well with experiment, be applied to superconductors. Shockley's expression is

$$\omega = 2.2\, E_g + \eta E_r \qquad (3\text{-}13)$$

where ω is the mean energy required to create an electron-hole pair, E_g is the gap energy, E_r is the phonon energy and

$$\eta = \frac{L_i}{L_R} = \frac{\text{carrier mean free path between ionizations}}{\text{mean free path between scattering by phonons}}$$

On the basis of a two-fluid model the quantity L_R must be considered for both the paired superconducting electrons and the unpaired normal electrons. It is a basic tenet of the BCS theory that the paired electrons are not easily scattered by phonons so that $L_R(SC)$ may be roughly taken to be infinite. The normal electrons, however, are scattered by phonons thereby having a finite mean free path. Therefore, one may take

$$L_R = \left(1/L_R(SC) + 1/L_R(N) \right)^{-1} \cong L_R(N)$$

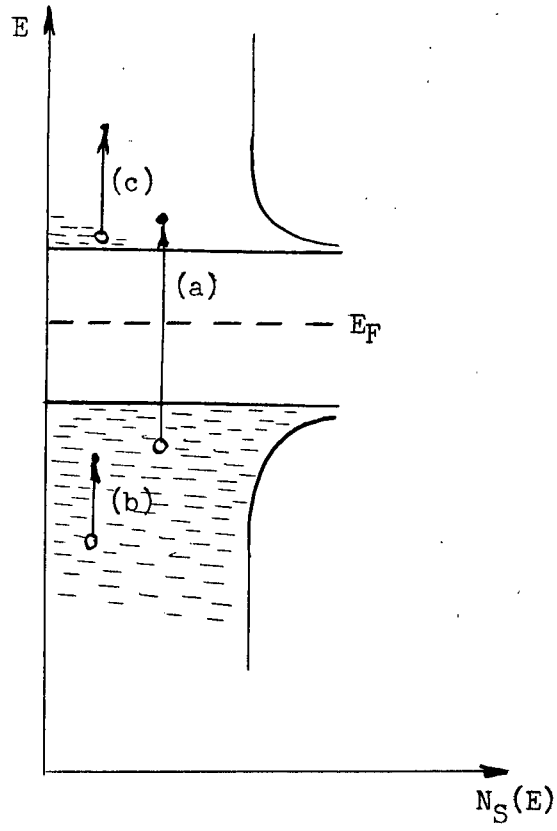

Figure 16: Modes of Excitation

The quantity L_i, which should be quite insensitive to temperature, is quoted by Shockley (1961) to be about 880Å for germanium at 300°K; L_R is given as 50Å for germanium under similar conditions.

Lynton (1962) shows that for a pure metal at low temperatures, the amount of electron scattering by phonons is proportional to T^2/T_D^2 where T_D is the Debye temperature. If it is assumed that the same reasoning can be applied to normal electrons in a superconductor at T = 1°K then, for $T_D(Pb) = 96°K$, the mean free path $L_R(N)$, being inversely proportional to the amount of scattering, is proportional to a factor of $T_D^2/T^2 = 10^4$. Similarly, with the crude assumption that the mean free path between phonon collisions is still proportional to T_D^2/T^2 at room temperatures, the mean free path $L_R(300)$ is proportional to a factor of approximately 10^{-1}. On this basis, there is reason to expect $L_R(N)$ to be significantly greater than $L_R(300)$ so that γ, instead of being about 18 as it is for a semiconductor, might be less than one for a superconductor.

Consider now the relative size of the first and second terms in equation 3-13. E_g for lead is about .003ev making the first term roughly .006ev. An experimental value for E_r of 0.04ev for germanium is given by Shockley (1961) which, since the present estimate is at best an order of magnitude calculation, may be taken to be the same as for lead. Immediately, one observes that the first and second terms are comparable for $\gamma = 0.15$. Accordingly, if γ were 0.01 or less, which means ultimately that $L_R(N) \gtrsim 1800\ L_R(300)$, the second term could be safety neglected.

Experimental evidence indicates that quite possibly this criterion can be satisfied. Wyder (1964) has found that the mean free path

of normal electrons in a superconductor is the same as that of electrons in the normal metal in which superconductivity has been quenched. Furthermore, he was able to estimate the path length $L_R(N)$ to be of the order of 0.1 mm. By accepting his value for $L_R(N)$ and regarding boundary scattering as elastic, one finds $L_R(N) = 2 \times 10^4 L_R(300)$ which would completely justify ignoring the second term of equation 3-13.

2. Energy Resolution

A convenient estimate of energy resolution R in an energy loss charge carrier conversion spectrometer is $R = (N)^{-\frac{1}{2}}$ where N is the number of electron-hole pairs generated by a charged particle (Dearnaley and Northrop, 1963). If W is the incident particle energy then $N = W/\omega$ so that

$$R = (\omega/W)^{\frac{1}{2}}$$

The excellent theoretical energy resolution of the superconducting particle detector is best illustrated by a comparison with the energy resolution of a semiconductor device. Typically, the mean energy per ion pair in a semiconductor is $\omega_{ss} = 3.5$ ev at room temperature; whereas for a superconducting detector, $\omega_{sc} = 6 \times 10^{-3}$ ev at $1^{\circ}K$. Therefore, for the same particle, the ratio of the resolutions is

$$\frac{R_{sc}}{R_{ss}} = (\omega_{sc}/\omega_{ss})^{\frac{1}{2}} = .04$$

For charged particles, R_{ss} is nominally 0.5% so that $R_{sc} = .02\%$ might be attained--a value comparable to that achieved by some magnetic spectrometers.

It is unlikely that such high resolution would obtain in

practice because of internal and external noise (see Section G). At worst, however, R_{sc} should be 5 to 10 times better than R_{ss}; this, essentially, is the "raison d'être" of the superconducting detector.

E. Tunneling Probability and Recombination Time

When a quasi-particle is excited above the energy gap of one superconducting member of a "sandwich", it may decay via one of three modes:

(1) recombine with a hole across the gap in time τ_{eh}

(2) recombine with another electron to form a "Cooper pair" and fall below the gap in time τ_R

(3) diffuse to the barrier, subsequently tunneling through it to an energetically favourable unoccupied state on the opposite side in time τ_t

Immediately, it is apparent that the relative probabilities of these processes is of great importance in predicting the performance of a non-equilibrium device like the superconducting particle detector.

Let P_{eh} be the probability per unit time of electron-hole recombination; P_R the probability per unit time of electron-electron recombination and P_t the probability per unit time that an excited electron will diffuse to the barrier and tunnel. Now,

$$P_{eh} = \frac{1}{\tau_{eh}} , \quad P_e = \frac{1}{\tau_R} , \quad P_t = \frac{1}{\tau_t}$$

so that the probability of decay per unit time is

$$P(\text{decay}) = P_{eh} + P_R + P_t = \frac{1}{\tau_{eh}} + \frac{1}{\tau_R} + \frac{1}{\tau_t} = \frac{1}{\tau}$$

Burstein (1961) gives a theoretical estimate for τ_{eh} of 0.4 sec. at $2^{\circ}K$. Comparing this to a value for τ_R, estimated theoretically by Rothwarf (1963), of 5×10^{-10} sec. at $2^{\circ}K$, one can safety dismiss electron-hole recombination as being the dominant decay process. Thus, the total decay time is

$$\tau \approx (1/\tau_t + 1/\tau_R)^{-1} \qquad (3\text{-}14)$$

which clearly demonstrates the need for τ_t to be at least as short as τ_R for a given temperature.

Consider therefore some of the recent estimates which have been carried out for τ_R in lead. Ginsberg (1962) arrived experimentally at an upper limit for τ_R of 2.2×10^{-7} sec. at $1.44^{\circ}K$. For the same temperature, theoretical estimates of τ_R by Schrieffer (1962) and Rothwarf (1963) yielded values of 0.43×10^{-7} sec. and 0.17×10^{-7} sec. respectively which are consistent with Ginsberg's experimental results.

The expression for $\tau_R(T)$ given by Rothwarf has been evaluated (see Appendix B) at numerous temperatures, the results of which are shown in figure 17 . A remarkable feature of this plot is that a reduction in temperature from $1.44^{\circ}K$ to $1.0^{\circ}K$ causes a corresponding lengthening in τ_R of two orders of magnitude. Because $\tau_t \leq \tau_R$ is imperative for operation of the detector, it is advantageous to have τ_R as large as possible, which forcibly indicates the need for the lowest convenient experimental temperatures.

Using a method suggested by Ginsberg (1962), it is possible to obtain a rather rough estimate of τ_t. For voltages $V \gg \varepsilon_o/e$, which as pointed out previously gives an I-V characteristic very similar to that of normal metals

Figure 17: Recombination Times of Electrons in Superconducting Lead

$$\tau_R = \frac{3.03\times10^{-13}\ \exp(15.5/T)}{T^{\frac{1}{2}}}$$, (Rothwarf, 1963)

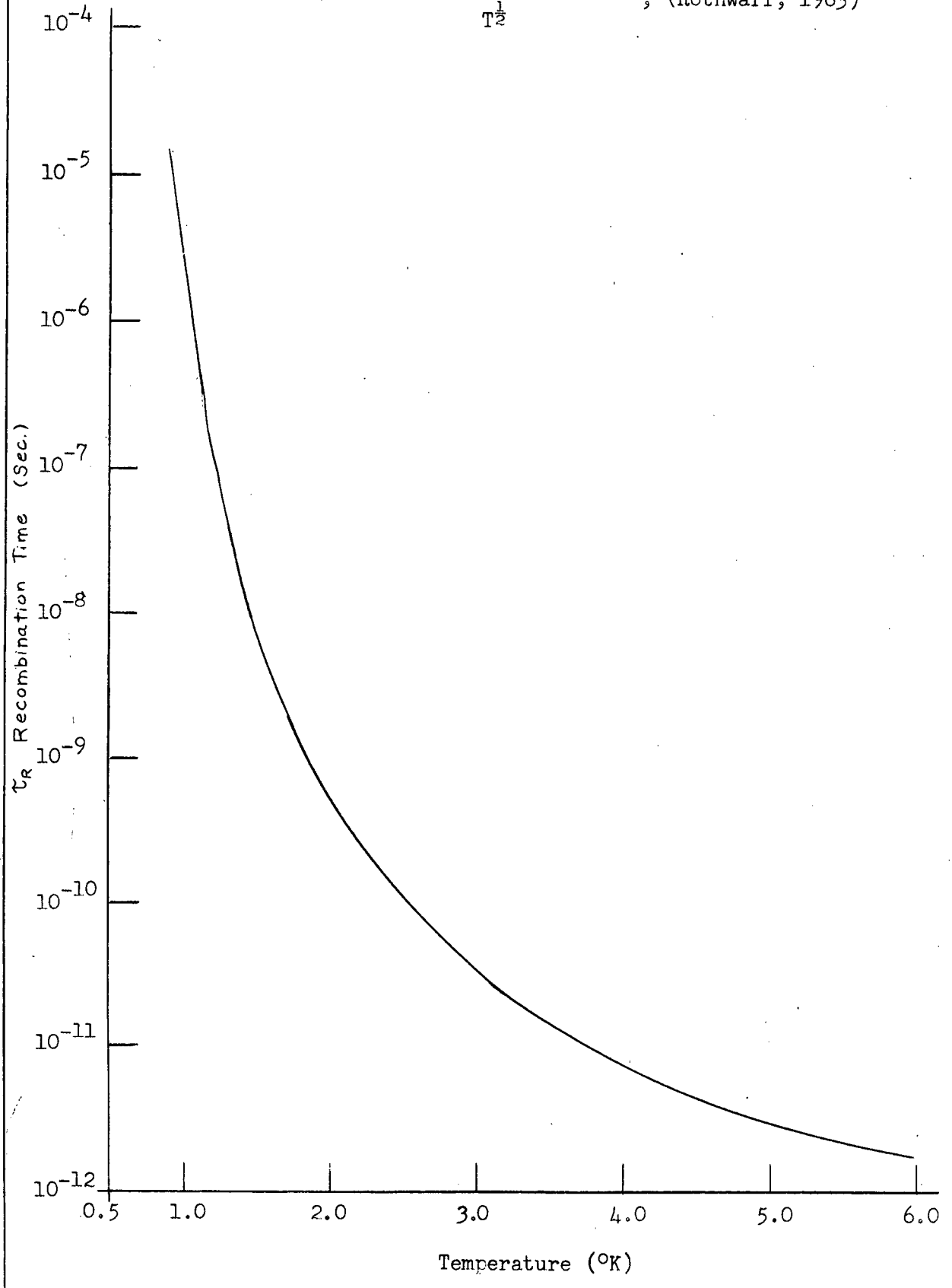

the current I through the barrier should be given by

$$I = e^2 \bar{N}(E_F)\, \lambda A V P_t \tag{3-15}$$

where
e = electronic charge
$\bar{N}(E_F)$ = average density of free electron states/unit volume/unit energy range near the Fermi surface of the normal metal
λ = film thickness
A = junction area
V = bias voltage

The tunneling current between normal metals is used because the tunneling time should be characteristic of the barrier thickness alone and not of the state of the electrodes on either side of it. In addition, it is shown in Appendix A that the decrease in barrier thickness in going from room to helium temperatures is only about 0.2%.

The number of free electron states per unit volume per unit energy range is given by Kittel (1956) as

$$N(E)\, dE = \frac{1}{2\pi^2} \left(\frac{2m}{\hbar^2}\right)^{3/2} E^{\frac{1}{2}} = k\, E^{\frac{1}{2}} dE \tag{3-16}$$

To find the average value of $N(E)$ near the Fermi surface ($E = E_F$), consider the variation in $N(E)$ over a small energy range $\delta E \ll E_F$, then

$$\bar{N}(E_F)\, \delta E = \int_{E_F - \delta E/2}^{E_F + \delta E/2} k E^{\frac{1}{2}}\, dE \approx k\, E_F^{\frac{1}{2}}\, \delta E \tag{3-17}$$

Rather than evaluate k explicitly, one requires that the number of free electrons N_f be given by

$$N_f = \int_0^{E_F} N(E) dE = 2/3\, k\, E_F^{3/2} \tag{3-18}$$

Eliminating k between 3-17 and 3-18, one obtains

$$\bar{N}(E_F) = 3/2\, N_f\, E_F^{-1} \tag{3-19}$$

N_f is estimated for lead (Ginsberg, 1962) by assuming 1.24 free electrons per atom so that

$$N_f = 1.24\, N_o = 4.1 \times 10^{22} \text{ electrons/cm}^3 \tag{3-20}$$

where N_o is Avogadro's number.

Substituting 3-19 into 3-15 and re-writing the equation in a more convenient form, one finds

$$P_t = \frac{2\, E_F}{3e^2 N_f \lambda A} \cdot \frac{I}{V} = \frac{2\, E_F}{3e^2 N_f\, \lambda AR} \tag{3-21}$$

where R is the junction resistance at room temperature.

It is well known that for room temperatures $E_F(T) = E_F(0)$ to a good approximation. Kittel (1956) gives

$$E_F(0) = \frac{h^2}{8m} \left(\frac{3\, N_f}{\pi}\right)^{2/3}$$

where h is Planck's constant and m the electron mass. For lead, $E_F(0)$ is 4.34 ev. Expressing R in ohms, λ in cm and A in cm^2, one may evaluate 3-21 as

$$P_t = \frac{4.41 \times 10^{-4}}{R\, \lambda\, A} \text{ sec}^{-1}$$

For a typical junction, A is about 10^{-4} cm^2 and, if the lead film is to stop 5 Mev alpha particles say, λ must be at least 1.4×10^{-3} cm. These

values make

$$P_t = \frac{3.15 \times 10^3}{R} \text{ sec}^{-1} = \frac{1}{\tau_t}$$

From figure 17 , the theoretical value for τ_R at $1^\circ K$ is 1.6×10^{-6} sec; therefore, in order to satisfy the condition $\tau_t \leq \tau_R$, R must be

$$R \leq (1.6)10^{-6} \times (3.15)10^{-3} = 5 \times 10^{-3} \text{ ohms.}$$

One factor of concern is that, based on the result of Simmons shown in figure 8 , a junction having a resistance of 5×10^{-3} ohms $\times 10^{-3}$ cm^2 is only about 6 Å thick--a size not easily attained experimentally.

Also, it was stated at the beginning of this derivation that the tunneling time and hence P_t should be relatively independent of temperature. That this assumption was justified is shown in Appendix A where a change in barrier thickness of 0.2% is found to increase P_t by only about 3.6%.

A final point to note is that P_t is, in fact, the product of two other probabilities; P_t = P (striking barrier) x P (transmission). P (transmission) is fairly well understood from quantum mechanics (see, for example, Simmons, 1963a); P (striking barrier), however, is not so well understood for it depends on the initial location of the excited particle as well as its resultant diffusion velocity. An estimate of the diffusion velocity will be presented in the next section but it is obvious that much remains to be learned concerning these topics, and something may be learned about them from superconducting detector experiments.

F. Diffusion Velocity

To optimize the efficiency of the superconducting particle detector, it is imperative that an excited electron traverse the distance from its site of "creation" to the barrier in as short a time as possible.

According to Ginsberg (1962), the normal electrons in a superconductor diffuse in a manner effectively described by a one-dimensional random walk with a mean free path approximately equal to the average film thickness and a diffusion velocity given by the group velocity

$$v(E) = \frac{v_F}{\sqrt{3}} \frac{(E^2 - \varepsilon_o^2)^{\frac{1}{2}}}{E} \tag{3-23}$$

As before, E is the BCS excitation energy, ε_o is one-half the gap width and v_F is the Fermi velocity in the normal state. Now $\frac{1}{2} mv_F^2 = E_F$, where m is the mass of the electron and E_F was found in section E to be 4.34 ev for lead, so that

$$v_F = (2E_F/m)^{\frac{1}{2}} = 1.23 \times 10^8 \text{ cm/sec} \tag{3-24}$$

In order to obtain a usuable form of the diffusion velocity, it is within the spirit of this estimate to use the thermal average;

$$\bar{v}_{DIFF} = \frac{\int_{\varepsilon_o}^{\infty} f(E)\, N_s(E)\, v(E)\, dE}{\int_{\varepsilon_o}^{\infty} f(E)\, N_s(E)\, dE} \tag{3-25}$$

where

$$f(E) = (e^{\beta E} + 1)^{-1}$$

$$N_s(E) = N_s(0)\, E\, (E^2 - \varepsilon_o^2)^{-\frac{1}{2}}$$

$$\beta = 1/kT$$

It will be shown in Appendix B that the solution of equation 3-25 is

$$\bar{v}_{DIFF} = \frac{v_F \; e^{-\beta \mathcal{E}_o}}{\sqrt{3} \int_{\mathcal{E}_o}^{\infty} \exp\left(-\left(x^2 + \beta^2 \mathcal{E}_o^2\right)^{\frac{1}{2}}\right) dX} \qquad (3\text{-}26)$$

Equation 3-26 has been evaluated for several temperatures (Appendix B) with the results plotted in figure 18 .

To appreciate the effect of $\bar{v}_{DIFF}$ on the overall tunneling probability, consider $\bar{v}_{DIFF}$ at 1^{o}K which, from figure 18 , is about 1.4×10^{7} cm/sec. With the assumption that the mean free path is roughly the film thickness λ, then τ_c, the mean time between collisons, is approximately 10^{-10} sec for a film thickness of 10μ. The inference of this estimate is that, at low temperatures, P (striking barrier) per unit time is reasonably large and relatively independent of temperature variations which, in turn, implies that the normal electron diffusion velocity should not be a limiting factor in developing a superconducting detector.

G. Signal and Noise

As mentioned in Section D, noise could prove to be a critical factor in the energy resolution of the superconducting nuclear particle detector. In this section, an estimate of the magnitudes of the signal and of several noise sources and the effect of the resulting signal to noise ratio on resolution are discussed.

1. Signal Size

Figure 19 shows an equivalent circuit of the junction and a charge sensitive amplifier with open loop gain A. The amplifier magnifies

Figure 18: Variation of Theoretical Diffusion Velocity With Temperature

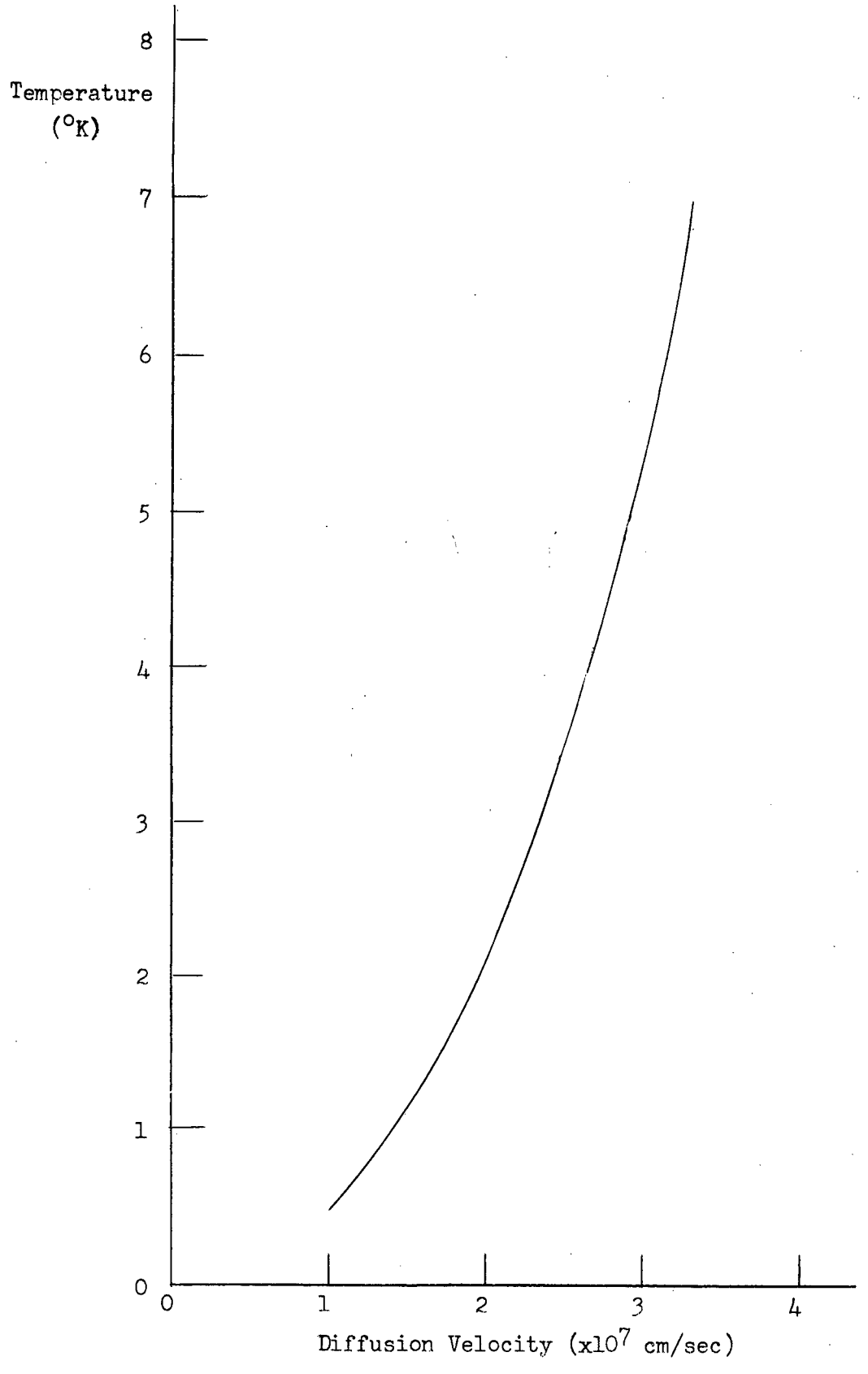

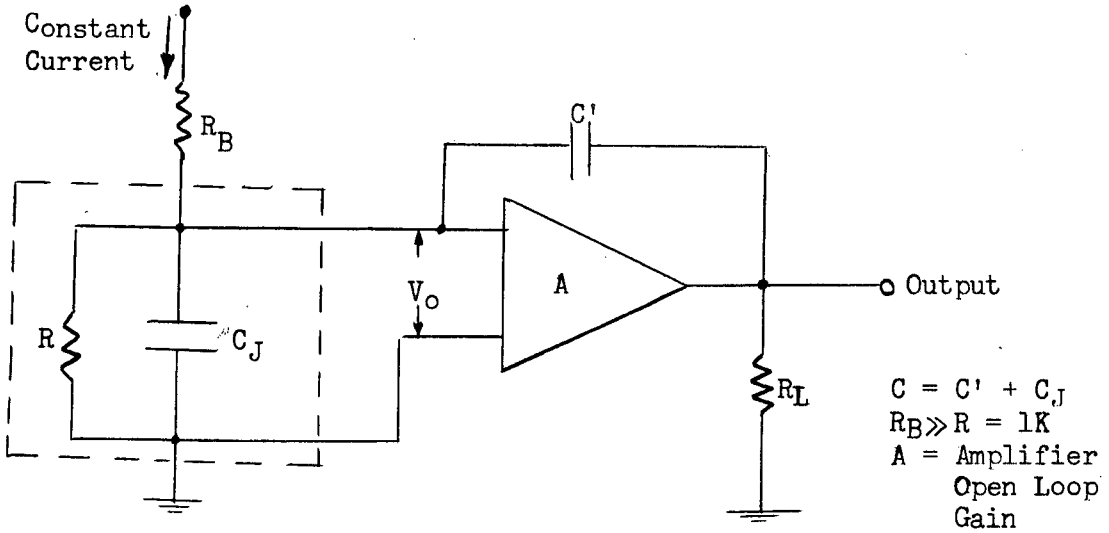

Figure 19: Junction Equivalent Circuit and Amplifier

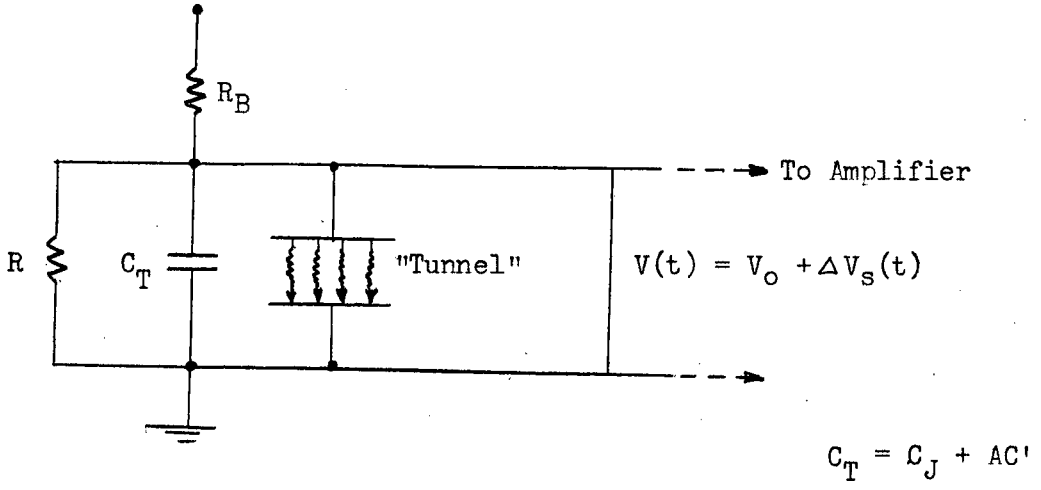

Figure 20: Model for Voltage Pulse Estimate

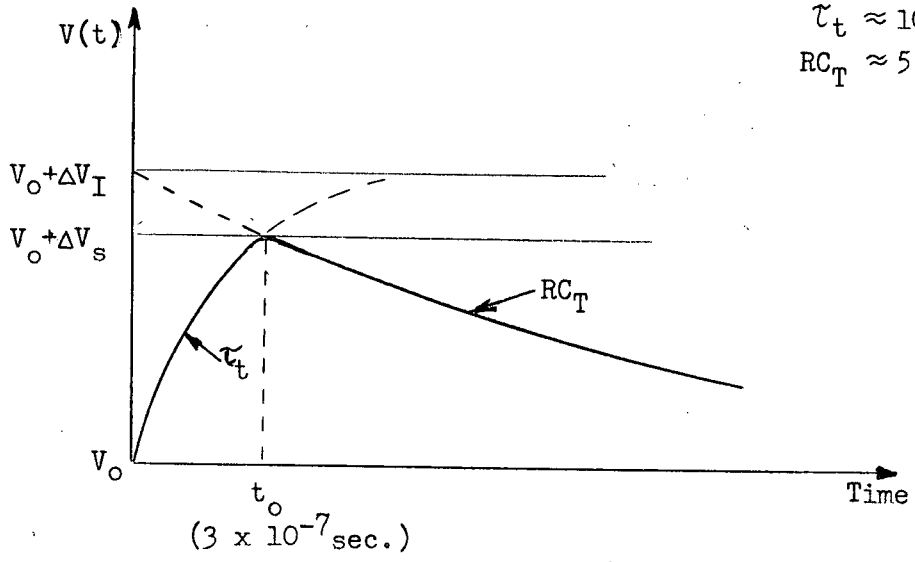

Figure 21: Theoretical Signal Pulse Shape

the feedback capacitance C' making the effective capacitance $C_T = C_J + AC'$ so that, with the feedback loop in place, one obtains the equivalent circuit of figure 20 . When a nuclear particle liberates a number of charges N in the lead, the ideal voltage change across the junction is given by $\Delta V_I = \Delta Q/C_T = Ne/C_T$ where e is the electronic charge. But $N = W/\omega$ where W is the particle energy and ω is the excitation energy which makes $\Delta V_I = e\, W/\omega\, C_T$. Typical values of the parameters are

$$\omega = 6 \times 10^{-3} \text{ ev}$$

$$C_J = 100 \text{ pf}$$

$$C' = 50 \text{ pf}$$

$$A = 10{,}000$$

so that for a 5 Mev alpha particle,

$$\Delta V_I = \frac{(5 \text{ Mev})\,(1.6 \times 10^{-19} \text{ coul})}{(6 \times 10^{-3} \text{ ev})(100 + 500{,}000 \text{ pf})} = .00026\text{v}$$

and the voltage pulse at the output of the amplifier will be $A \cdot \Delta V_I = 2.6\text{v}$. In practice, however, the actual voltage pulse appearing at the input of the amplifier (ΔV_S) might be less than ΔV_I because of the two following effects.

It is highly unlikely that all of the charge liberated by the ionizing particle will survive long enough to tunnel because of recombination effects in the region near the particle track where there exists a high carrier density. The second effect is best explained with the use of figure 21 . After the excited carriers have been generated--in a time assumed to be much less than the tunneling time τ_t--they leak off the capacitor C_T by tunneling through the junction and thereby raise the junction voltage $V(t)$. As soon

as some electrons have leaked off, however, a potential is developed across the junction resistance R. By drawing electrons through R the capacitor tries to return to the bias voltage V_o with a time constant $R\,C_T$. Depending on the relative sizes of τ_t and $R\,C_T$, there will be a time t_o at which the "recharging" process through R will catch up to the tunneling "leakage" and return the system to V_o. To evaluate t_o, one writes the following equations for V (t)

$$V_1(t) = V_o + \Delta V_I \left(1 - \exp(-t/\tau_t)\right),\ 0 \leq t \leq t_o$$
$$V_2(t) = V_o + \Delta V_I \exp(-t/R\,C_T),\quad t_o \leq t \leq \infty$$

Setting $V_1(t_o) = V_2(t_o)$, one obtains

$$\exp(-t_o/R\,C_T) + \exp(-t_o/\tau_t) = 1$$

which, using $\tau_t = 10^{-7}$ sec and $R\,C_T = 10^3 \times 5 \times 10^{-9} = 5 \times 10^{-6}$ sec, has the approximate solution $t_o = 3 \times 10^{-7}$ sec. (R is taken to be 10^3 ohms because the junction resistance, when one of the electrodes is superconducting, is found experimentally (Chapter VII) to be roughly a factor of 10^5 or 10^6 greater than the normal resistance which, as mentioned in Section E, will be about 5×10^{-3} ohms.) The actual voltage pulse, neglecting any other effect, would be therefore

$$\Delta V_S' = \Delta V_I \left(1 - \exp(-t_o/\tau_t)\right) = \Delta V_I\,(1-.05) = .95\,\Delta V_I$$

From this analysis, it is apparent that if any cause is going to significantly attenuate the actual voltage signal input to the amplifier, it will be incomplete charge collection and not unfavourable time constants. Fortunately, almost all of any signal loss thus incurred can be compensated

for by suitable adjustment of A and C'.

2. Shot Noise on the Leakage Current

At any finite temperature, thermally excited electrons will be present and give rise to, depending on the bias voltage, a "steady" leakage current I_S. An average thermal current is about 10^{-6} amps. for 1 mv. bias which implies 6×10^{12} electrons/sec. are tunneling through the junction. Therefore in a time of $\tau_t = 10^{-7}$ sec, which is the characteristic time for the observation of a radiation-induced tunneling charge impulse, the number of leakage electrons N_L present is 6×10^5 which makes the noise due to leakage current fluctuations about $N_L^{\frac{1}{2}} \approx 800$. Compared, for instance, to the statistical fluctuations in the number of excited carriers generated by a 5 Mev alpha particle, which is roughly $(10^9)^{\frac{1}{2}} \approx 3 \times 10^4$, the leakage noise is seen to be very small. This would not be so in the case of a solid state device with a similar leakage current, for the same charged particle would produce only about 10^6 charges whose statistical fluctuation (10^3) is clearly comparable to that of the leakage current.

For purposes of comparison to other sources of noise, note that the energy of a particle required to produce $N_L^{\frac{1}{2}}$ carriers would be

$$W_{LC} = \omega(800) = 4.8 \text{ ev} \qquad (3\text{-}27)$$

3. Thermal Noise

Thermal noise arises because the velocity distribution of the excited electrons leads to a fluctuating and, in general, a non-uniform spatial distribution of the electrons in the superconductor. Its average

value is zero but its rms value in a bandwidth δf is

$$\overline{V^2}(f) = 4\,k\,T\,R\,\delta f$$

where k is Boltzmann's constant and T is the absolute temperature. The mean square voltage $\overline{V_o^2}(f)$ observed at the input to the amplifier (figure 19) is limited to an upper frequency set by R and $C = C' + C_J$ which together act as a frequency dependent (potentiometer). It can be readily shown that the rms noise voltage developed at the amplifier input is

$$\overline{V_o^2}(f) = \frac{4\,k\,T\,R\,\delta f}{1 + \nu^2 C^2 R^2}$$

where $\nu = 2\pi f$. Thermal noise is uniformly distributed over an infinite frequency band (Dearnaley and Northrop, 1963) so to find the most pessimistic value for $\overline{V_o^2}(f)$ one sets

$$\overline{V_o^2} = 4\,k\,T\,R \int_0^\infty \frac{df}{1 + \nu^2 C^2 R^2} = \frac{kT}{C}$$

To observe the effect of $\overline{V_o^2}$ upon resolution, one observes that the number of electron-hole pairs required to produce a signal $(\overline{V_o^2})^{\frac{1}{2}}$ is

$$\Delta N = \frac{\Delta Q}{e} = \frac{C}{e}\,\Delta V = \frac{C}{e}\,\frac{(kT)^{\frac{1}{2}}}{(C)^{\frac{1}{2}}}$$

The energy of a particle necessary to produce this number of pairs, or the equivalent noise appearing at the amplifier input, is

$$\Delta W_{th} = \frac{\omega}{e}\,(kTC)^{\frac{1}{2}} = 1.3 \text{ ev} \qquad (3\text{-}28)$$

where

$\omega = 6 \times 10^{-3}$ ev/electron

$e = 1.6 \times 10^{-19}$ coul/electron

$k = 8.65 \times 10^{-5}$ ev/deg

$T = 1^{\circ}K$

$C = 1.1 \times 10^{-10}$ farads

4. Generation-Recombination (GR) Noise in Leakage Current

GR noise is due to fluctuations in the density of thermally excited carriers brought about by variations in the generation and recombination rates. Dearnaley and Northrop (1963) quote Van der Ziel's estimate for GR noise as

$$\overline{I_{GR}^2}(f) = 4 \frac{\overline{\Delta N_L^2}\, e^2}{\tau_t^2} \cdot \frac{\tau_1^2}{(1 + \omega^2 \tau_1^2)} \delta f$$

which is valid for $\tau_1 < \tau_t$ where τ_1 is the mean life-time of the excited carriers. Now, it was shown in Section C that for about $1.4^{\circ}K$

$$\tau_1 \approx \left(\frac{1}{\tau_R} + \frac{1}{\tau_t}\right)^{-1} \approx \left(\frac{2}{\tau_t}\right)^{-1} = \tau_t/2 \qquad (3\text{-}29)$$

where τ_R is the recombination time. Furthermore, it can be shown (Dearnaley and Northrop, 1963) that the mean square voltage seen at the amplifier input is

$$\overline{V_{GR}^2} = \int_0^{\infty} \frac{2 N_L e^2}{\tau_t^2} \cdot \frac{\tau_1^2}{1 + \omega^2 \tau_1^2} \cdot \frac{R^2}{1 + \omega^2 C^2 R^2} \, df$$

For the conditions $RC > \tau_t > \tau_1$, which hold for the superconducting detector,

this equation can be integrated to give

$$\overline{V_{GR}^2} = \frac{N_L e^2 \tau_1 R}{2 \tau_t^2 C}$$

The number of electron-hole pairs necessary to make a signal equal to $(\overline{V_{GR}^2})^{\frac{1}{2}}$ is

$$\Delta N = \frac{C}{e} \Delta V = \frac{(N_L e^2 \tau_1 RC)^{\frac{1}{2}}}{(2 \tau_t^2)^{\frac{1}{2}}}$$

so that the energy required by a particle to produce ΔN pairs is

$$\Delta W_{GR} = \omega \Delta N = \omega (N_L e^2 \tau_1 RC/2 \tau_t^2)^{\frac{1}{2}}$$

Using all the previous values and the estimate for τ_1, (equation 3-29) one obtains

$$\Delta W_{GR} = 2.5 \text{ ev} \qquad (3\text{-}30)$$

5. Input Noise of Amplifier

Heywood (1963) gives an experimental value for the "equivalent input noise charge" of a good low noise amplifier with 100pf input capacitance as roughly 2×10^3 electrons. Thus, the energy of a particle needed to produce that many excited electrons in superconducting lead is

$$\Delta W_A = \omega (2 \times 10^3) = 6\text{ev} \qquad (3\text{-}31)$$

6. GR Noise in Signal

Variations in the generation and recombination rates will produce changes in the density of radiation-excited carriers and consequently fluctuations in the magnitude of the signal ΔV_S.

The fluctuation in the generation rate is taken to be equal to the statistical fluctuations (ΔN) in N, the number of carriers excited by an ionizing particle. Now ΔW, the particle energy required to produce a voltage signal equivalent to that caused by ΔN is

$$\Delta W = \omega N^{\frac{1}{2}} = \omega (W/\omega)^{\frac{1}{2}} = (\omega W)^{\frac{1}{2}}$$

where W is the incident energy of the nuclear particle and ω is the excitation energy. Thus, for a 5 Mev alpha particle,

$$\Delta W_G = (6 \times 10^{-3} \times 5 \times 10^{6})^{\frac{1}{2}} = 173 \text{ ev}$$

Recombination rate fluctuations are difficult to analyze but for purposes of this calculation may be assumed to also vary as ΔN. Thus,

$$\Delta W_R \leq 173 \text{ ev}$$

To facilitate ready comparison between the signal noise and leakage current noise, it is necessary to compute the root square sum of the two contributions, so that

$$\Delta W_{GRS} \leq (\Delta W_G^2 + \Delta W_R^2)^{\frac{1}{2}} = 245 \text{ ev}$$

The important aspect about GR noise is that is depends on the number of initially excited carriers not on the number remaining after

recombination. Thus, unlike other types of noise, GR signal noise cannot be minimized indefinitely by lower experimental temperatures and becomes, therefore, an irreducible factor which sets the lower limit on detector resolution.

7. Net Contribution of Noise to Resolution

The overall effect of noise on the resolution of the detector is computed by summing the squares of all the various contributions and taking the square root of the total. Thus,

$$\Delta W_N = \left((\Delta W_{LC})^2 + (\Delta W_{th})^2 + (\Delta W_{GR})^2 + (\Delta W_A)^2 \right)^{\frac{1}{2}} \text{ ev}$$

$$= \left(4.8^2 + 1.3^2 + 2.5^2 + 6^2 \right)^{\frac{1}{2}} \text{ ev}$$

$$= 8.25 \text{ ev}$$

To appreciate the magnitude of ΔW_N, one need only compare it to ΔW_{GRS} to see immediately that leakage current noise will have little effect on detector resolution. In fact, the resolution of the detector appears to be limited essentially only by statistical fluctuations in the number of electron-hole pairs produced by an ionizing particle. Thus, for a 5 Mev alpha particle the resolution of the superconducting detector is about 245 ev which is roughly 25 times better than the resolution of a solid state device.

8. Signal to Noise Ratio

Converting ΔW_N into a corresponding rms voltage signal, one obtains

$$\Delta V_N = \frac{\Delta W_N}{\omega} \cdot \frac{e}{C_T} = 4.4 \times 10^{-10} \text{ v}$$

The voltage signal resulting from a charged particle was discussed earlier in this section and it was stated that the pulse might be about 0.26 mv in magnitude. Therefore, for a 5 Mev alpha particle,

$$\frac{\Delta V_S}{\Delta V_N} \geq \frac{2.6 \times 10^{-4}}{4.4 \times 10^{-10}} \approx 6 \times 10^5$$

which implies that further attenuation of the ideal voltage pulse by a factor of 10^5, due to incomplete charge collection, would still be tolerable.

At this juncture, it is necessary to clarify two approximations that have been made in deriving these estimates. Up to this point, the equivalent noise at the input of the amplifier was taken to be

$$\Delta W' = (\Delta W_N^2 + \Delta W_{GRS}^2)^{\frac{1}{2}} \text{ ev}$$

and it was assumed that since $\Delta W_N \ll \Delta W_{GRS}$ the resolution is chiefly limited by the factor

$$\Delta W_{GRS} = (\Delta W_R^2 + \Delta W_G^2)^{\frac{1}{2}} = (2)^{\frac{1}{2}} \Delta W_G$$

This, however, was a pessimistic estimate for it assumes the recombination-rate fluctuations are always as large as generation-rate fluctuations which will not be true at sufficiently low temperatures. Thus, if V_o is the voltage signal with no recombination attenuation and V_a is the attenuated voltage signal, it is more realistic to write

$$\Delta W'_{GRS} = (1 + \varepsilon)^{\frac{1}{2}} \Delta W_G$$

where $\varepsilon = V_o - V_a / V_o$ and $0 < \varepsilon < 1$. If recombination attenuation became large however, such that $\varepsilon \rightarrow 1$, then $V_a \rightarrow 0$ which implies that the equivalent noise is infinite. To incorporate this fact into the expression for $\Delta W'$, it is

assumed that, at any time, the number of noise electrons present ΔN_N is given, not simply by $\Delta W_N/\omega$ as has been assumed previously, but by $x(\Delta W/\omega)$ where $x = V_a/V_o$. Thus, for a fixed bandwidth, the more general expression for the equivalent noise at the amplifier input is

$$\Delta W = (\Delta W_N^2/x^2 + (1 + \varepsilon) \Delta W_G^2)^{\frac{1}{2}} \text{ ev}$$

where $x = 1 - \varepsilon$. Assuming a typical value of $\frac{1}{2}$ for ε, one obtains a slightly more refined estimate of

$$\Delta W = (4(8.25)^2 + (3/2)(173)^2)^{\frac{1}{2}} = 212 \text{ ev}$$

In summary, the key to the low noise level and superior theoretical energy resolution of the superconducting detector is the extremely large number of carriers produced by a charged particle. On the average, there are 500 to 1,000 times more carriers produced in a superconductor than in the best semiconductor. Statistical fluctuations, which are the fundamental limitation to resolution in any detector, are proportional to the square root of the number of excited carriers and clearly become relatively less important as the number of carriers increases.

H. Josephson Tunneling

Josephson (1962) predicted theoretically an additional kind of tunneling current that could flow between two superconducting metals. Essentially, this current behaves like the direct tunneling of "Cooper pairs" between the Fermi surfaces of the two metals.

Feynman (1965) finds the net Josephson current density to be

$$J = J_o \sin \delta(t)$$

where J_o is a constant characteristic of the junction and

$$\delta(t) = \delta_o + q/\hbar \int V(t)\, dt$$

In the latter expression, V is the voltage applied across the junction, q is twice the electronic charge, and $\delta_o = \theta_2(0) - \theta_1(0)$ where θ_1 and θ_2 are the phases of the wave function on their respective sides of the junction.

Now, if a d-c voltage V_o is applied for a time t then

$$\delta = \delta_o + (q/\hbar)\ V_o t = \delta_o + wt$$

But w is very large because $\hbar$ is about 10^{-12} smaller than qV_o for ordinary voltages; therefore the sine oscillates rapidly resulting in zero net Josephson current. The remarkable result, however, is that for $V = 0$ there exists a current ranging between $-J_o$ and $+J_o$ depending on the value of δ_o.

Furthermore, it was predicted by Josephson (1962) that this "supercurrent" would be sensitive to magnetic fields to such an extent that if the flux in the barrier region approached $hc/2e \approx 2 \times 10^{-7}$ Maxwells, the "supercurrents" would tend to cancel out.

That a Josephson current does indeed exist was verified experimentally by Anderson (1963). Using low resistance, thin junctions (approximately 6.5×10^{-4} ohm cm^2) he observed a current at and near zero d-c voltage for fields of 6×10^{-3} gauss and 0.4 gauss but was unable to observe such a current at 20 gauss. Thus, the Josephson current could flow even with a flux of 6.5×10^{-4} Maxwells in the barrier region.

If, as was analyzed in section E, it is necessary in the present experiment to make R about 10^{-3} ohm, and consequently the junction resistance about 10^{-7} ohm cm^2, it is fairly likely that Josephson currents might be observed.

The earth's field in the laboratory is about 0.2 gauss; therefore, because the junction area is roughly $10^{-4} cm^2$, the flux through the barrier should be 2×10^{-5} Maxwells. In the light of Anderson's findings, this flux will probably not be large enough to seriously inhibit the Josephson current.

In the experiment at hand, of course, a bias voltage of 1 mv or so will be applied which should reduce the Josephson current to negligible proportions. This is the desired result for it is obviously in the best interests of the detector to minimize the Josephson current as it would constitute a significant contribution to the leakage current.

I. Comparison Between Solid State and Superconducting Detectors

Having now considered some of the theoretical aspects of the superconducting counter, it is enlightening to make a practical comparison between the solid state and superconducting devices.

Based on the same figures of merit as defined in Chapter II, the comparison is shown in Table III. (For convenience, the solid state parameters from Tables I and II are repeated here.)

TABLE III

COMPARISON OF SUPERCONDUCTING AND SOLID STATE DETECTORS

	SOLID STATE DETECTOR	SUPERCONDUCTING DETECTOR
R (%) ENERGY RESOLUTION	0.3 - 0.7	.01 - .03
η (%) DETECTOR EFFICIENCY	100	100
ω (%) SOLID ANGLE (BEST VALUE)	50	50
$F = \frac{\eta\omega}{R}$	10,000	250,000
W (ev) ENERGY/ION PAIR	3 - 4	5 - 6 ($\times 10^{-3}$)
TIME RESOLUTION (SEC.)	10^{-8}	$O(10^{-8})$
AVAILABLE SIZES	.025 - 25cm^3	10^{-7} - 10^{-6}cm^3
ENVIRONMENT REQUIRED	Portable Easily Mounted in Arrays Room Temperature or Liquid Nitrogen Operation No Special Power Supply Requires Amplifying Electronics Source Size not critical	Liquid Helium operation necessitates cryostat Ponderous (because of cryostat) Requires Constant Current Source Requires Amplifying Electronics Source size limited Introducing radiation into cryostat could be a major problem

CHAPTER IV

FABRICATION OF TUNNELING JUNCTIONS

The tunneling junctions were prepared by evaporating aluminum and lead to form a thin film "sandwich" of aluminum, aluminum oxide and lead on a glass substrate. Masks were used to delineate the aluminum and lead thin film strips.

A. Preparation of Substrate

The substrates, 1 cm by 2 cm in area, were cut from glass photographic plates about 1 mm thick. Because it was imperative (Balser, 1954) that the glass be scrupulously clean before attaching the electrical contacts, the photographic emulsion was removed with household cleanser and the substrate was placed in a standard glass-cleaning solution of 100 parts concentrated sulphuric acid ($H_2 SO_4$) to 3.5 parts potassium dichromate ($K_2Cr_2O_7$). Then, after the slide had been rinsed in distilled water and ethanol and dried with compressed air, the electrical contacts were formed by smearing indium solder onto each corner of the glass surface formerly covered by the emulsion. Finally, the substrate was cleaned again in household cleanser, rinsed in distilled water and ethanol and dried with compressed air.

B. Evaporation Procedure

The completed substrates were mounted in the evaporator in such a manner that they could be positioned behind either of two masks while under vacuum. In this way, it was possible to avoid exposing the specimen to the atmosphere between the aluminum and lead evaporations and so to oxidize the aluminum film at reduced pressures.

Tungsten filaments, 40 mils in diameter, were used to evaporate the aluminum; tantalum boats, approximately 1 by $\frac{1}{2}$ by .005 in, were used to evaporate the lead. It was found necessary to use a new filament for each evaporation because every time a filament was re-used the subsequent junction was found to have little or no tunneling resistance. The short circuit was probably caused by lead that had been deposited on the filament during the previous lead evaporation. This lead would then be re-evaporated as an impurity with the aluminum and would form a bridge through the insulating aluminum oxide layer. The additional refinement of making the tantalum boat into a "point" source by covering it with a thin tantalum sheet pierced with a small hole, enhanced the sharpness of the edges of the lead films.

The evaporations, performed at a pressure not greater than 5×10^{-5} mm Hg, were carried out in three steps (see figure 22). Firstly, a layer of aluminum, estimated (See Appendix C) to be about 6 μ thick, was evaporated onto the substrate between two diagonally opposite contacts. The mask, made from .002 aluminum shim, was designed so that the evaporated strip was about 3 mm wide. Secondly, the freshly evaporated strip was oxidized at a reduced pressure, usually about 50 microns Hg, by admitting room air into the evaporator bell jar for a period of about ten minutes. Thirdly, a layer of lead, roughly 10 μ thick (See Appendix C) and the same width as the aluminum, was evaporated over the aluminum oxide layer between the two remaining contacts. In this case, a mask cut from .002 brass shim was employed.

C. Geometric Effects

The capacitance of the junctions was discovered to be of the order of 0.1 μf-- a value much too large if the junction were to be used to detect

Figure 22: Evaporation Procedure

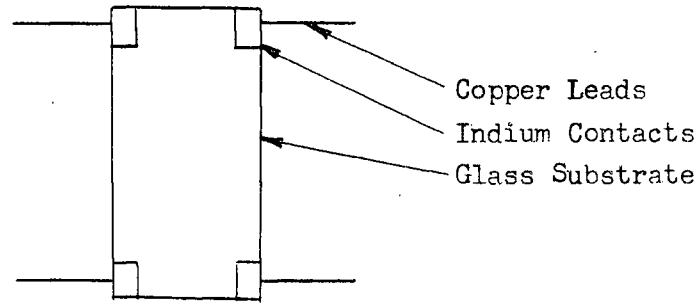

(a) Completed Substrate

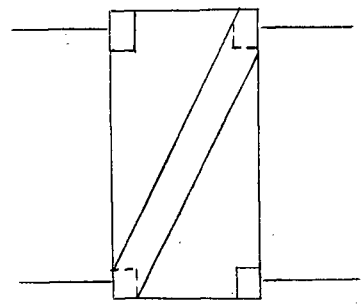

(b) Aluminum Evaporated

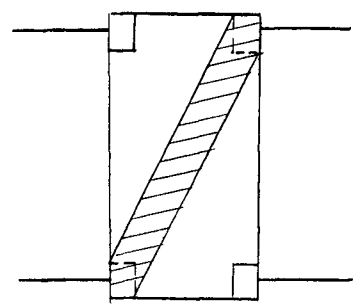

(c) Aluminum Oxide Formed

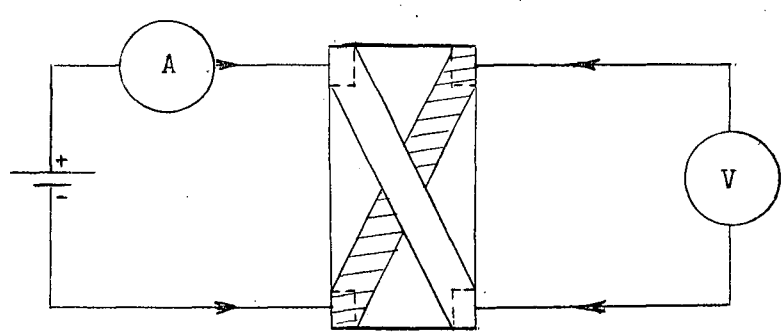

(d) Lead Evaporated

radiation, for any pulses generated by nuclear particles would be shorted to ground. To reduce this capacitance, the masks were re-designed thereby reducing the area of the junction from about 10 mm^2 to 10^{-2} mm^2. Because of the low resistance in parallel with the capacitance, it was difficult to measure the capacity with much accuracy. The best estimate that could be obtained, for the smaller area junctions, with the use of an externally biased General Radio Impedance Bridge, was an upper limit of 100 $\mu\mu$f.

Reducing the junction area, however, pointed up a hitherto unnoticed property of the junction resistance. As the junction aged, its resistance increased quite rapidly and, as discussed more fully in Chapter VII, considerable effort was required to understand and control this undesirable effect.

CHAPTER V

CRYOGENIC APPARATUS

A. Introduction

Basically, the apparatus is a glass dewar vessel containing liquid helium-4--referred to hereafter as the helium dewar--which sits inside a larger dewar vessel filled with liquid nitrogen and referred to as the nitrogen dewar (see figure 23). The liquid nitrogen acts as a pre-coolant and as a heat shield for the liquid helium bath. Inside the helium dewar is a cryostat whose inner chamber is connected to the helium bath by means of a needle valve. Provision is made for differential pumping on the liquid helium baths in both the cryostat and the helium dewar giving the system a capability of attaining temperatures close to 1.2°K.

B. Dewars

Both the nitrogen and helium dewars, constructed by the departmental glass blower, are of conventional design except that a pyrex tee (3x3x2 in) is affixed to the top of the double walled portion of the helium dewar. The tee was necessitated by the fairly unconventional manner in which the dewars were installed. Both dewars were mounted in a firmly anchored table, the top of the tee being about four feet above floor level, thereby making possible the installation and removal of the cryostat and specimens without disturbing the dewars. One port of the tee thus provided an opening for pumping on the helium dewar, the other port provided a readily demountable vacuum coupling for the cryostat.

Figure 23: Cryogenic Apparatus (Schematic)
(See Page Following for Key)

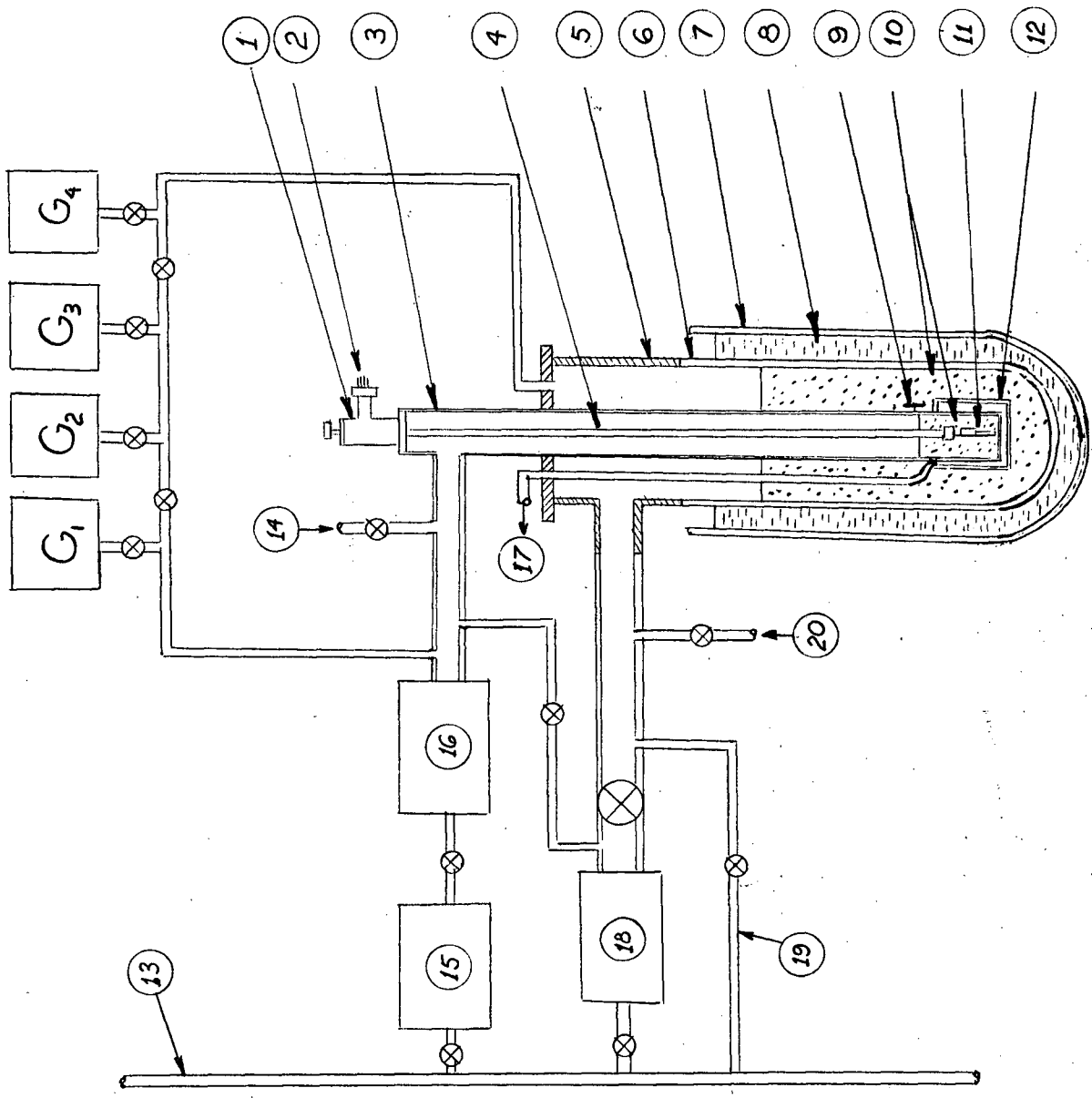

KEY TO FIGURE 23

G_1 Dial Gauge, 0-30 in.Hg.

G_2 Dial Gauge, 0-20 mm.Hg.

G_3 Vacustat, 0-1 mm.Hg.

G_4 Dial Gauge, 0-30 in.Hg.

1. Cryostat Cap
2. Electrical Leads
3. Cryostat
4. Sample Mount and Control Shaft
5. Pyrex Tee
6. Helium Dewar (Glass)
7. Nitrogen Dewar (Glass)
8. Liquid Nitrogen
9. Needle Valve
10. Liquid Helium-4
11. Sample & R-C Filter
12. Vacuum Jacket
13. Helium Return Line
14. Roughing & Flushing
15. Mechanical Pump (Welch 1402)
16. Diffusion Pump (PMC 115)
17. Pumping & Flushing
18. Low Temperature Laboratory Pump (Stokes #49-10, 80 cfm)
19. Helium Flush and Atmospheric Return Line
20. Roughing

C. Pumps

All pumps and their connections, except the roughing pump, are shown schematically in figure 23. The diffusion pump, a C.V.C. model PMC-115A, has a quoted unbaffled pumping speed of about 100 litres per second at input pressures ranging from 3×10^{-3} mm Hg to 2×10^{-5} mm Hg. This is backed by a Welch model 1402B rotary pump. A Stokes pump model 49-10, a permanent "community" installation of the Low Temperature laboratory, has also been incorporated into the experimental system. Both sets of pumps exhaust into the laboratory helium-4 recovery lines.

A judicious location of valves makes it possible to have either set of pumps pumping on either the main helium bath in the dewar or the experimental helium bath in the cryostat. Normally, the diffusion pump and its backing pump operate on the cryostat bath and should be capable of lowering the vapour pressure to correspond to a temperature of about $1.2^{\circ}K$. The Stokes pump is usually connected to the main helium bath and, on a preliminary test, a temperature of about $2^{\circ}K$ was attained with it.

D. Pressure-Temperature Measurement

Temperatures are measured by observing the helium vapour pressure and relating it to the temperature with a standard table. The vapour pressure-temperature relationship of liquid helium-4 has been extensively investigated and it is found in many standard references. (Mendelssohn, 1960). An Edwards vacustat, model 2E, and two dial gauges (figure 23) provide adequate coverage of the pressure range from 1 μHg to 1 atmosphere for either bath.

E. Cryostat

It is in the cryostat that the specimens are placed and the low temperatures necessary for operation of the junction are reached. The needle

valve and the vacuum jacketed-region (figure 24) are of particular importance.

Liquid helium from the dewar is admitted to the cryostat by means of the externally operated needle valve. Thus, the cryostat can be filled with liquid helium to any hydrostatically possible level thereby providing a suitable bath for cooling the tunneling junctions. When the inner bath is pumped away, the needle valve is simply opened and more liquid helium flows in from the outer bath. In this way, experimental time is extended to 10 or 12 hours and the outer bath serves as both an additional heat shield and a storage volume. The needle valve, constructed in the physics workshop, has been found to work satisfactorily thus far. It is not perfectly vacuum tight, however, and it remains to be seen if it will maintain isolation between both inner and outer baths when both are below the lambda point and superfluid is present on both sides of the valve.

The vacuum jacket, about four inches in length, provides the necessary thermal insulation between the outer "warm" bath and the inner "cold" bath. The interspace thus formed is filled with nitrogen exchange gas during pre-cooling and evacuated before the helium dewar is filled.

F. Cryostat Cap and Sample Mount

The cryostat cap (see figure 25) is vacuum coupled to the top flange of the cryostat. Two thin-walled stainless steel tubes extending below the cap provide support for the specimen mount and a means for adjusting the Spectrol potentiometer. The distinguishing feature of this design is that, in order to change specimens, only this single piece of apparatus need be removed.

It is through the cryostat cap that the electrical leads and mechanical

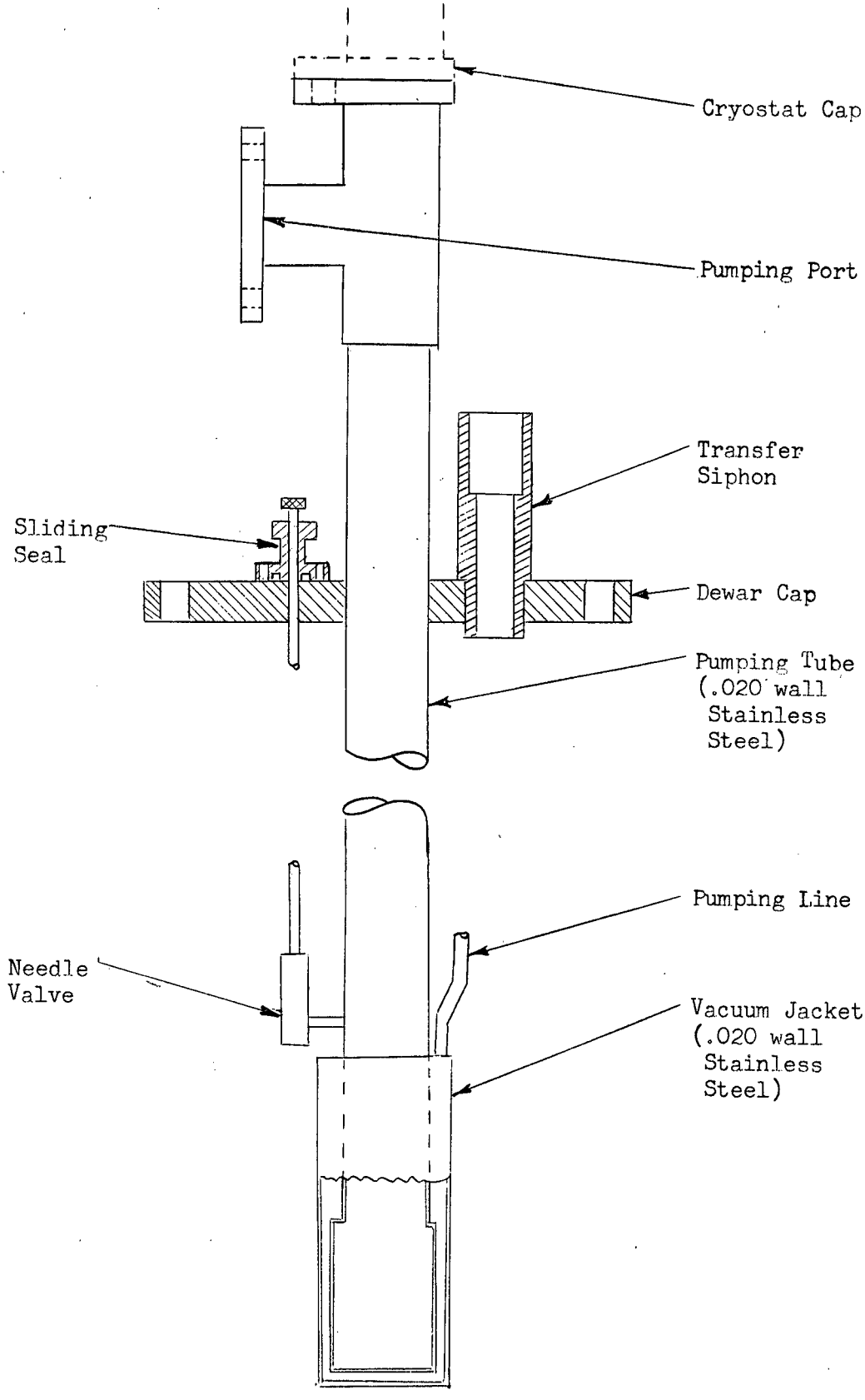

Figure 24: Cryostat (Simplified)

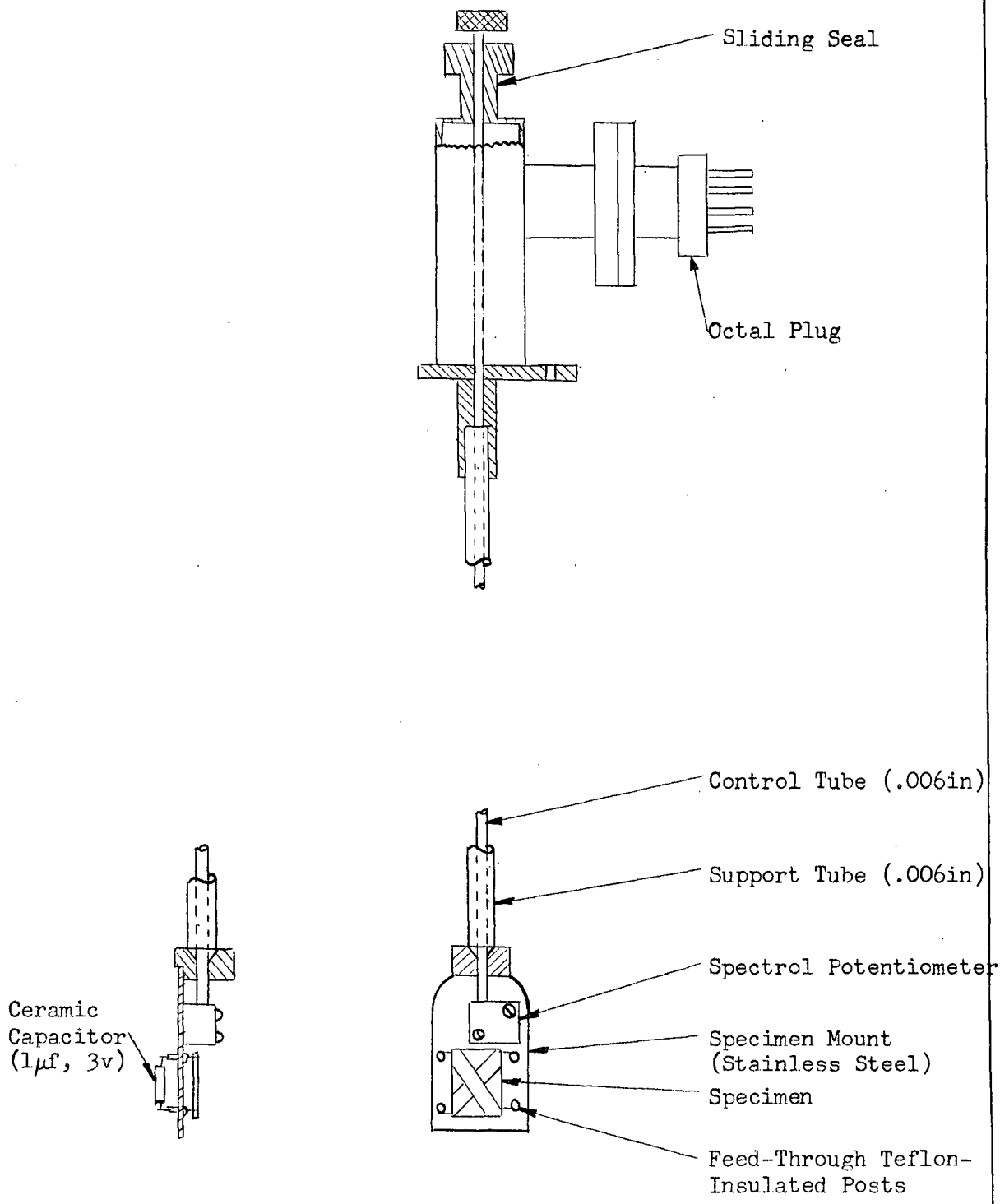

Figure 25: Cryostat Cap and Specimen Mount

motion are introduced. Provision has been made for eight leads, the glass-to-metal seals being obtained by using the base of a discarded octal electronic tube. The sliding seal is, of course, vacuum tight and permits vertical and rotational motion of the control tube.

Two main functions are demanded of the sample mount: it must hold the sample firmly and yet not so rigidly that the substrate can crack as a result of differential contraction; it must have space for a resistive-capacitive filter (see Chapter VI) and be sufficiently rigid that torque can be applied to the shaft of the potentiometer. As evident in figure 25 , both requirements are met without great difficulty or complexity.

CHAPTER VI

ELECTRICAL MEASUREMENT TECHNIQUES

A. Power Supply

The power supply, shown in figure 26, was energized by a battery as the current load was small and a minimum of a-c ripple imperative. Normally, potentiometer R1 was set at 50K making the power supply effectively a constant current source.

In practice, the voltages applied to the sample were very small--one or two millivolts--and therefore voltages induced by fluctuating stray fields were, even after shielding, not negligible. Such noise causes "ripple" and hysteresis in the characteristics traced out by the X-Y recorder. It was to minimize this induced noise that potentiometer R2 was placed in series with the sample for it served as a voltage divider thereby causing only a small fraction of the noise to appear across the sample. Furthermore, when R2 was set at the usual value of 50K, the output impedance of the power supply increased so that it more closely approximated a constant current source.

B. High-Pass Filter

Giaever and Megerle (Giaever, 1961) reported high frequency oscillations when their samples were biased into the negative resistance region (see Chapter III) and found that the oscillations could be greatly reduced by placing a high-pass filter in parallel with their sample. Their filter consisted of a variable resistor in series with a capacitor large in comparison to the sample

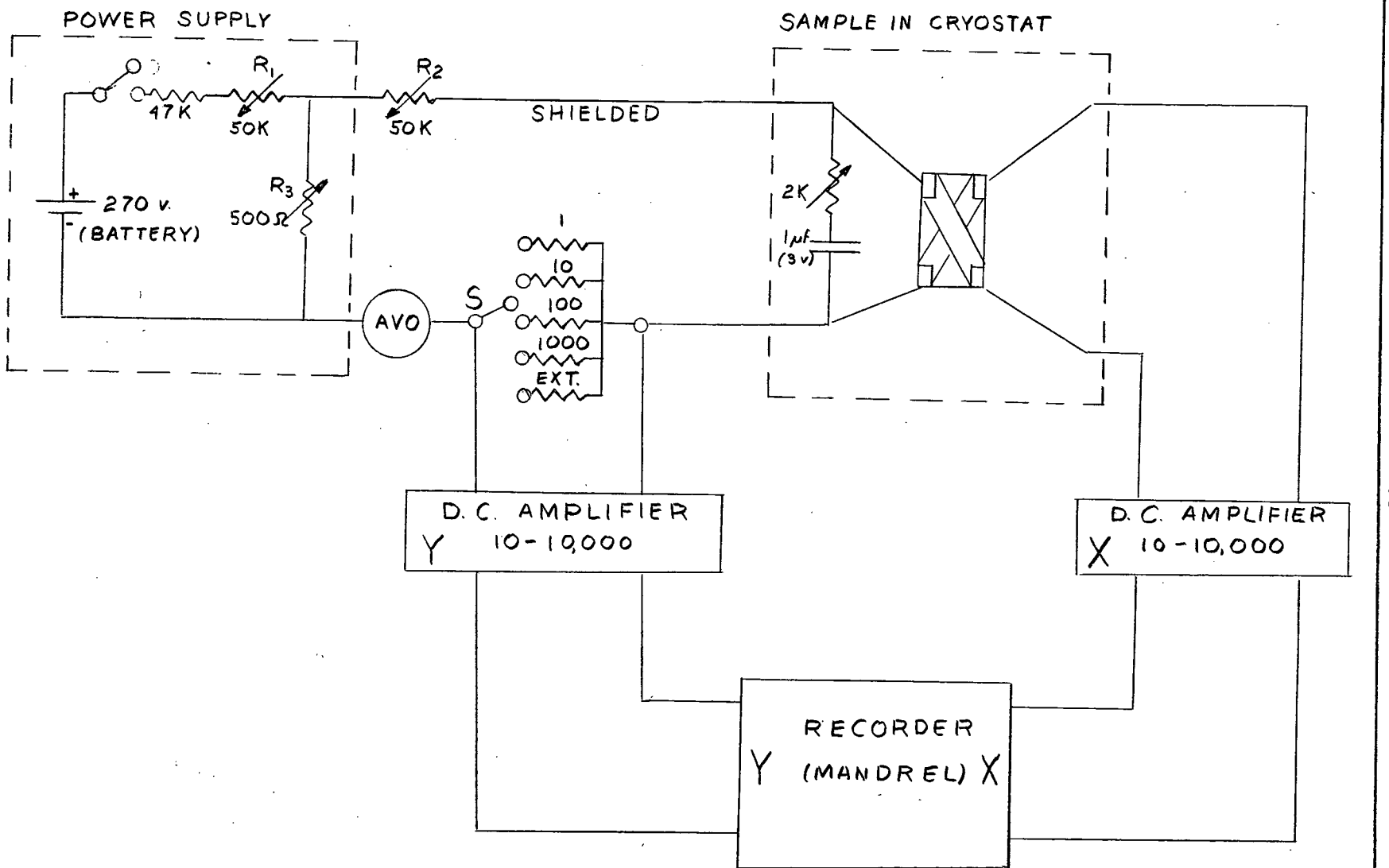

Figure 26: Electrical Circuit (Schematic)

capacitance and it was mounted inside the cryostat in proximity to the sample.

The high-pass filter used in the present experiment was a small (1/2 x 1/2 x 3/16 in) Spectrol 2K potentiometer, model 60-1-1, in series with a Centralab 1 μf - 3v ceramic capacitor type UK - 105. Both components were mounted (see figure 25) on the sample mount to minimize lead inductance and they performed satisfactorily at liquid helium temperatures. As mentioned in Chapter V, the potentiometer could be adjusted externally. This feature made it possible to match the negative resistance of the sample and attempt to tune out the oscillations.

C. Electrical Connections

To obviate the problems arising from indium-thin film contact resistance and the significant resistance of the thin films and wire leads, a four-terminal network was used. A reduction in induced noise was attained by shielding the two current and two voltage leads both inside and outside the cryostat. Inside the cryostat, the leads were shielded by the grounded stainless steel cryostat body; outside the cryostat, the leads formed part of a multi-strand cable shielded in the conventional manner.

In order to minimize heat leakage, Driver-Harris, size 38 (4 mil), double nylon-covered "Advance" Cu-Ni wire was used inside the cryostat. The estimated thermal conductivity (see Appendix D) of the four leads was approximately a factor 10^3 smaller than the thermal conductivity of the main stainless steel tube of the cryostat and was therefore completely negligible.

D. Measuring Circuitry

Figure 26 shows the apparatus required to provide a trace of the current-voltage characteristics of the sample. The sample voltage was amplified and

displayed on the X axis of the recorder. The current display was obtained by passing the sample current through an appropriate precision (1%) resistor at S, amplifying the voltage thus developed and feeding it into the Y axis of the recorder.

A schematic of the twin d-c amplifiers is shown in figure 27 . Two Philbrick operational amplifiers, model P65AU, powered by a Philbrick power supply, model PR-30C, were the principal components. In this configuration the input impedance of each amplifier, as specified by the manufacturer, was about 10M and the output impedance so large that the device was quoted as a current source. By selecting various feedback resistors at multipole switches S_x and S_y, it was possible to attain voltage gains of 11, 51, 101, 501 or 1001. Experience showed that a warm-up time of at least one-half hour was required for stability and, even after this period, periodic checks for drift were necessary.

A Mandrel X-Y recorder, model ER 90-1, was employed to trace the current-voltage characteristics of the tunneling junctions. It was because maximum sensitivity of this device was only 10 mv/in and the input impedance only 10K, that the d-c amplifiers described above were essential. To permit accurate attenuation of incoming signals, the two attenuating potentiometers supplied with the recorder were by-passed and replaced by two 10K Spectrol type 860 ten-turn precision potentiometers. In addition, a calibration circuit was appended to the recorder to facilitate frequent calibration checks.

With these instruments, voltages in a range from 100 μv to 1v and currents in a range from less than 1 μa to 100 ma could be conveniently displayed.

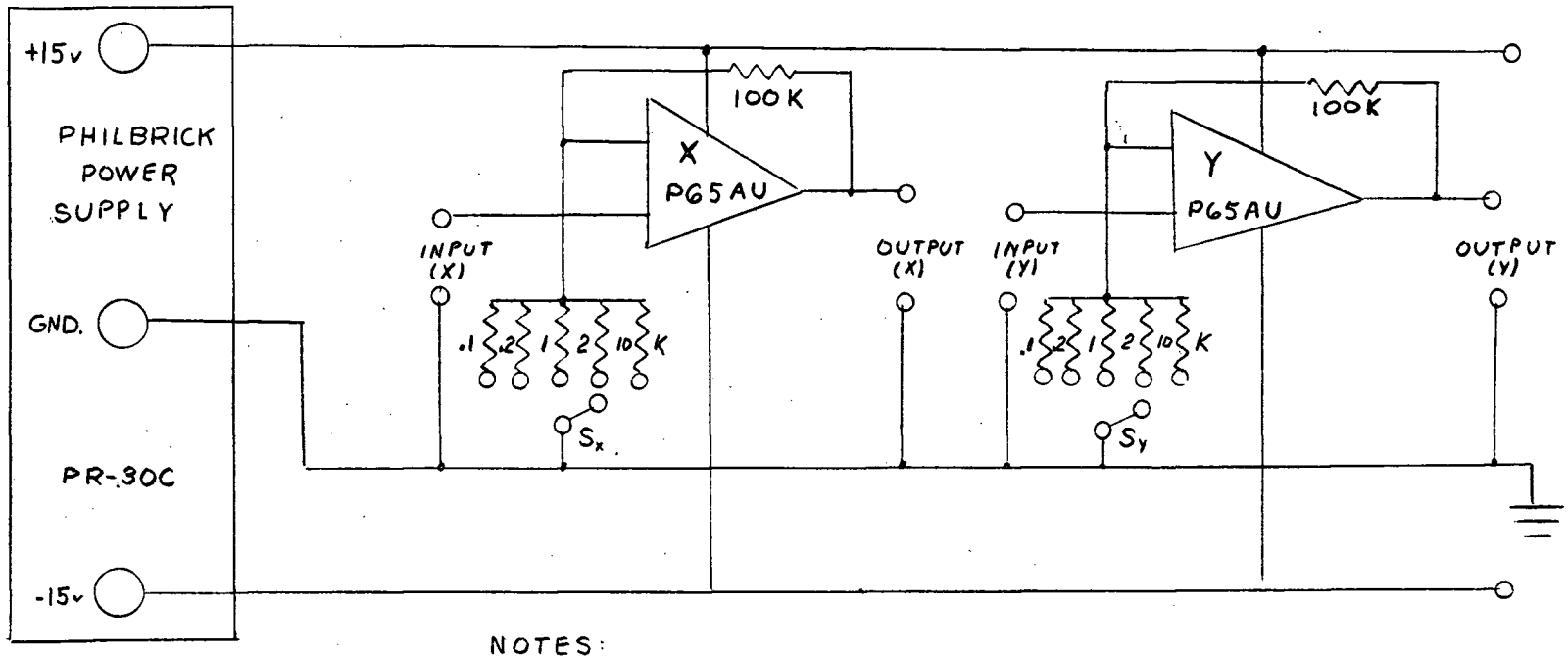

NOTES:

- $e_{out} = (R_f/R_i + 1)\, e_{in}$
- ALL RESISTOR PRECISION (1%)
- S_x, S_y BY CENTRALAB, # PA 1004
- OPERATIONAL AMPLIFIERS BY PHILBRICK

Figure 27: Twin D.C. Amplifiers (Schematic)

In an attempt to detect changes in the ambient d-c voltage of the specimen while it was being subjected periodically to a strong flux of gamma rays, a model 153X Brown strip-chart recorder was used. A Hewlett Packard model 412A vacuum tube voltmeter and d-c amplifier provided the necessary loading isolation and signal amplification.

CHAPTER VII

RESULTS

A. Normal Metal Junction Resistance

The thickness of the Al_2O_3 layer, and hence the magnitude of the junction resistance, is dependent upon a number of variables. Specifically, the oxidation rate depends on pressure, time, temperature, humidity, evaporation rate and evaporation temperature of the metal film covering the oxide layer. Eley and Wilkinson (1959) give a fairly complete summary of the pressure and time dependence of the oxidation rate; Giaever and Megerle (1961) show a few experimental results relating pressure and time to junction resistance; Handy (1962) relates the evaporation temperature of the covering metal film to the ultimate junction resistance.

For purposes of the present experiment, it was concluded that junctions with a sufficiently wide range of resistance could be most easily prepared by varying only the oxidation time and holding all the other parameters as constant as possible. Accordingly, several junctions were prepared, the oxidations taking place at room temperature and atmospheric pressure with no measurement being made of the other "constant" parameters. The room temperature junction resistance for each sample was obtained by placing a vacuum tube voltmeter across two adjacent terminals and passing a known current through the remaining two terminals (see figure 22). In agreement with the theory of Chapter III, no rectification effects were observed. Table IV summarizes the results:

TABLE IV

Relation between oxidation time and Junction resistance for Al-Al_2O_3 - Pb "sandwiches"

Oxidation Time	Low Voltage Junction Resistance ohm cm^2
10 Min	10^3
5 Hr.	10^4
46 Hr.	10^7

As predicted in the theory of Simmons (1963), the resistivity was relatively constant for low voltages but, at higher voltages, it decreased rapidly with increasing voltage until, at about 1 or 2 volts, destructive breakdown occurred. A typical I-V characteristic is shown in figure 28 .

B. Time Dependence of Junction Resistance

It was found that the resistance of the completed Al-Al_2O_3 - Pb junctions increased with time. Typically, the junction resistance of samples stored at atmospheric pressure was observed to increase by an order of magnitude in about 40 hours (figure 29). Primarily, this effect meant that, unless a junction were used immediately after fabrication, in a short while its resistance would have increased to a value that would severely inhibit non-equilibrium tunneling (Chapter III). Secondly, this effect implied that the junction resistance could increase significantly during the six or more hours required for an experiment. Finally, it was apparent that, even if the time constant were sufficiently large that the resistance change during an experiment would be negligible, the time dependence of the resistance would

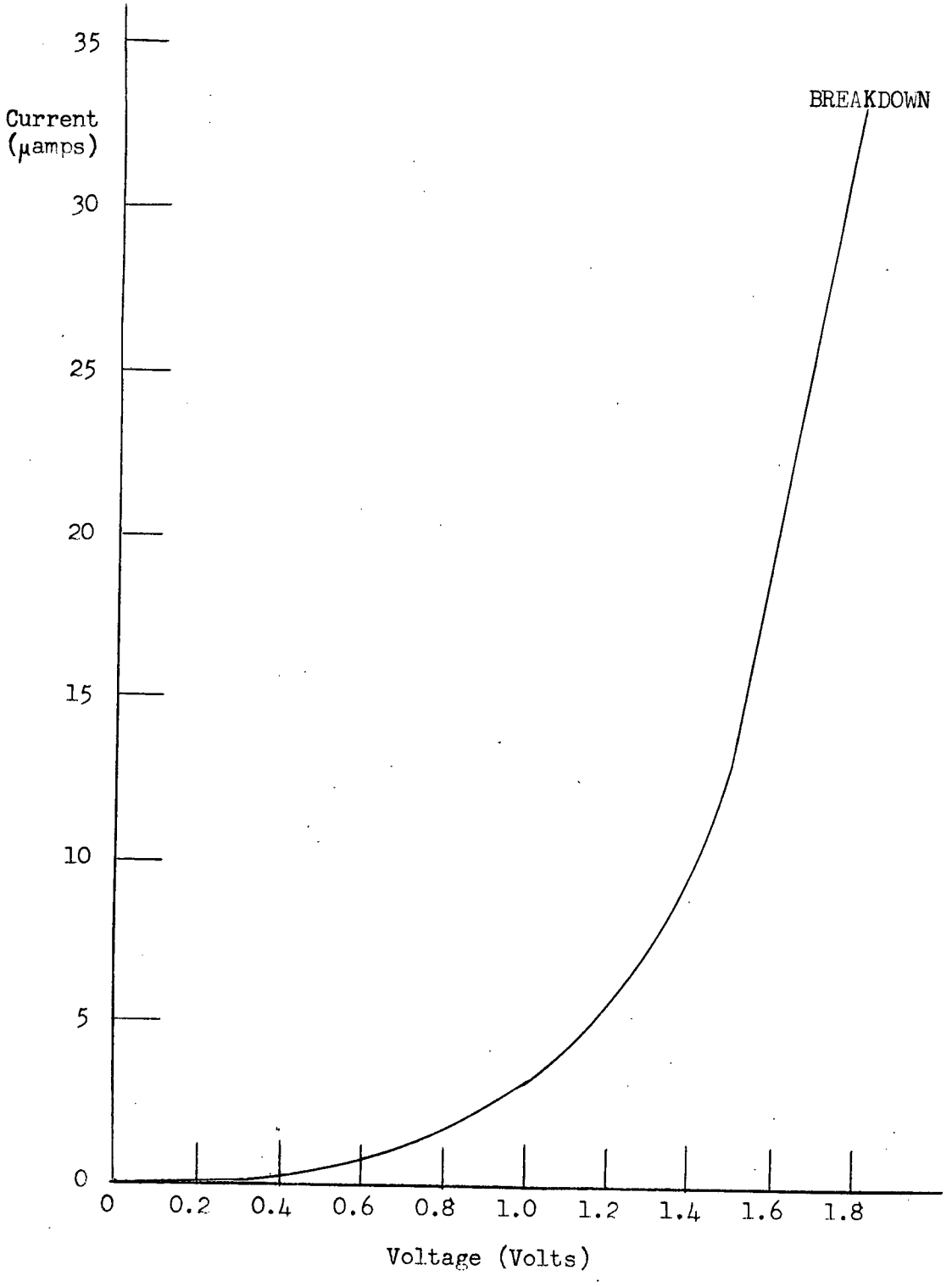

Figure 28: I-V Characteristic for Normal Metal Junction

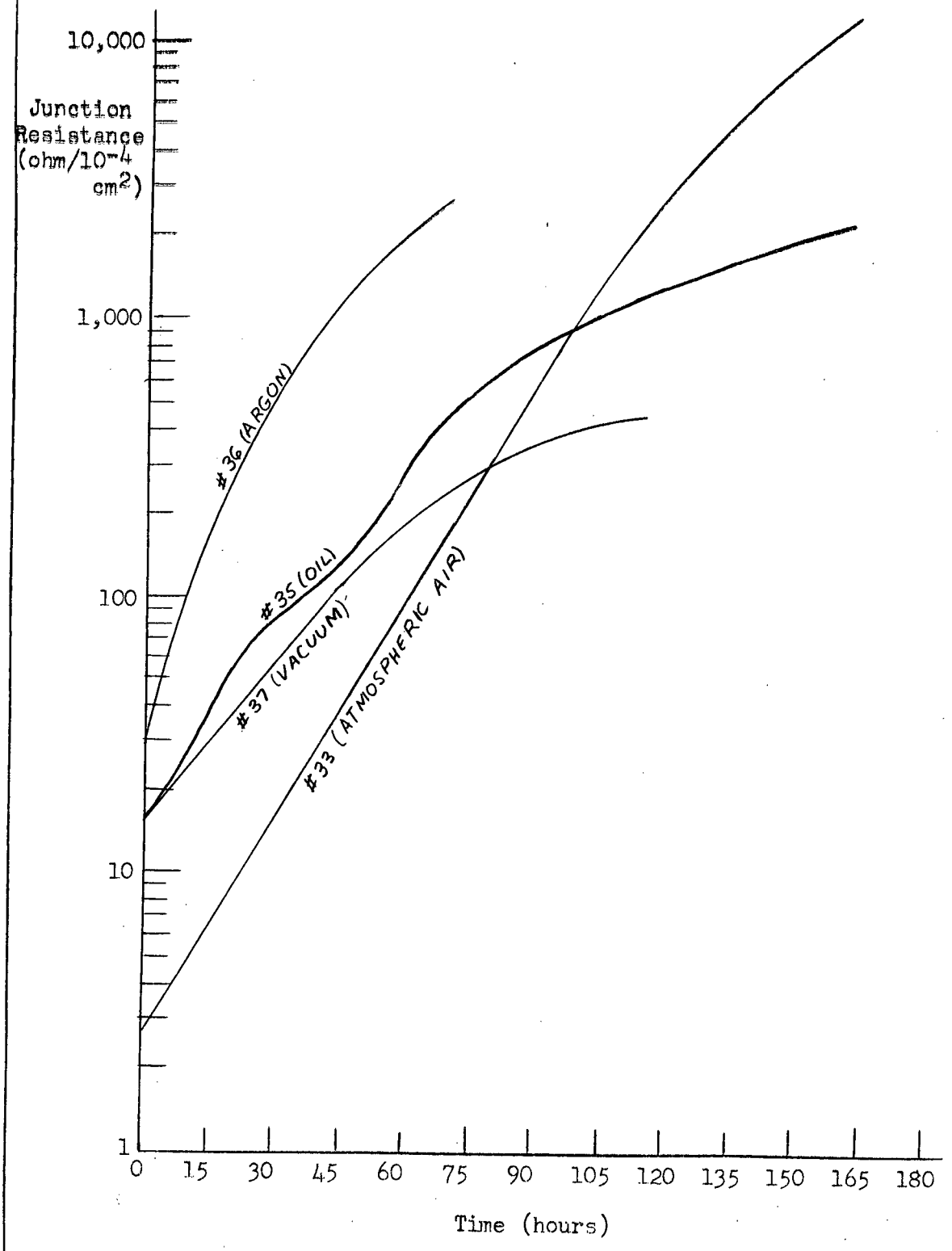

Figure 29: Time Dependence of Junction Resistance in Various Environments

preclude re-using a junction at a later time for calibration purposes. In an attempt to reduce these undesirable effects, steps were taken to lengthen the time constant as it seemed improbable that the time dependence could ever be completely removed.

The immediate inference from the time-dependent effect is that somehow oxygen is diffusing from or through the lead film to the oxide layer thereby giving rise to further oxidation. To obviate this an effort was made to coat the completed junction with a layer of calcium or magnesium fluoride. Little success was found with this method because of the difficulty in forming a sufficiently thick fluoride layer. When the evaporating furnace was placed near the junction so that more fluoride might be deposited, the heat destroyed the junction; when a "cold" mask was interposed between the furnace and the junction, insufficient fluoride was deposited. Storing the junction in pump oil or an inert atmosphere like argon proved beneficial but still unsatisfactory (figure 29). A measure of success was found, however, by evaporating the lead slowly at first, to prevent overly - energetic atoms from piercing the oxide to form a "bridge", and then very quickly evaporating the remaining lead to form a fine-grained film (Holland, 1956)--presumably less permeable to oxygen atoms. Further improvement was obtained by storing the junctions in a vacuum maintained by a mechanical pump (figure 29). At this point, it was felt that the time constant was sufficiently large to make the experiment feasible so that no further study of this effect was carried out.

Handy (1962) also reported the junction resistance to be time dependent, but with one important distinction. For the system Al-Al_2O_3 - M, where M was Al, Sn, Cu, Ni, Ag or Au, the resistance increased with time even when the junction was stored in a vacuum of 5×10^{-7} mm Hg but, when M was Pb, the

resistance was reported to not only decrease with time but to be independent of storage pressure. As his result for lead is diametrically opposed to that found in the present experiment, further investigations of this phenomenon would be valuable.

C. Superconductive Tunneling

To ascertain the quality of the junctions which had been prepared, a simple experiment was performed to test their low-temperature d-c characteristics against those of other workers and the theoretical model.

A sample was prepared using 3 mm wide aluminum and lead films of the usual thickness (Chapter IV). The oxidation took place at about 50 μHg for 10 minutes which resulted in an initial junction resistance of about 1/3 ohm x 10^{-1} cm^2 = .033 ohm cm^2. Eight days later, when the experiment was actually conducted, the junction resistance had only risen to 1.5 ohm cm^2 which was low enough for a preliminary test.

Two representative plots from the X-Y recorder are reproduced in figures 30 and 31 . At 1.46°K, the Al-Al_2O_3 - Pb system actually belongs to the M-B-S class discussed in Chapter III since T_c for aluminum is 1.19°K. For the M-B-S structure, a theoretical estimate of the total tunneling current gave

$$I_T = A|M|^2 N_m(0)\, n_o\, e^{eV/kT} \qquad (3\text{-}8)$$

at which time it was pointed out that when eV is close to $\mathcal{E}_o$, $eV \gg kT$, and the current increases very rapidly with increasing voltage. Now for lead, the theoretical value for $\mathcal{E}_o$ is (BCS, 1957)

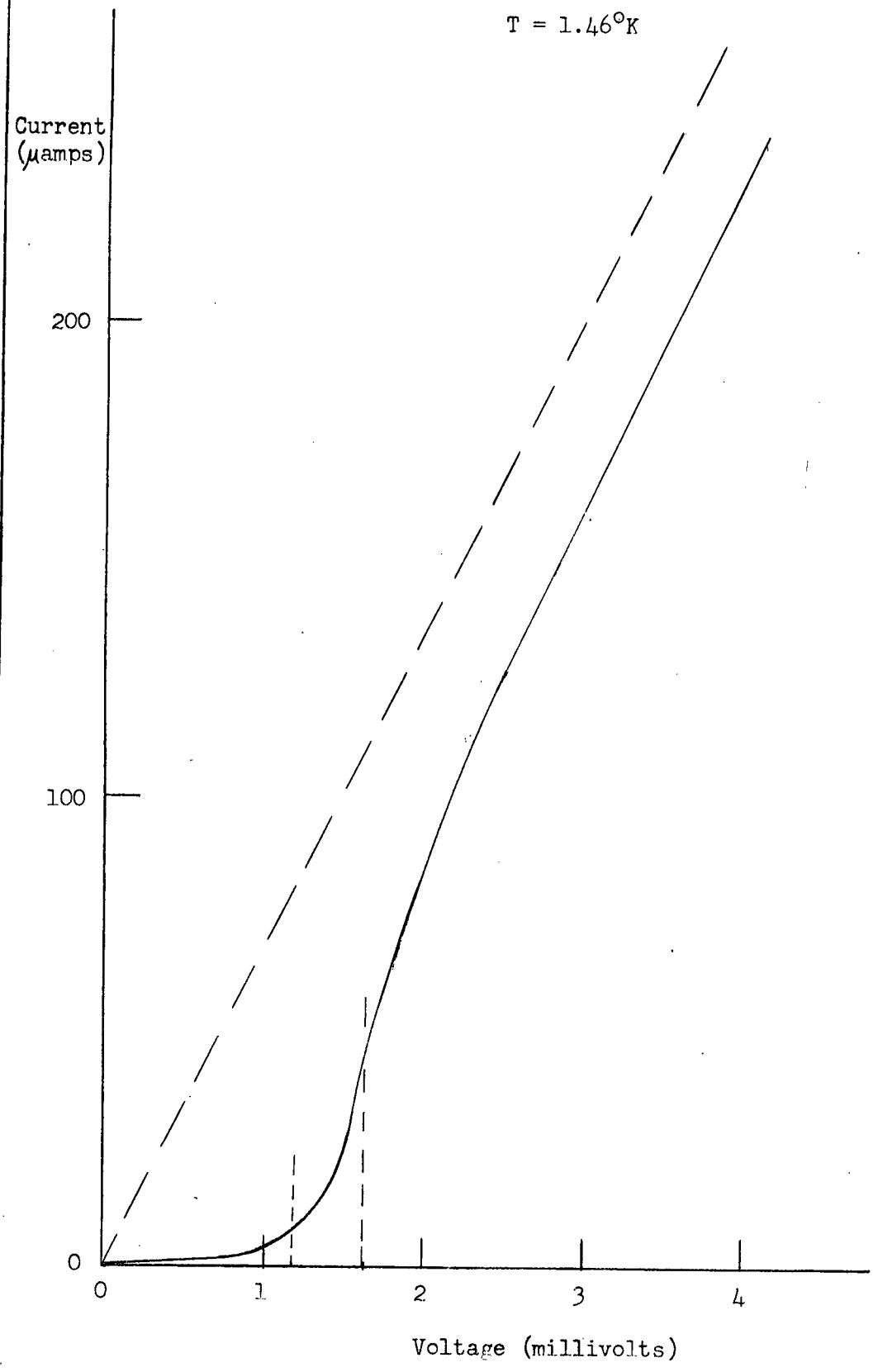

Figure 30: I-V Characteristic for Al-Al_2O_3- Pb Sandwich

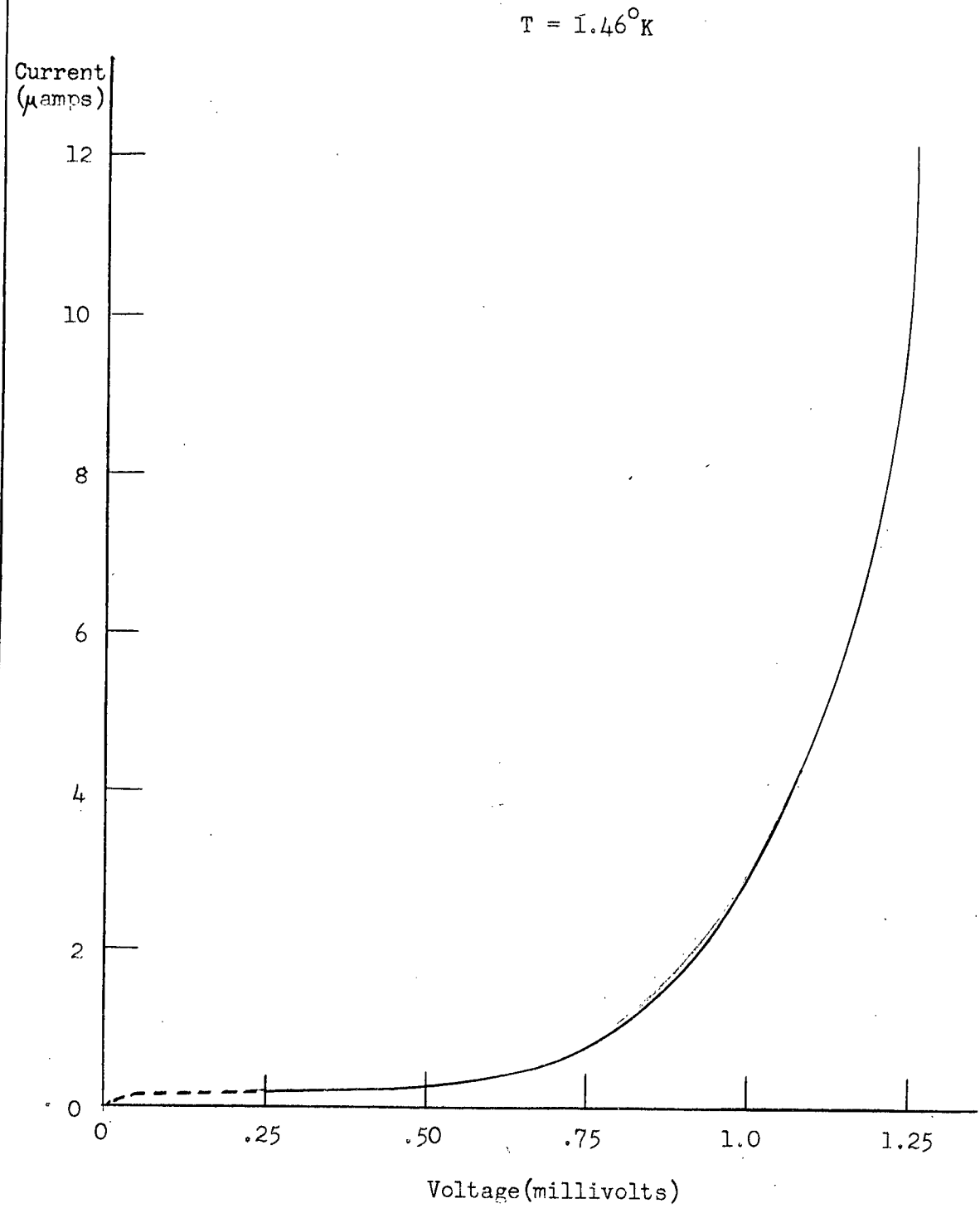

Figure 31: I-V Characteristic for Al-Al_2O_3-Pb Sandwich

$$\mathcal{E}_o = \tfrac{1}{2}\,(3.50)\,kT_c(\mathrm{Pb}) = 1.09 \text{ mev.}$$

From figure 30 the current is seen to start increasing rapidly in the neighbourhood of $1.4 \pm .2$ mv which indicates fair agreement with the model previously described. In addition, the value of $\mathcal{E}_o(\mathrm{Pb}) = 1.4 \pm .2$ mev obtained in this experiment corroborates quite satisfactorily the value of 1.34 mev obtained by Giaever and Megerle (1961).

D. Effect of Radioactive Source

It was shown in Chapter III, that the tunneling current in a M-B-S system depends almost entirely on the density of excited electrons in the normal metal and not in the superconductor. To test the validity of this prediction, an attempt was made to see if the gamma radiation from a radium-beryllium source would produce observable changes in the d-c tunneling current.

With the junction biased at 0.6 mv, a strip-chart recorder was connected across the voltage terminals and back-biased in such a way that its middle scale reading corresponded to zero volts input. To optimize the probability of observing any current fluctuations induced by the radiation, the source was placed as close as possible to the junction (about 8 cm.) for 10 minutes and then removed to a considerable distance for 10 minutes. This cycle was repeated four consecutive times but no correlation significantly larger than the noise fluctuations could be discerned between the source period and variations in the ambient current.

The reason for this negative result can be explained in the following way. Consider the number N_c of excited carriers that would be generated in the superconducting lead by the gamma radiation. If N_γ is the source

strength in photons/sec, ρ is the attenuation in the beam between the source and the junction, Ω is the fraction of a sphere subtended by the junction, $\mathcal{E}$ is the probability that a photon is absorbed in the lead and η is the number of excited electrons generated per absorbed photon, then

$$N_c = N_\gamma \rho \Omega \mathcal{E} \eta \qquad (7\text{-}1)$$

The radium-beryllium source is assumed to have a gamma activity of roughly 1 millicurie so that $N_\gamma \approx 3.7 \times 10^7$ photon/sec. For the experimental set-up, ρ is estimated to be 0.7; $\mathcal{E} = 1\text{-}e^{-\mu \cdot d} \approx 3.4 \times 10^{-4}$ where $\mu = 0.34$ is the absorption coefficient and $d = 10^{-3}$ cm is the lead thickness. For a junction 10^{-1} cm^2 in area located 8 cm from the source, Ω is 1.3×10^{-4}. The quantity η is estimated by assuming that every photon absorbed generates electrons of roughly the same energy which, in turn, ultimately lose their energy in the breaking up of many superconducting paired electrons. Thus,

$$\eta = \frac{(dE/dx)_{\text{electron}} \times (\text{mean free path of electrons})}{\text{excitation energy } (\omega)}$$

From Marion (1960), the range of 1.6 Mev electrons (the average photon energy) is found to be 2 kev cm^2/mgm. It is assumed that the electron mean free path is roughly d/2 so that, using $\omega = 6 \times 10^{-3}$ ev/excited electron, one finds

$$\eta = 1.9 \times 10^6 \text{ excited electrons/photon absorbed}$$

which, upon substitution, gives $N_c = 2.2 \times 10^6$ electrons/sec.

Previously, when analyzing the pulse amplitudes, it was necessary to consider the total number of electrons present during the pulse period. In d-c calculations, the number of excited carriers present per unit time is all that is required.

The fraction of the N_c electrons that actually tunnel is given by

$$F = \frac{P_t}{P(\text{decay})} \cong \frac{P_t}{P_t + P_R} = \frac{\tau_R}{\tau_t + \tau_R} \lesssim \frac{1}{2}$$

(at the present experimental temperatures). Therefore, the change in current induced by the gamma radiation is roughly

$$(\Delta I)_R = e N_c F \leq 1.7 \times 10^{-13} \text{ amps} \qquad (7\text{-}2)$$

The noise level in the system measuring the voltage across this specimen was, at best, 0.5 μv which means that, for the experimental junction resistance of 10^4 ohms, the minimum detectable change in current was

$$\Delta I = \frac{(\Delta v)_{\text{instrument}}}{R_{\text{junction}}} \geq 5 \times 10^{-11} \text{ amps} \qquad (7\text{-}3)$$

Thus, even the most optimistic estimate of $(\Delta I)_R$ shows that it was significantly less than ΔI and consequently unobservable. If charged particle radiation had been used instead, the number of excited electrons generated, N_c, would have been roughly 10^9 thereby increasing $(\Delta I)_R$ to a detectable level of about 10^{-10} amps. It may be concluded therefore that the negative result with gamma radiation does not necessarily foreshadow the failure of an S_1-B-S_2 structure to detect charged particles.

CHAPTER VIII

CONCLUSIONS

The experimental and theoretical study reported in this thesis has shown the plausibility of successfully developing a superconducting charged particle detector. Because its theoretical energy resolution is superior to that of any comparable device, the superconducting counter would be capable of making important contributions to the field of nuclear spectroscopy. There is, however, a considerable difference between a device working in theory and a device working in practice.

Although none seems insuperable, there are several obstacles which will no doubt impede the rapid development of a practicable detector. Fabrication techniques are readily refined to the point where samples are fairly reproducible but making a junction of only 5×10^{-7} ohm cm^2 resistance, as stipulated by the theory of Chapter III, might prove to be a problem. In preliminary work, the smallest junction resistance yet attained has been about 5×10^{-5} ohm cm^2. To enhance the tunneling probability, it may be imperative to use experimental temperatures somewhat lower than $1^{\circ}K$. If this were the case, it would be expedient to use He^3 rather than He^4 as the coolant thereby adding an additional complication to the already complex ancillary apparatus. (To alleviate such inconvenience, the present cryostat was designed for future conversion to He^3). Needless to say, because of the apparatus needed to attain low temperatures, the superconducting counter would be bulky and have little or no portability

even though the junction itself is very small. Another obstacle, perhaps the most formidable of all, is the tendency of the junction resistance to increase with age, for this property will make calibration difficult and reproducible results impossible.

To put a superconducting detector "on line" with an accelerator-produced beam experiment involves still other difficulties. Because of the tiny junction area, the solid angle subtended by the junction to a source external to the cryostat is very small indeed. Thus, good spatial resolution is possible but only at the expense of detection efficiency. Introducing the radiation into the cryostat in such a way as to minimize energy straggling and intensity attenuation could very well prove to be a challenging cryogenic--and nuclear-engineering feat. Finally, too high a radiation flux might saturate the junction and produce non-linearities by generating sufficient heat to drive the entire lead electrode into the normal state.

It is reassuring to note, however, that even if a workable detector can never be developed, much important information may still be learned about fundamental aspects of superconductive tunneling. Specifically, these are: the excitation mechanism for breaking up "Cooper pairs" by charged particle radiation; the relative sizes as well as some estimate of the absolute recombination and tunneling times of excited electrons; the diffusion velocity of excited electrons in a superconductor.

Clearly, the superconducting nuclear particle detector experiment holds considerable promise. "Positive" results imply the feasibility of developing a detector valuable to nuclear spectroscopy; "negative" results imply, not

failure, but a significant contribution to present knowledge of basic physical processes in superconductors.

APPENDIX A

EFFECT OF THERMAL CONTRACTION ON JUNCTION THICKNESS AND TUNNELING PROBABILITY

It will be shown that the change in thickness of the $Al_2 O_3$ layer is only about 0.2% and that the resulting change in tunneling probability is small.

Holland (1956) states that the oxide layer formed on an aluminum film is amorphous in structure. Consequently, for the purpose of this estimate, it will be assumed that the oxide layer has the same expansion coefficient at 25°C as does alumina, viz. 8×10^{-6} deg^{-1} (Wilkes, 1927). In general, the expansion coefficient (α) is not constant with respect to temperature and is found to vary roughly as the specific heat C_v (White, 1959) so that

$$\frac{\alpha(T)}{\alpha(295)} = \frac{C_v(7)}{C_v(295)} \qquad \text{(A-1)}$$

Unfortunately, data on the specific heat of alumina at low temperatures are not available but such data are available for a crystalline form of $Al_2 O_3$ called sapphire (McFarlane). The expansion coefficient for sapphire at room temperature is 5.8×10^{-6} deg^{-1} which is very close to that of alumina. Because of the similarity of expansion coefficients at room temperature, it is reasonable to assume that, although the lattice forces in alumina and sapphire are different, their net effect on the expansion coefficient is slight. Therefore, to within the accuracy of this estimate, it may be assumed that the lattice-force effect remains small even down to low temperatures and

that α(alumina) will change with temperature similarly to α(sapphire). McFarlane gives the specific heat of sapphire as C_v (291°K) = 0.1813 and C_v (91°K) = 0.0249. Therefore, from equation A-1,

$$\alpha(\text{sapphire, } 91^\circ\text{K}) \approx 8 \times 10^{-7}\,\text{deg}^{-1} \approx \alpha(\text{alumina, } 91^\circ\text{K}) \qquad \text{(A-2)}$$

The thickness t of the barrier at temperature θ may therefore be written as

$$t(\theta) = t_o\,(1 + \alpha(\theta)\theta), \qquad (22^\circ\text{C} > \theta > -182^\circ\text{C})$$

where t_o is the thickness at $\theta = 0^\circ$C. Hence, at temperature $\theta_1 = 22^\circ$C one may write, since the variation between $\alpha(0^\circ)$ and $\alpha(22^\circ)$ is completely negligible,

$$t(\theta_1) = t_o\,(1 + \alpha(\theta_1)\,\theta_1) \qquad \text{(A-3)}$$

At temperature $\theta_2 = -182^\circ$C, it is within the spirit of this estimate to assume an average value of $\langle\alpha\rangle$ such that

$$\langle\alpha\rangle \equiv \frac{\alpha(\theta_1) + \alpha(\theta_2)}{2} = 4.4 \times 10^{-6} \qquad \text{(A-4)}$$

which makes,

$$t(\theta_2) = t_o\,(1 + \langle\alpha\rangle\theta_2)$$

White (1959) states that, for practical purposes, all the contraction has taken place in the range 300°K to about 50°K. For the present estimate, therefore, it will be assumed that $t(\theta_2) = t\,(-182^\circ\text{C}) \approx t\,(-272^\circ\text{C})$. The change in barrier thickness is

$$t\ (22^{\circ}C) - t\ (-272^{\circ}C) \approx t\ (\theta_1) - t\ (\theta_2) = \Delta t$$

It follows then that

$$t = t_o \left[(1 + \alpha(\theta_1)(22) - (1 + \langle\alpha\rangle(-182)) \right]$$

$$= t_o\ (22\ \alpha(\theta_1) + 182\langle\alpha\rangle)$$

From equation A-4, it is clear that $\langle\alpha\rangle < \alpha(\theta_1) = \alpha$. Hence, to simplify the above expression and establish an upper bound on Δt, one may write

$$\Delta t = t\ (\theta_1) - t\ (\theta_2) < t_o\ (22\alpha + 182\alpha) = t_o\ \alpha\ (204)$$

Evaluating equation A-3, one finds that

$$t\ (\theta_1) = t_o(1 + 8 \times 22 \times 10^{-6}) = t_o\ (1 + .00018) \qquad \text{(A-6)}$$

Substituting equation A-6 into A-5 it is seen that

$$t\ (\theta_1) - t\ (\theta_2) < t\ (\theta_1)\ (1 - .00018)\ \alpha\ (204)$$

which may be re-written as

$$t\ (\theta_2) > t\ (\theta_1)\ (1 - .00163) = t\ (\theta_1)\ (.998) \qquad \text{(A-7)}$$

The change in barrier thickness is therefore

$$\Delta t = t\ (\theta_1) - t\ (\theta_2) < t\ (\theta_1) - t\ (\theta_1)\ (.998)$$

or $$\Delta t < (.002)\ t\ (\theta_1)$$

so that

$$\frac{\Delta t}{t\ (\theta_1)} < 0.2\% \qquad \text{(A-8)}$$

On the basis of this result, an expression was derived in Section E of Chapter III which related the tunneling probability P_t to the junction resistance R as follows

$$P_t = \frac{K'}{R} \tag{A-9}$$

where K' is a constant. To justify the ignoring of the variation in thickness when deriving P_t, it will now be demonstrated that the percentage change in P_t due to thickness changes is not only relatively small but, in fact, conducive to more efficient detector operation.

The relation between junction resistance R and junction thickness t is given in figure 8 as

$$\log R = .775t - 10.1 = Ct + M \tag{A-10}$$

so that $R = 10^{Ct + M}$ which makes equation A-9

$$P_t = \frac{K'}{10^M \times 10^{Ct}} = \frac{K}{10^{Ct}}$$

Clearly,

$$\Delta P_t = P_t(\theta_2) - P_t(\theta_1) = K\left(10^{-Ct_2} - 10^{-Ct_1}\right)$$

where $t_1 = t(\theta_1)$ and $t_2 = t(\theta_2)$. Consequently,

$$\frac{\Delta P_t}{P_t(\theta_1)} = \frac{10^{-Ct_2} - 10^{-Ct_1}}{10^{-Ct_1}} = 10^{C(t_1 - t_2)} - 1 = 10^{C\Delta t} - 1$$

and, by invoking equation A-8, one finds

$$\frac{\Delta P_t}{P_t(\theta_1)} < 10^{Ct_1(.002)} - 1$$

Upon substituting a typical value for $t_1 = t\ (25^{\circ}C) = 10\ \text{Å}$ and, from equation A-10, the value for C, one has

$$\frac{\Delta P_t}{P_t(\theta_1)} < 10^{.0155} - 1 = 1.0364 - 1 = 0.0364$$

In conclusion, a 0.2% decrease in barrier thickness is seen to produce an increase in the tunneling probability per unit time of

$$\frac{\Delta P_t}{P_t(\theta_1)} < 3.6\%$$

Though but a small effect, it is observed that thermal contraction of the insulating barrier actually enhances the operation of the detector by increasing the proportion of excited electrons that tunnel.

APPENDIX B

CALCULATION OF DIFFUSION VELOCITY AND RECOMBINATION TIME

In this section, the detailed solution of equation 3-25 and the computer programme used to numerically solve the integral appearing in that equation will be discussed.

Equation 3-25 can be written as

$$\bar{v}_{DIFF} = \frac{\int_{\varepsilon_o}^{\infty} f(E)\, N_s(E)\, v(E)\, dE}{\int_{\varepsilon_o}^{\infty} f(E)\, N_s(E)\, dE} = \frac{I}{n_o}$$

where the symbols are all defined in Chapter III.

First of all, consider the upper integral I

$$I = \int_{\varepsilon_o}^{\infty} \frac{1}{\exp(\beta E) + 1} \cdot \frac{N_s(0)\, E}{(E^2 - \varepsilon_o^2)^{\frac{1}{2}}} \cdot \frac{v_F (E^2 - \varepsilon_o^2)^{\frac{1}{2}}}{\sqrt{3}\, E} \cdot dE$$

$$= (v_F N_s(0)/\sqrt{3}) \int_{\varepsilon_o}^{\infty} (\exp \beta E + 1)^{-1}\, dE$$

The minimum value of E is ε_o and for helium temperatures, $\beta \varepsilon_o$ is about 10 so that $e^{\beta E} \gg 1$ to a good approximation. Hence,

$$I = K N_s(0) \int_{\varepsilon_o}^{\infty} e^{-\beta E} dE = \frac{K N_s(0)\, e^{-\beta \varepsilon_o}}{\beta}$$

With the assumption $e^{\beta E} \gg 1$, n_o becomes

$$n_o = \int_{\varepsilon_o}^{\infty} e^{-\beta E} N_s(0)\, \frac{E\, dE}{(E^2 - \varepsilon_o^2)^{\frac{1}{2}}}$$

n_o can be somewhat simplified by introducing a change of variable,

$$X^2/\beta^2 = E^2 - \varepsilon_o^2$$

making n_o of the form

$$n_o = \frac{N_s(0)}{\beta} \int_o^\infty \exp - (X^2 + \beta^2 \varepsilon_o^2)^{\frac{1}{2}} dX$$

It immediately follows, therefore, that

$$\bar{v}_{DIFF} = \frac{v_F}{\sqrt{3}} \frac{e^{-\beta\varepsilon_o}}{\int_o^\infty \exp - (X^2 + \beta^2 \varepsilon_o^2)^{\frac{1}{2}} dX} \qquad 3\text{-}26$$

The integral n_o does not integrate exactly, so a computer programme was written to numerically evaluate this integral by 16-point Gaussian quadrature and give $\bar{v}_{DIFF}$ as a function of temperature.

In addition, the expression given by Rothwarf shown in figure 17 was evaluated for temperatures ranging from 0.5°K to 8°K.

The results of the following programme are summarized in figures 17 and 18 .

```
C     PROGRAMME FOR EVALUATING DIFFUSION VELOCITY
      AND RECOMBINATION TIME
      READ (5,20) EPSO, VF
20    FORMAT (F10.5, E 12.5)
      COMMON EPSO
      WRITE (6,25)
25    FORMAT (9X, 5HVDIFF, 12X, 1HT, 10X, 5HAREAB, 10X, 5H  E. 10X, 6HTRECOM,//)
      R = 3.03 E-13
      BK = 8.65 E-5
      V = VF/ 1.7321
      READ (5,21) AB,BB
21    FORMAT (2F 15.5)
      READ (5,21) T
5     CONTINUE
      P = 15.5/T
```

```
      S = SQRT (T)
      Q = EXP (P)
      TRECOM = (R*Q)/S
      U = BK * T
      BETA = 1.0/U
      G = EPSO * BETA
      COMMON BETA
      E = EXP (-G)
      CALL GAUSSB (AB, BB, AREAB)
      VDIFF = (V * E)/AREAB
      WRITE (6,30) VDIFF, T, AREAB, E, TRECOM
30    FORMAT (6 X,E 12.5, 7 X, F3.1, 6X, E 12.5, 3X, E12.5, 3X, E12.5, /)
      T = T + 0.5
      IF (T.LE. 8.0)  GO TO 5
      STOP
      END
```

```
      SUBROUTINE GAUSSB (A, B, AREA)
```

This was a standard subroutine available from the U.B.C. Computing Centre Library. It numerically evaluated the integral between the limits AB and BB and stored the answer in AREAB. GAUSSB in turn called another subroutine AUXB(X,Y) which contained the function to be integrated.

```
      SUBROUTINE AUXB(X,Y)
      COMMON EPSO
      COMMON BETA
      C= (BETA * EPSO) **2
      F= SQRT (X * X + C)
      Y= EXP (-F)
      RETURN
      END
```

The following data were used:

EPSO = ε_o = .00134

VF = v_F = 1.23 x 10^8 cm/sec

AB = 0.0

BB = 100.0

T = 0.5

APPENDIX C

ESTIMATE OF THE THICKNESS OF LEAD AND ALUMINUM FILMS

Consider a mass M of lead or aluminum placed in a covered furnace whose top is pierced with a small hole of area A (see figure 32). The evaporated metal atoms effuse through this hole with a certain fraction eventually striking a substrate located a distance R and angle θ from the furnace.

For this cylindrical symmetry, Kennard (1938) gives the number of atoms crossing A per unit area per second, with speed in the range dv and with a direction of motion that makes an angle lying in the range $d\theta$ with respect to the normal to A, as

$$dN' = 2\pi n B v^3 e^{-\gamma^2 v^2} \sin\theta \cos\theta \, dv \, d\theta$$

In this expression,

n = number of atoms/unit volume (inside the furnace)

$B = (M_o/2\pi RT)^{3/2}$

$\gamma^2 = (M_o/2 RT)$

where M_o is the molecular weight, R the gas constant and T the absolute temperature.

From figure 32 it is evident, assuming the pressure is sufficiently low that the molecular mean free path is greater than R, that only those atoms whose velocity is sufficient to allow them to just reach the substrate are of interest.

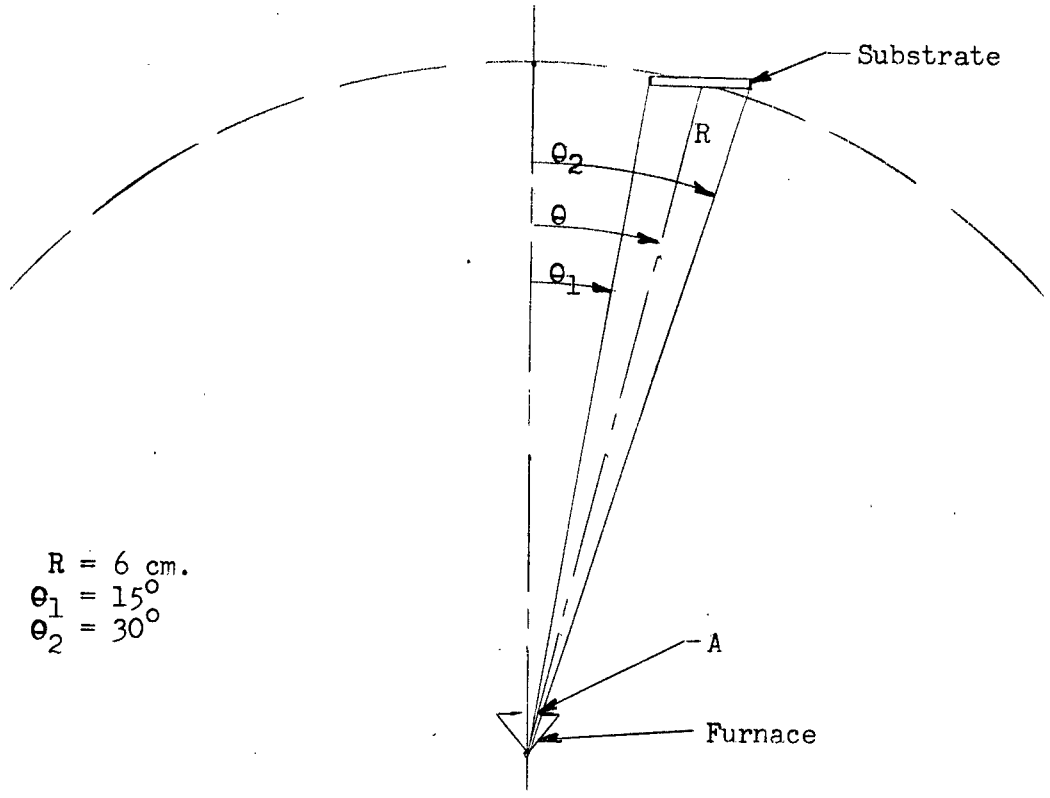

Figure 32: Geometry of Evaporator

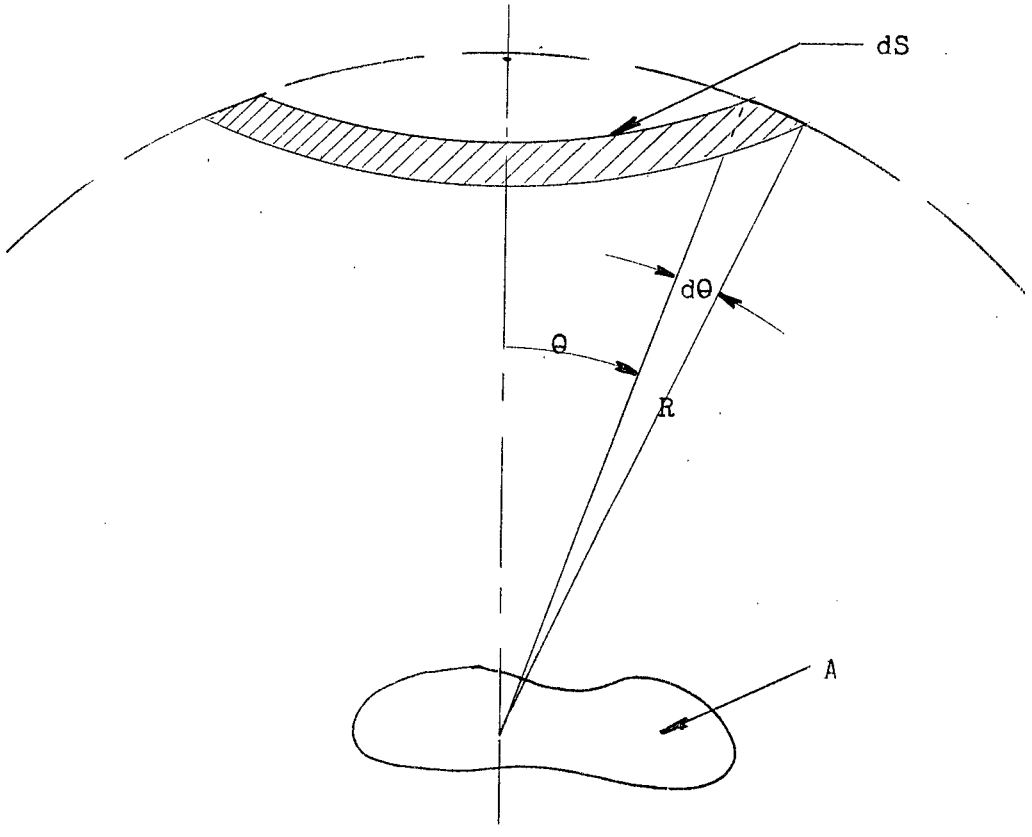

Figure 33: Geometry for Molecular Effusion

This number is given by

$$dN = A2\pi nB \int_{v=v_{min}}^{\infty} v^3 e^{-\gamma^2 v^2} \sin\theta \cos\theta \, d\theta \, dv \text{ atoms/sec.} = A2\pi nBI$$

Now $v_{min} = (2gR)^{\frac{1}{2}} = 108.5$ cm/sec. Performing the integral I by parts, one obtains

$$I = \frac{e^{-\gamma^2 v_{min}^2}}{2\gamma^2} \left(v_{min}^2 + 1/\gamma^2 \right)$$

But $\gamma^2 = M_o/2RT = 207/(2)(8.31)10^7(1300) = 9.6 \times 10^{-10}$ cm^{-2} sec^2 so that $e^{-\gamma^2 v_{min}^2} = e^{-.000011} \approx 1$ and

$$I \approx \frac{1}{2\gamma^2} \left(v_{min}^2 + 1/\gamma^2 \right)$$

It is readily seen that $1/\gamma^2 \gg v_{min}^2$ so that to a very good approximation

$$I \approx \tfrac{1}{2}\gamma^{-4} = \int_0^{\infty} v^3 e^{-\gamma^2 v^2} \, dv$$

Hence, the fractional number of atoms with acceptable velocities and with direction of motion in range $d\theta$ is

$$dN = \frac{2\pi nAB}{2\gamma^4} \cdot \sin\theta \cos\theta \, d\theta = K' \sin\theta \cos\theta \, d\theta$$

If m is the atomic mass and τ is the time required for all the metal to evaporate, then the mass eventually deposited on elemental area dS (see figure 33) is given by

$$dM = m\tau K' \sin\theta \cos\theta \, d\theta = K \sin\theta \cos\theta \, d\theta \qquad \text{C-1}$$

From figure 33 it is clear that $dS = 2\pi R^2 \sin\theta \, d\theta$ and if the deposited metal film has density ρ_f and thickness $t(\theta)$, it follows that

$$dM = \rho_f \, t(\theta) \, dS = \rho_f \, t(\theta) \, 2\pi R^2 \sin\theta \, d\theta \qquad \text{C-2}$$

Equating C-1 and C-2, one finds

$$t(\theta) = K \cos\theta / \rho 2\pi R^2 \qquad C\text{-}3$$

To evaluate K, one notes that in time τ all of the original mass M is deposited over a hemisphere. Therefore, from C-1,

$$M = \int dM = K \int_0^1 \sin\theta \, d(\sin\theta) = \tfrac{1}{2}K \qquad C\text{-}4$$

Substituting C-4 into C-3 one finally obtains

$$t(\theta) = M \cos\theta / \rho \pi R^2 \qquad C\text{-}5$$

Assuming that the films are sufficiently thick that $\rho_f = \rho_B$, where ρ_B is the bulk density of the metal, one calculates the following values for the average thickness $\bar{t} = (t(15^\circ) + t(30^\circ)) / 2$:

Material	Density (gm/cm^3)	M (gm)	$\bar{t}$ (μ)
Aluminum	2.7	0.2	5.98
Lead	11.37	1.5	10.7

APPENDIX D

ESTIMATE OF HEAT LEAKAGE AND RESULTING LIQUID HELIUM LOSS

As can be seen from figures 23 and 24 , heat is transferred to the liquid helium bath in the cryostat mainly via the following four paths: the stainless steel body of the cryostat, the sample mount tube, the control tube and the electrical leads.

It is assumed, for purposes of calculation, that the warm end of the thermal conductors is at 300°K and the cold end at 4°K. Between these temperatures, the mean values of the thermal conductivity λ are (White, p186):

Material	(watts/cm/deg)
Stainless Steel	0.103
Constantan	0.20

Note: Constantan (60 Cu-40 Ni) has almost exactly the composition of the alloy of Cu-Ni called "Advance" (see Chapter VI).

Using these values for λ and the relation

$$\dot{Q} = \frac{A}{L} \lambda (T_w - T_c)$$

where the symbols have the following meanings:

$\dot{Q}$ - heat flux
A - Cross-sectional area of conductor
L - length of conductor
T_w - Temperature at warm end (300°K)
T_c - Temperature at cold end (4°K)

one obtains:

Conductor	A (cm^2)	l (cm)	$\dot{Q}$ (watts)
Cryostat Body	0.4	136	8.4×10^{-2}
Control Tube	0.059	122	1.4×10^{-2}
Sample Mount Tube	0.029	122	0.7×10^{-2}
4 "Advance" leads	7.8×10^{-5}	122	1.4×10^{-4}
Total			10.5×10^{-2}

It is of interest to compare the heat leak of the stainless steel apparatus to the electrical leads.

$$\frac{\dot{Q}_{\text{stainless steel}}}{\dot{Q}_{\text{wires}}} = \frac{10.5 \times 10^{-2}}{1.4 \times 10^{-4}} = 7.5 \times 10^{2}$$

Finally, the relation between the rate at which liquid helium evaporates and the rate at which heat is transferred to the helium is given (White, p. 198; Hoare, p. 142) as 1.43 litre/hour/watt. Therefore, with a total heat leak of 10.5×10^{-2} watts, the estimated loss of liquid helium is 0.15 litres/hr.

APPENDIX E

PROCEDURE FOR LIQUID HELIUM RUN

START UP

1. Siphon in (blanked off)
2. Open stop cock on helium dewar interspace
3. Rough out He dewar, cryostat, interspace and vacuum jacket (with Helium pump)
4. Shut needle valve
5. Close cryostat and dewar roughing valves
6. Flush interspace with N_2
   - close rough main valve, open "air" to N_2, close "air", when P = 1 atm., open main valve to pump, close stop cock and interspace valve when P = 2 cm.
7. Flush vacuum jacket with N_2
   - close rough main valve, open "air" to N_2, close "air" when P = 1 atm., open main valve to pump, close vacuum jacket toggle valve when P = 2 cm.
8. Open lower "He flush" valves on dewar and cryostat
9. Fill dewar and cryostat with He gas from the atmospheric return line.

LEAVE RETURN LINE WIDE OPEN

10. Fill Nitrogen dewar
11. Wait for 1-2 hours for pre-cooling
12. Turn on electronics $\frac{1}{2}$ hour before end of pre-cooling period
13. Close lower "He" flush valves and open 1" ball valve joining cryostat to main return line.
14. Obtain He cylinder and mercury monometer
15. Transfer liquid helium

16. Remove siphon (leaving He dewar open to return line)

17. Allow 5-10 min. for He to boil less violently

18. Open needle valve, admit He to cryostat chamber and close valve (measure difference in level of liquid He in the dewar)

19. Close off cryostat from return line

20. Open bellows valve connecting cryostat to He^4 pump.

SHUT DOWN

1. Valve off He^4 pump

2. Crack needle valve and allow cryostat to come to $4^{\circ}K$ (atmospheric pressure)

3. Open cryostat to return line

4. Make sure there is sufficient liquid N_2 until He has evaporated (make sure no more than 0.8 litres of liquid He remain if compressor not on)

BIBLIOGRAPHY

ABELES, B. and Goldstein, Y., (1965), Phys. Rev. Letters, 14, 595.

AJZENBERG-SELOVE, F., ed., (1960), Nuclear Spectroscopy, Part A, Academic Press, New York.

ANDERSON, P.W., (1963), Phys. Rev. Letters, 10, 525.

BALSER, R.B., (1954), Indium Solder Techniques, Rev. Sc. Instr., 25, 180.

BARDEEN, J., Cooper, L.N., Schrieffer, J.R., (1957), Phys. Rev., 108, 1175.

BARDEEN, J., (1961), Phys. Rev. Letters, 6, 57.

BIRKS, J.B., (1953), Scintillation Counters, Pergammon, London.

BROMLEY, D.A., (1961), "Semiconductor Detectors in Nuclear Physics", Semiconductor Nuclear Particle Detectors, eds. J. W. T. Dabbs and F. J. Walter, N.R.C.- N.A.S., Nuclear Science Series, Report No. 32.

BUECHNER, W.W., (1956), Progress in Nuclear Physics, 5, 1.

BURSTEIN, E., Langenberg, D.N., and Taylor, B.N., (1961) "Quantum Detection of Microwave and Submillimetre-Wave Radiation based on Electron Tunneling in Superconductors", Advances in Quantum Electronics, ed., J. R. Singer, Columbia University Press, p. 480.

CHASE, R.L., (1961), Nuclear Pulse Spectrometry, McGraw-Hill, Toronto.

CROSS, W.G., (1951), Rev. Sc. Instr., 22, 717.

CURRAN, S.C., (1953), Luminescence And The Scintillation Counter, Academic Press, New York.

DEARNALEY. G., and Northrop, D.C., (1963), Semiconductor Counters for Nuclear Radiations, E. & F. N. Spon Ltd., London.

DOUGLASS, D.H., and Meservey, R., (1964, a), Phys. Rev., 135, A19.
Meservey and Douglass, (1964,b), Phys. Rev., 135, A24.

DOUGLASS, D. H., and Falicov, L. M., (1964, c), "The Superconducting Energy Gap", Progress in Low Temperature Physics., C. J. Gorter, ed., Vol. IV, North Holland, Amsterdam.

ELEY, D.D., and Wilkinson, P.R., (1959), "Kinetics of Oxidation of Aluminum Films", Structure and Properties of Thin Films, John Wiley, New York.

FEYNMAN, R.P., et al, (1965), The Feynman Lectures on Physics, Vol. III, Addison-Wesley, New York.

GIAEVER, I. and Megerle, K., (1961), Phys. Rev., 122, 1101.

GIAEVER, I., (1960), Phys. Rev. Letters, 5, 147.

GINSBERG, D.M., (1962), Phys. Rev. Letters, 8, 204.

HANDY, R.M., (1962), Phys. Rev., 126, 1968.

HEALEY, D.C., (1965), A He^3-Filled Ionization Chamber as a Neutron Detector, Thesis.

HEYWOOD, D.R., and White, B.L., (1963), Rev. Sc. Instr., 34, 1050.

HOARE, F.E., et al, eds., (1961), Experimental Cryophysics, Butterworth, London.

HOLLAND, L., (1956), Vacuum Deposition of Thin Films, Chapman and Hall, London.

JOSEPHSON, B.D., (1962), Phys. Letters, 1, 251.

KENNARD, E.H., (1938), Kinetic Theory of Gases, McGraw-Hill, New York.

KITTEL, C., (1956), Introduction to Solid State Physics, J. Wiley, New York.

LAX, E., and Vernon, F.L., (1965), Phys. Rev. Letters, 14, 256.

LEIGH, J.L., (1964), The Efficiency of Scintillation Counters for Gamma Ray Detection, Thesis.

LYNTON, E.A., (1962), Superconductivity, Methuen, London.

McFARLANE, R.A., Summary of Available Data on the Physical Properties of Synthetic Sapphire, Adolf Meller Co., (unpublished).

MARION, J.B., (1960), Nuclear Data Tables, Part 3 "Nuclear Reaction Graphs", N.A.S.-N.R.C., Washington.

MENDELSSOHN, G.K., (1960), Cryophysics, Interscience, New York.

NEILER, J. H., and Good, W.M., (1960), "Time of Flight Techniques", Fast Neutron Physics, Marion, J.B. and Fowler, J.L., eds., Interscience, London.

NICOL, J., et al, (1960), Phys. Rev. Letters, 5, 461.

REIMANN, M.A., (1964), Charged Photoparticles from Argon, Thesis.

ROSENBERG, H.M., (1963), Low Temperature Solid State Physics, Oxford.

ROSSI, B.B. and Staub, H., (1949), Ionization Chambers and Counters, McGraw-Hill, New York.

ROTHWARF, A., and Cohen, M., (1963), Phys. Rev. 130, 1401.

SCHRIEFFER, J.R., (1962), Phys. Rev. Letters, 8, 207.

SEGRÈ, E., (1964), Nuclei and Particles, Benjamin, New York.

SEITZ, F., (1940) Modern Theory of Solids, McGraw, New York.

SIEGBAHN, K., ed., (1955), Beta and γ-Ray Spectroscopy, North-Holland, Amsterdam.

SHAPIRO, S., et al, (1962), IBM Journal Research and Development, 6, 34.

SHERMAN, N.K., (1964), Can. J. Phys., 40, 372.

SHIN, E.E., (1964), Phys. Rev., 135, A299.

SHOCKLEY, W., (1961), Czech. J. Phys., B11, 81.

SIMMONS, J.G., (1963,a), J.A.P., 34, 1793, J.A.P., 34, 2581, (1963,b)

SMITH, A.J.S., (1961), The Development of a Double Focusing Spectrometer, Thesis.

TAYLOR, J.M., (1963), Semiconductor Particle Detectors, Butterworth, London.

TOVE, P.A., and Falk, K., (1961), Nuclear Instruments and Methods, 12, 278.

WHITE, G.K., (1959), Experimental Techniques in Low-Temperature Physics, Oxford University Press, London.

WILKES, G.B., (1927), "Refractory Materials", International Critical Tables, E.W. Washburn, ed., McGraw-Hill, New York.

WILKINSON, D.H., (1950), Ionization Chamber and Counters, Cambridge University Press.

WYDER, P., (1964), Rev. Mod. Phys., 36, 116.

YUAN, L.C., and Wu, C., eds. (1963), Methods of Experimental Physics, Vol. 5, "Nuclear Physics", Part A.